

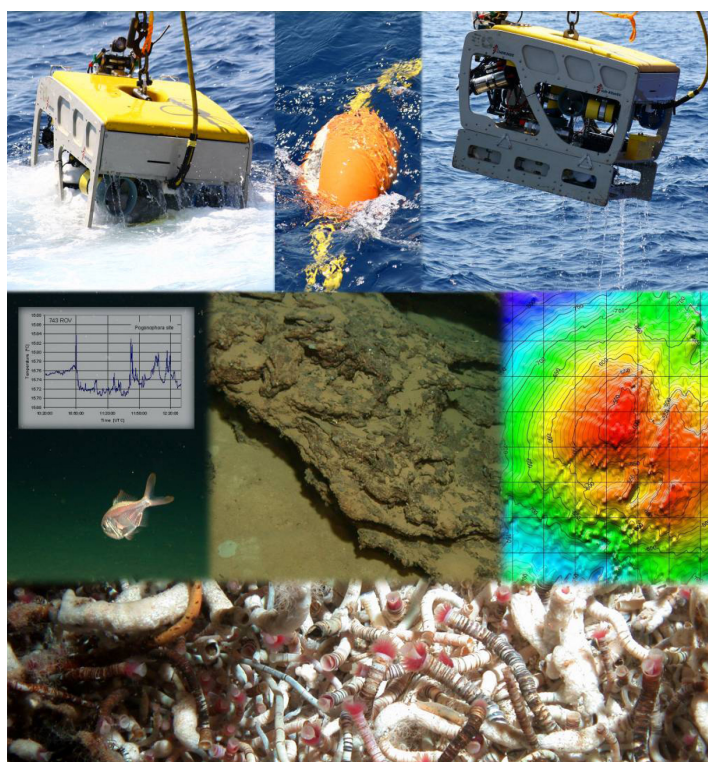


IFM-GEOMAR

Leibniz-Institut für Meereswissenschaften
an der Universität Kiel

FS Poseidon
Fahrtbericht / Cruise Report P340
TYMAS
"Tyrrhenische Massivsulfide"

Messina - Messina
06.07.-17.07.2006



Berichte aus dem Leibniz-Institut
für Meereswissenschaften an der
Christian-Albrechts-Universität zu Kiel

Nr. 21
September 2008

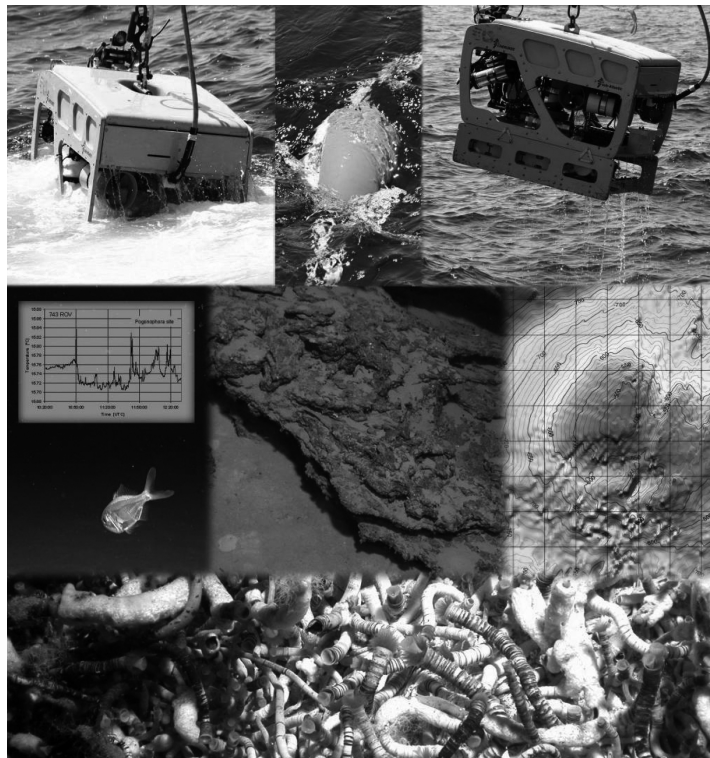


IFM-GEOMAR

Leibniz-Institut für Meereswissenschaften
an der Universität Kiel

FS Poseidon Fahrtbericht / Cruise Report P340 TYMAS "Tyrrhenische Massivsulfide"

Messina - Messina
06.07.-17.07.2006



Berichte aus dem Leibniz-Institut
für Meereswissenschaften an der
Christian-Albrechts-Universität zu Kiel

Nr. 21, September 2008

ISSN Nr.: 1614-6298



IFM-GEOMAR

Leibniz-Institut für Meereswissenschaften
an der Universität Kiel

Das Leibniz-Institut für Meereswissenschaften
ist ein Institut der Wissenschaftsgemeinschaft
Gottfried Wilhelm Leibniz (WGL)

The Leibniz-Institute of Marine Sciences is a
member of the Leibniz Association
(Wissenschaftsgemeinschaft Gottfried
Wilhelm Leibniz).

Herausgeber / Editor:

Sven Petersen and Thomas Monecke

IFM-GEOMAR Report

ISSN Nr.: 1614-6298

Leibniz-Institut für Meereswissenschaften / Leibniz Institute of Marine Sciences

IFM-GEOMAR
Dienstgebäude Westufer / West Shore Building
Düsternbrooker Weg 20
D-24105 Kiel
Germany

Leibniz-Institut für Meereswissenschaften / Leibniz Institute of Marine Sciences

IFM-GEOMAR
Dienstgebäude Ostufer / East Shore Building
Wischhofstr. 1-3
D-24148 Kiel
Germany

Tel.: ++49 431 600-0
Fax: ++49 431 600-2805
www.ifm-geomar.de

1 Scientific Party & Crew

Scientific Party

Sven Petersen	IFM-GEOMAR ¹	Chief scientist
Thomas Monecke	University of Ottawa	Co-Chief scientist
Nico Augustin	IFM-GEOMAR ¹	Bathymetry
Alessandra Esposito	INGV ² , Rome	Volcanology
Dieter Garbe-Schönberg	University of Kiel	Fluid sampling
Guido Giordano	University of Rome	Volcanology
Mark D. Hannington	University of Ottawa	Mapping
Mike Hocking	University of Ottawa	Geology
Bernd Melchert	IFM-GEOMAR ¹	Bathymetry
Harry Schulz	Fielax, Bremen	ROV-pilot
Inken Suck	Fielax, Bremen	ROV-pilot

¹ IFM-GEOMAR, Leibniz Institute of Marine Sciences at the University of Kiel

² Istituto Nazionale di Geofisica and Vulcanologia, Rome

Crew

Michael Schneider	Captain
Theo Griese	First mate
Holger Voigt	Second mate
Frank-Werner Dohmann	First engineer
Mohammed Al-Tamini	Second engineer
Werner-Dietmar Klare	Electrician
Rüdiger Engel	Motorman
Hans-Ulrich Schade	Cook
Frank Liiders	Steward
Frank Schrage	Bosun
Bernd Rauh	Ship mechanic
Thomas Radisch	Ship mechanic
Jürgern Sauer	Ship mechanic
Pedro M. Barbosa	Seaman

2 Introduction & Scientific Background

S. Petersen and T. Monecke

Massive sulfide deposits hosted by ancient volcanic successions typically contain low amounts of precious metals, with Au contents ranging from an average of approximately 1 to 3 ppm. However, some deposits are typified by elevated Au concentrations with Au being one of the primary commodities. Important examples of massive sulfide deposits with anomalous Au enrichments are the Jurassic Eskay Creek deposit in Canada (1.08 Mt ore at 65.6 g/t Au), the Cambrian Henty deposit in Tasmania (1.7 Mt ore at 11.3 g/t), and the Proterozoic Boliden deposit in Sweden (8.5 Mt ore at 15.2 g/t Au). In addition to the enrichment of this precious metal, these deposits are also characterized by elevated concentrations of the epithermal suite of elements – As, Sb, and Hg (Hannington et al., 1999).

Research on ancient deposits suggests that massive sulfides showing high gold concentrations may have formed in unusual shallow water environments (<1,500 m; Hannington et al., 1999; Hannington and Herzig, 2000). Fluid inclusion studies revealed that Eskay Creek formed at a water depth of less than 1,500 m (Sherlock et al., 1999). This finding is corroborated by the presence of shallow marine fossils and wood fragments in a coarse volcanoclastic unit underlying the sulfide mineralization (Nadaraju, 1993; Sherlock et al., 1999). The Henty deposit in Tasmania is located in a sequence of rhyolites and coarse volcanoclastic sediments that locally contain welded ignimbrites, which suggests that the deposit formed in a shallow marine environment or close to a nearby subaerial volcanic centre (Halley and Roberts, 1997; White and McPhie, 1997). In the case of the Boliden deposits, Allen et al. (1996) have shown that the host rock sequence was exposed above storm wave base during the mineralizing event.

Hydrothermal fluids forming Au-rich massive sulfide deposits at shallow water depth are likely to have boiled during ore deposition. Ascent of the boiling hydrothermal fluids is accompanied by a dramatic cooling, which influences the capability of the fluids to transport metals (Drummond and Ohmoto, 1985; Cole and Drummond, 1986; Butterfield et al., 1990). Due to the pronounced decrease in temperature, reduced and slightly acidic hydrothermal fluids cannot transport significant amounts of Cu to a vent site located at shallow water depth, whereas the precious metals Au and Ag and the epithermal suite of elements As, Sb, and Hg can be transported under these conditions. Sulfide deposits formed at shallow water depth may, therefore, be enriched in these elements (Hannington et al., 1999). In many respects, deposition of metals in the shallow water environment can be compared to the formation of epithermal deposits on land suggesting that there is a continuous transition from submarine base metal massive sulfides to subaerial epithermal Au deposits (Hannington et al., 1999; Hannington and Herzig, 2000).

Despite compelling evidence for the formation of Au-rich massive sulfide deposits in the shallow marine environment, considerable ambiguity remains because water depth cannot be directly measured or constrained in ancient volcanic successions (Huston and Cas, 2000). Direct evidence proving a possible link between water depth and the metal content of massive sulfide deposits can only be provided by research on modern seafloor hydrothermal systems.

The southeastern Tyrrhenian Sea represents one of the best localities worldwide to study the formation of shallow marine massive sulfide mineralization and the processes that result in metal enrichment in this environment. Hitherto, three different sites of polymetallic sulfide mineralization have been recognized. Detailed investigations of these sites should provide an ideal basis for the development and testing of new genetic models explaining the formation of shallow water, precious metal-rich marine massive sulfide deposits.

Research cruise P340 forms part of a large international research project aiming to constrain the nature of shallow hydrothermal activity in the Tyrrhenian Sea and is the first of two consecutive cruises organized by the Leibniz Institute of Marine Sciences at the University of Kiel. The cruise with R/V Poseidon represents a reconnaissance survey of the known hydrothermal sites in the Tyrrhenian Sea using the remotely operated vehicle Cherokee of the University of Bremen. It is the aim of this research to define targets that will be revisited during a cruise with R/V Meteor in 2007. During this second cruise, shallow drilling at the identified targets will be conducted using the lander-type drilling device Rockdrill 1 of the British Geological Survey. This portable drilling device was successfully used during cruise SO-166 aboard R/V Sonne (Herzig et al., 2003; Petersen et al., 2005) and permits drilling to a maximum penetration of 5 m at a core diameter of 50 mm.

3 Regional Geology

T. Monecke and S. Petersen

The Tyrrhenian Sea represents a semi-closed basin in the western Mediterranean that is bounded by mainland Italy to the northeast, Sicily to the southeast, and the islands of Corsica and Sardinia to the west. The southeastern portion of the Tyrrhenian Sea comprises the Marsili abyssal plain and the volcanoes of the Aeolian archipelago (Fig. 3-1).

The Marsili abyssal plain is interpreted to represent a small oceanic back-arc basin that formed as a consequence of roll-back of the northwestward-dipping Ionian subduction zone and migration of arc volcanism from the island of Sardinia towards the east-southeast (Barberi et al., 1974; Gasparini et al., 1982; Ellam et al., 1989; Argnani and Savelli, 1999; Savelli, 2001). Opening of the Marsili back-arc basin was initiated close to the Pliocene-Pleistocene boundary at approximately 1.9 Ma (Savelli, 1988; Savelli and Schreider, 1991). The presence of oceanic crust in the Marsili basin has been confirmed by ODP Leg 107 Hole 650 (Kastens et al., 1986, 1988).

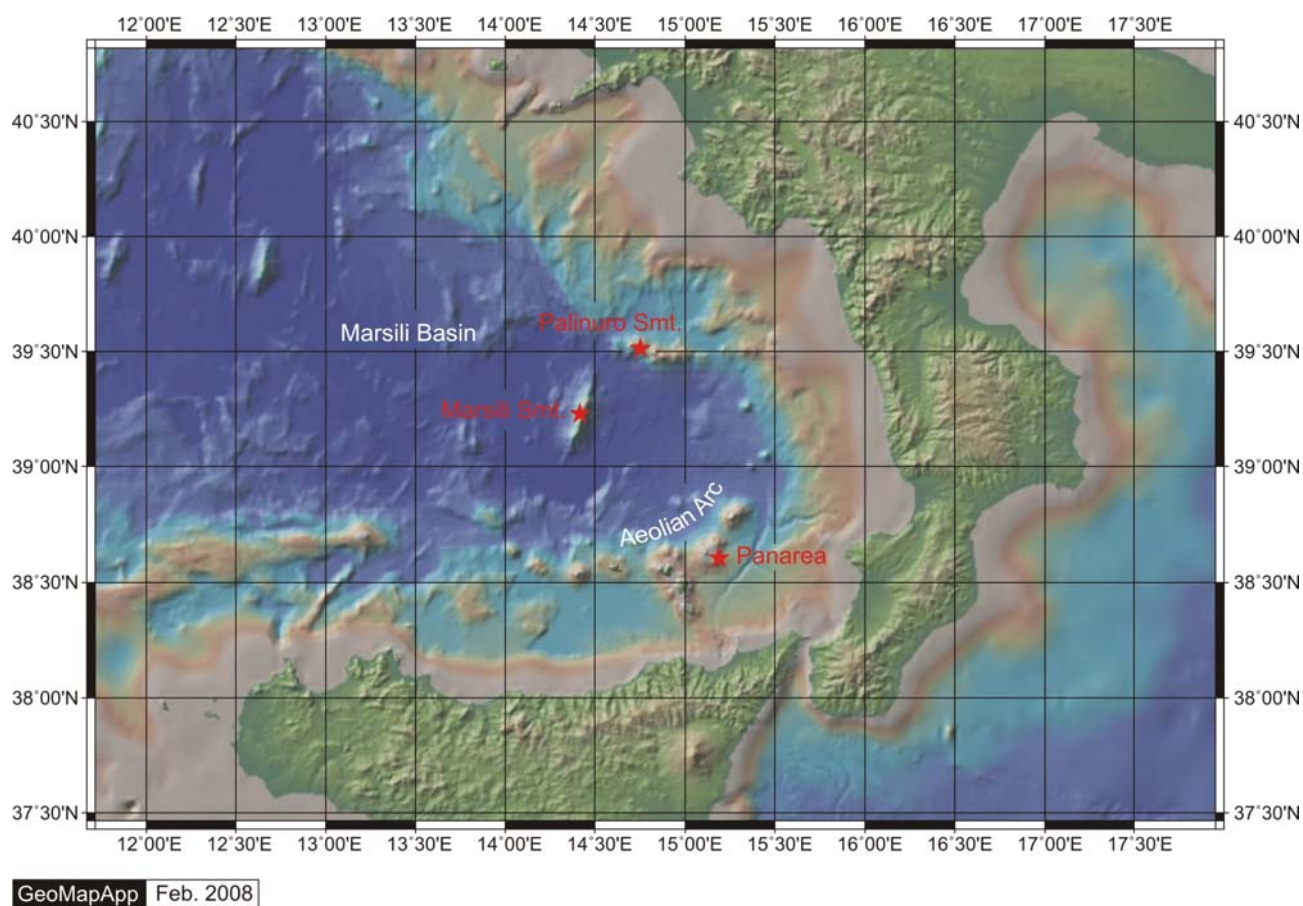


Fig. 3-1: Bathymetric map of the Tyrrhenian Sea showing the location of the working areas visited during P340.

The central part of the Marsili abyssal plain is occupied by Marsili Seamount, a prominent volcanic feature interpreted to be the superinflated spreading ridge. Superinflation may have been the result of robust volcanism occurring within a restricted, slow spreading environment (Marani and Trua, 2002). Due to the contamination of the mantle by the subducted Ionian slab, Marsili Seamount is composed of volcanic rocks having a calc-alkaline affinity. The seamount consists largely of medium-K basalts, with high-K andesites form-

ing small volcanic cones in the summit area (Del Monte, 1972; Brusilovskiy and Gorodnitskiy, 1990; Sborshchikov and Al'mukhamedov, 1992; Savelli and Gasparotto, 1994; Gasparotto and Savelli, 1994; Trua et al., 2002). Age constraints on the volcanism are scarce. Lava sampled from the summit region of Marsili Seamount yielded K/Ar ages of <0.2 Ma (Selli et al., 1977), which is consistent with magnetostratigraphic data suggesting that the bulk of Marsili Seamount is <0.8 Ma in age (Brusilovskiy and Gorodnitskiy, 1990; Faggioni et al., 1995).

The Marsili back-arc basin is surrounded by the tightly arcuate chain of Aeolian volcanoes (Fig. 3-1) that rests on an up to 20 km thick continental basement (Morelli et al., 1975) formed by metamorphic and sedimentary rocks (Honnorez et al., 1968; Bargossi et al., 1989). The volcanic chain comprises seven major islands and several seamounts extending for approximately 200 km parallel to the continental slope of northern Sicily and western Calabria. Volcanism in the Aeolian archipelago commenced ca. 1.5 Ma ago in the western part of the volcanic chain (Beccaluva et al., 1985). Subaerial volcanic activity was restricted to the past 500 ka. Volcanic eruptions occurred during historical times at Stromboli, Lipari, and Vulcano. Today, only Stromboli exhibits ongoing eruptive volcanism, but fumarolic activities also occur on Salina, Lipari, and Vulcano.

The Aeolian volcanoes are located in three structurally and volcanologically distinct sectors. The western sector extends from Sisifo Seamount to the islands of Alicudi and Filicudi. Calc-alkaline volcanism in this sector was probably initiated 1.3 Ma ago. Shoshonitic rocks (K-basalt, shoshonite, rhyolite, and trachyte) with an age of about 0.8 Ma occur at Eolo and Enarete Seamounts (Beccaluva et al., 1985). Filicudi Island represents the emergent part of several overlapping volcanic centers. Volcanic rocks have a calc-alkaline or high-K calc-alkaline affinity ranging in composition from basalt and basaltic andesite to high-K andesite (Santo et al., 2004).

The central sector comprises the islands of Salina, Lipari, and Vulcano. Salina is composed of several basaltic and andesitic volcanic centers that are older than 230 ka. Volcanism at this island ceased approximately 13 ka ago (De Rosa et al., 1989). At Lipari, subaerial high-K calc-alkaline volcanism commenced at approximately 223 ka producing rocks of andesitic to rhyodacitic composition. Volcanism lasted until 98 ka in the central part of Lipari and resumed at 42 ka producing rhyolitic rocks on the southernmost part of the island. Younger volcanic activities resulted in the deposition of pyroclastic rocks and thick viscous, mainly obsidian, lava flows. The island of Vulcano is composed of four major volcanic complexes. Volcanic activity on this island started 120 ka ago with the formation of the South Vulcano edifice, which consists of old lavas and scoria fall and flow deposits. The formation of the Piano Caldera occurred between 107 and 99 ka and was followed by the eruption of scoriae and lavas between 99.5 and 48.5 ka. Volcanism resumed in the northern, western, and southern sectors of Vulcano between 28 and 7.6 ka with the emplacement of rhyolitic to trachytic domes. Younger volcanic activity resulted in the formation of the Fossa cone and the peninsula of Vulcanello. The last eruption in the Fossa cone took place between 1880 and 1890 AD (Gioncada et al., 2003). Salina, Lipari, and Vulcano form a NNW-SSE alignment which runs orthogonal to the general orientation of the Aeolian volcanic chain. The development of these volcanic islands is linked to the presence of major extensional tectonic structures cutting the pre-volcanic basement. These structures are interpreted to represent the offshore extension of the Tindari-Letojanni fault system on Sicily. The structural evolution of this area is similar to that found in zones of transition from arc-related to rift volcanism (Barberi et al., 1994; Ventura et al., 1999).

The eastern sector of the Aeolian volcanic chain extends from Panarea Island to Palinuro Seamount. The oldest subaerial lavas on Panarea Island were deposited at approximately 150 ka. The formation of the volcanic edifice was completed by 120 ka. The mainly extrusive and explosive volcanic rocks have a high-K calc-alkaline affinity and are of andesitic to dacitic composition. The youngest volcanic activities at Panarea resulted in the deposition of basaltic pyroclastic rocks and the formation of the rhyolite dome of Basiluzzo Island

at approximately 42 to 13 ka (Gabbianelli et al., 1990; Calanchi et al., 1999, 2002). Stromboli represents the largest volcano in the Aeolian archipelago (Favalli et al., 2005). Its subaerial portion was built in the last 100 ka through four main periods of volcanic activity (Hornig-Kjarsgaard et al., 1993). The composition of the volcanic products is variable, belonging to calc-alkaline, high-K calc-alkaline, and shoshonitic series (Francalanci et al., 1993). In contrast to Panarea and Stromboli, little is known on the nature and age of volcanism at Alcione and Lametini Seamount. Arc tholeiitic basalts have been dredged from Lametini Seamount (Beccaluva et al., 1985). Palinuro Seamount is located at the northern tip of the Aeolian volcanic chain. Its location appears to be controlled by the occurrence of a major E-W trending structure that represents the offshore continuation of the Sanginetto line separating Calabria and the southern Apennines. Volcanic rocks recovered from the upper portion of Palinuro Seamount have a calc-alkaline affinity and range from basalt to basaltic andesite (Del Monte, 1972; Colantoni et al., 1981). Radiometric K-Ar dating of one volcanic sample collected on the shallowest portion of Palinuro yielded an age of 0.35 ± 0.05 Ma (Colantoni et al., 1981).

The geodynamic significance of the Aeolian volcanism is controversial. The geochemical composition of the volcanic rocks and the occurrence of a deep seismicity in the southern Tyrrhenian Sea led many authors to interpret the Aeolian volcanoes as a volcanic arc related to the northwest-ward subduction of the Ionian microplate beneath the Tyrrhenian plate (Barberi et al., 1974; Beccaluva et al., 1982, 1985; Ferrari and Manetti, 1993). More recently, however, it has been proposed that subduction ceased approximately 1 Ma ago, when a general uplift coupled with extensional tectonics started to affect Calabria and the southern Apennines (Westaway, 1993; Hippolyte et al., 1994; Milano et al., 1994; Carmignati et al., 1998). Following this interpretation, present-day deep seismicity in the southern Tyrrhenian Sea is caused by passive subduction of the detached Ionian slab. Consequently, the volcanism in the Aeolian archipelago would take place in a post-subduction extensional tectonic regime (De Astis et al., 2003).

4 High temperature hydrothermal sites

T. Monecke, S. Petersen, M. Hocking, and M.D. Hannington

Submarine hydrothermal precipitates have been recorded at several localities in the southeastern Tyrrhenian Sea. Hitherto, research in the area has mainly focused on low-temperature precipitates, the characteristics of which are described in detail by Dekov and Savelli (2004). In addition to these deposits, three sites containing polymetallic high-temperature precipitates have been recognized, namely Palinuro Seamount, Marsili Seamount, and the Panarea hydrothermal field located between the islands of Panarea and Basiluzzo (Fig. 3-1).

4.1 Palinuro Seamount

Palinuro Seamount represents a complex volcanic feature that consists of five coalesced volcanic edifices lying along an E-W trending fault system extending seaward off the northern limit of Calabria. The seamount is elongated and extends about 50 km in an E-W direction, with a maximum width of about 25 km at its base. Palinuro Seamount is bounded to the north by the continental slope of the Southern Apennines and faces Marsili basin to the south. The seamount can be divided into two sectors. The western and central sector has a minimum water depth of 570 m, whereas the eastern sector shoals to a water depth of 70 m. The two sectors appear to be offset by about 7 km by an N-S or NE-SW trending fault system. The peaks of Palinuro Seamount are regularly shaped and probably represent former centers of eruption (Fabbri et al., 1973; Colantoni et al., 1981; Minniti and Bonavia, 1984; Stüben et al., 1993; Yevsyukov, 1994). The shallow peak on the eastern part of Palinuro Seamount is built on a plateau that is about 2 km in diameter, and probably formed as a result of erosion during the last glacial low-stand of the sea level (Fabbri et al., 1973).

Seafloor observations have shown that large parts of Palinuro Seamount are covered by sediments with outcrops of volcanic rocks being relatively rare in the upper portion of the coalesced volcanic edifices. The occurrence of massive sulfides and, more extensive, Mn-Fe-oxide deposits has been established by seafloor sampling and TV-guided camera surveys (Kidd and Ármannson, 1979; Minniti and Bonavia, 1984; Puchelt and Laschek, 1986; Eckhardt et al., 1997; Marani et al., 1999; Dekov and Savelli, 2004).

Massive sulfide fragments have been recovered from the western portion of the seamount at a water depth of approximately 600 m by gravity coring (Minniti and Bonavia, 1984; Marani et al., 1999), dredging (Marani et al., 1999), and TV-guided grab sampling (Puchelt and Laschek, 1986). The distribution of the polymetallic mineralization at Palinuro Seamount is poorly constrained; the samples collected during several research cruises originate from two localities that are approximately 5 km apart. No information on the sub-seafloor nature of the mineralization is available. Sulfide samples recovered during earlier research cruises appear to have been buried in sediment (Puchelt and Laschek, 1986; Marani et al., 1999). The occurrence of sulfide chimneys has not been reported. However, high concentrations of flocculent white and yellow bacterial mats as well as yellow, brown, and green staining of sediments and outcrops have been recognized suggesting relatively recent hydrothermal activity in the area (Minniti and Bonavia, 1984; Puchelt and Laschek, 1986; Stüben et al., 1993; Eckhardt et al., 1997). The hydrothermal fluids responsible for the formation of the massive sulfides locally altered the surrounding volcanic host rocks, resulting in the formation of abundant clay minerals (Marani et al., 1999).

The recovered sulfides are highly porous, macroscopically layered or rhythmically banded, and typically botryoidal (Tufar, 1991). The recovered massive sulfide fragments showed concentrations of up to 14.5 wt.% Pb, 28.2 wt.% Zn, 1.21 wt.% Cu, 6,700 ppm Hg, 5,540 ppm As, 2,000 ppm Sb, 1,270 ppm Ag, and 7.1 ppm Au (Puchelt and Laschek, 1987; Bäcker et al., 1991; Tufar, 1991). The mineralization primarily consists of pyrite, galena, and sphalerite. Marcasite, chalcopyrite, and enargite represent minor phases. Bismuthinite, bravoite, covellite, eskebornite, jordanite, native silver, proustite-pyrargyrite, stibioluzonite, stibnite, tennantite-tetrahedrite, umangite, and wurtzite are present as accessory phases (Minniti and Bonavia, 1984; Tufar, 1991; Dekov and Savelli, 2004). The sulfide minerals are typically intergrown with barite, which forms tabular, euhedral crystals ranging up to several millimeters in size (Puchelt and Laschek 1987; Tufar, 1991). Sulfur isotopic ratios vary from -3.8 to -14.7 ‰ for pyrite and from -2.7 to -4.2 ‰ for other sulfide minerals. Barite has $\delta^{32}\text{S}$ values ranging from 9.0 to 11.4 ‰ (Puchelt and Laschek, 1987). The sulfur isotope values of the sulfides and associated barite are low, possibly indicating the contribution of a magmatic component to the mineralizing system.

In addition to the local occurrence of massive sulfides and associated hydrothermal alteration, a variety of hydrothermally derived Mn-Fe-oxide deposits have been observed at Palinuro Seamount at water depths between 90 m and 900 m (Kidd and Ármannson, 1979; Minniti et al., 1986; Glasby et al., 1995; Eckhardt et al., 1997; Dekov and Savelli, 2004). Manganese-rich crusts commonly form thin films on calcareous sediment and on fossil fragments such as shells and corals (Eckhardt et al., 1997). Besides these crusts, Mn-rich micronodules appear to be relatively abundant on the upper slopes and summits of Palinuro Seamount. The nodules have an average diameter of approximately 1 mm forming black gravelly sands at the seafloor. The well sorted nature of the micronodules may indicate that high energy bottom currents removed finer particles. The porous and black Mn-Fe-oxide deposits from Palinuro Seamount have distinctly high Mn/Fe ratios and possess low concentrations of Co, Ni, Cu, Zn, and Pb (Kidd and Armannson, 1979; Eckhardt et al., 1997).

4.2 Marsili Seamount

Marsili Seamount represents a prominent NNE-SSW trending volcanic feature located in the central part of the <2 Ma old ocean crust-floored Marsili basin (Fig. 3-1). It is the largest seamount in the Tyrrhenian Sea and has an overall length of 55 km, a maximum width of 30 km, and a height of approximately 3,000 m. The seamount possesses a long and narrow summit region that stretches approximately 20 km along the main axis of the volcano and rises to a minimum water depth of less than 500 m. The summit region, which occurs mainly above the 1,000 m isobath, is generated by the linear alignment of elongated ca. 200 m high volcanic cones and the occurrence of contiguous cones forming narrow cone ridges. The flanks of the seamount, in particular at its northern tip, are characterized by numerous circular, parasitic or flank cones that have a basal diameter of up to 1.5 km and a height of up to 300 m (Savelli, 1992; Sborshchikov et al., 1989; Sborshchikov and Al'mukhamedov, 1992; Marani and Trua, 2002; Trua et al., 2002). The basin to the east and west of the Marsili edifice exhibits several steep fault scarps. The faults have throws in the order of 200 to 400 m and are generally parallel to the trend of the summit region of Marsili Seamount. Small elongated volcanic cones occur on the hanging wall sides of the faults (Marani and Trua, 2002; Trua et al., 2002).

Video surveys showed that the summit region of the seamount is dominated by young lavas. The eruptive products of the summit area consist of viscous and scoriaceous lava flows and associated breccia, whereas pillow lavas and elongate tube flows form the deeper portions of the seamount at water depth greater than 1,000 m. Linear fault scarps

and several meters wide open fissures are abundant in the summit area, but also occur along the slopes of Marsili Seamount (Sborshchikov et al., 1989, 1991; Savelli, 1992; Sborshchikov and Al'mukhamedov, 1992). Sediments are scarce or absent in the summit area. The volcano flanks are overlain by a sediment cover that thickens considerably with depth (Sborshchikov et al., 1989).

Fe-oxide deposits, forming numerous mounds, stacks, and branch-like structures, occur in the central part of the summit region of Marsili Seamount (Uchupi and Ballard, 1989; Savelli, 1992; Sborshchikov and Al'mukhamedov, 1992). Submersible sampling revealed that the Fe-oxide precipitates are typified by distinctly low Si/Fe and Mn/Fe ratios (Dekov et al., 2006). The occurrence of shimmering water in the area suggests that low-temperature hydrothermal activity is probably still ongoing (Uchupi and Ballard, 1989; Savelli, 1992). In addition to Fe-oxide deposits, one massive sulfide fragment with abundant barite was discovered during dredging at Marsili Seamount (Marani et al., 1999).

4.3 Panarea

Panarea is the smallest island in the Aeolian archipelago. The island represents a small emerged volcanic complex set on a large, near circular platform that has a size of approximately 55 km². The platform is bounded by a shelf break at a water depth of 120 to 130 m. The submerged platform has steep slopes and a height of ca. 1,050 m above the surrounding seafloor. Taking the subaerial portion of the volcano into account, the total height of Panarea is ca. 1,600 m (Favalli et al., 2005). Subaerial parts of the volcanic complex include the main island of Panarea in the west, the island of Basiluzzo in the northeast, and the central islets and reefs in the east (Gabbianelli et al., 1990; Calanchi et al., 1999).

The morphology of the subaerial portion of Panarea Island is largely formed by lava domes. The presence of circular depressions and the occurrence of feeder dykes indicate the existence of two craters at Panarea. One is located at the NNW tip of Panarea between Scoglio La Nave and Punta Scritta and the other is situated further to the south at Cala Bianca. The main tectonic structures on Panarea Island are NE-SW trending faults that have been active up to <25 ka (Lanzafame and Rossi, 1984). A major normal fault of this orientation occurs at the southwestern tip of Panarea at Costa del Capraio, where a cliff formed by an 80 m high dip-slip. A second tectonic trend is represented by NNW-SSE trending normal faults. These structures are probably still active (Gabbianelli et al., 1990; Calanchi et al., 1999).

Shallow water gas venting is widespread in the submerged portion of the Panarea volcanic complex. Hydrothermal discharge is most pronounced in a 2.3 km² large area between the islets of Dattilo, Panarelli, Lisca Bianca, Bottaro, and Lisca Nera, where numerous shallow marine (<30 m) vents occur. Detailed bathymetric studies supplemented by scuba diving revealed that the submarine vents occur largely in relation to NE-SW and NW-SE trending faults (Gabbianelli et al., 1990; Calanchi et al., 1999; Esposito et al., 2006). The seafloor in the area between the central islets and reefs is dominated by dark to pale gray highly porphyritic andesitic lava, massive to flow-banded, gray basaltic andesite, and a sedimentary cover consisting of partly consolidated, stratified sand, gravel, and conglomerate that is laterally transitional to breccia. Hydrothermal alteration is widespread around the vent sites. In addition, abundant alunite veins have been recognized to the west of Lisca Bianca and Bottaro (Esposito et al., 2006).

Submarine gas emission between the central islets and reefs are known since historical times (Esposito et al., 2006). Total gas output in this area was estimated to be 9×10^6 liters/day (Italiano and Nuccio, 1991). Sampling of the vent sites showed that the

discharge consisted of CO₂ rich gases (>90 vol.%) with minor amounts of H₂S, H₂, N₂, He, Ar, CH₄, and CO (Italiano and Nuccio, 1991; Calanchi et al., 1995). The gas emissions at the seafloor were associated with the venting of thermal waters having temperatures of up to 100 °C. In comparison to seawater, the thermal waters exhibited increased concentrations of K, Ca, Li, and Cl, and decreased contents of Mg and SO₄ (Italiano and Nuccio, 1991). The compositions of the gases and their isotopic signatures suggested that the emissions originated from a geothermal reservoir fed by magmatic fluids (Italiano and Nuccio, 1991; Calanchi et al., 1995).

Since historical times, continuous gas venting in the area has been repeatedly interrupted by short periods of vigorous gas discharge, presumably due to new magmatic inputs into the geothermal reservoir (Caliro et al., 2004; Caracausi et al., 2005). The most recent hydrothermal crisis occurred between Lisca Bianca and Bottaro in the night between November 2nd and 3rd, 2002. The submarine explosion resulted in the formation of an ellipsoidal crater near Bottaro that has a dimension of 35 x 20 m and a depth of 8 m (Caliro et al., 2004; Caracausi et al., 2005; Esposito et al., 2006). The suspension of sediment during the hydrothermal explosion colored the sea forming whitish plumes that extended for several hectares to the SSE due to dispersal by the currents. The vigorous gas discharge near Bottaro was accompanied by a drop of the seawater pH to values between 5.0 and 5.5 (Capaccioni et al., 2003) and the death of thousands of fishes. The smell of H₂S was recognizable on Panarea Island, which is located about 3 km away from the vent site. The hydrothermal crisis was accompanied by a seismic swarm of low intensity (<1.8 M) and triggered gas venting in five other areas around Panarea (Caliro et al., 2004; Caracausi et al., 2005; Esposito et al., 2006). After a few days, the degassing activity decreased, but clearly remained higher than prior to the crises. Immediately after the hydrothermal crisis in early November 2002, the degassing rate in the area of the central islets and reefs increased by two orders of magnitude to about 10⁹ liters/day, but decreased over the following months to a level of 4 x 10⁷ liters/day, when the geothermal reservoir reached a new steady state (Caliro et al., 2004).

A highly unusual, shallow marine sulfide mineralization has been discovered at a water depth of only 80 m in a small, closed depression (about 1.2 km²) located to the north of the central islets and reefs. This depression is bounded to the north by the southern slope of the Basiluzzo rhyolite dome and to the west by two N-S and NNE-SSW trending linear faults that have throws of 10 to 15 m. Low volume gas venting is abundant at the floor of the depression as well as close to the bounding faults (Marani et al., 1997). Box coring in the depression revealed that the sedimentary column consists, from top to bottom, of a 10-20 cm layer of fine silty sand, an 8-10 cm thick layer of pumice breccia, followed by a relatively thick argillite unit that hosts base metal mineralization. Two massive sulfide fragments of decimeter size have been recovered from this stratigraphic position during a research cruise in 1995 (Gamberi et al., 1997; Marani et al., 1997). The massive sulfide fragments consisted mainly of pyrite, sphalerite, galena, and barite. Maximum values of 16.9 wt.% Zn, 4.8 wt.% Pb, 11.6 wt.% Ba, and 40 ppm Ag were observed (Marani et al., 1997; Savelli et al., 1999). The sulfur isotopic ratio of pyrite ($\delta^{34}\text{S} = -4.3 \text{ ‰}$) possibly indicates the contribution of magmatic derived H₂S to the mineralizing hydrothermal system (Hannington, unpubl. data). In addition to the massive sulfide mineralization, disseminated sulfides and sulfates, veinlets of pyrite, and siliceous concretions occur in the strongly altered argillite unit (Marani et al., 1997, 1999; Gamberi et al., 1999). Hydrothermal alteration of the argillite resulted in the formation of montmorillonite, kaolinite, cristobalite, and quartz (Marani et al., 1997). Sediment samples possessed a notable H₂S smell suggesting that sulfide precipitation is currently taking place at this locality (Marani et al., 1997; Savelli et al., 1999). Marani et al. (1999) showed that the mineralized and altered argillite unit grades into massive, strongly cemented gypsum aggregates containing disseminated pyrite crystals at about 2 m below seafloor.

In addition to the sulfide bearing site, low-temperature hydrothermal activity and associated hydrothermal precipitates have been recorded at five sites of the Panarea volcanic

complex (Gamberi et al., 1997; Savelli et al., 1999). Metalliferous deposits occur abundantly at the eastern slope of the NE elongation of the Panarea platform, north of the island of Basiluzzo, at a water depth ranging from 88 to 250 m. Fe-rich deposits in this area form numerous small chimneys consisting of soft mud which contains semi-consolidated crusts. The area is typified by active gas venting. Additional Fe-rich ochreous muds, forming mounds up to 1 m in high, also occur at the western slope of the NE elongation of the Panarea platform in a depression of 250 m water depth. The small locality between the island of Basiluzzo and Panarea is located close to a NNE-SSW oriented, meter-sized scarp. The top and bottom of the scarp is typified by white patches, interpreted to be sulfate precipitates, and gas venting. In addition, Fe-rich muds and crusts were recovered from this site. Active hydrothermal venting is also present at Secca di Pesci, the southeastern sector of the Panarea platform. The hydrothermal zone is located in a bathymetric low between highs rising up to 50 m above the adjacent platform. Vigorous hydrothermal discharges have been detected in the central bathymetric low, which is locally covered by Fe-rich sediments and white sulfate precipitates. Exhalites in the southwestern portion of the Panarea platform are characterized by the presence of Fe-rich crusts and white sulfate aprons (Gamberi et al., 1997; Savelli et al., 1999). Geochemical investigations on the Fe-oxide deposits from the different sites proved that the oxides formed from fluids of hydrothermal volcanogenic nature. The Fe-oxide deposits from Panarea are typified by distinctly low Mn/Fe ratios, high and variable Mo and As contents, and low concentrations of Cu, Co, and Ni (Savelli et al., 1999).

5 Cruise Narrative

S. Petersen

July 4th, 2006 - Tuesday

The participating scientists from Germany and Canada arrived at Messina. The container with the equipment was already unloaded by members of the scientific crew of the previous cruise (P339). The container was returned to Bremen. The participating Italian scientists from Rome tried to obtain permission to board the vessel at Panarea on July 14th.

July 5th, 2006 - Wednesday

The day was mainly used to set up the laboratories and to unpack the equipment. The ROV Cherokee and the winch were configured on deck and the first system checks were run.

July 6th, 2006 - Thursday

R/V Poseidon left port at ca. 09:00 local time and headed for Palinuro Seamount. The weather was fine and the sea was very calm.

Following arrival at Palinuro Seamount at 20:15 local time, a CTD-cast (721CTD) was conducted to generate a sound-velocity profile. This profile was required for calibration of the SEABEAM system. Bathymetric mapping of the area commenced at 24:00 local time (722SBM).

July 7th, 2006 - Friday

The ROV was deployed (723ROV) at 09:00 local time to conduct a seafloor survey at the eastern summit of the caldera at Palinuro Seamount. The dive aimed to constrain the distribution of hydrothermal precipitates in an area that was previously shown to host massive sulfide mineralization. Following deployment, a communication error between the ROV and the control room on board was experienced. The dive was aborted before reaching a water depth of 300 m.

During ongoing repair and onboard testing of the ROV, a dredge (724DR) was towed along a N-S transect across the eastern summit of the caldera at Palinuro. The dredge recovered a half-full load of pelagic sediment containing one large hydrothermal Fe-Mn-oxide crust. The sample was ca. 4 kg and contained numerous shell fragments that were incrustated by Mn-oxide indicating past hydrothermal activity. In addition, a number of Fe-Mn-oxide pebbles were recovered including one fragment of a chimney-like structure. Two subsequent dredges (725DR and 726DR) were towed over the seafloor on parallel tracks, but returned empty.

A fourth dredge was targeted further to the east (from 39°32.6'N / 14°42.55'E to 39°32.2'N / 14°42.6'E), but dredging was not commenced due to an upcoming thunderstorm. Due to unfavorable weather conditions, the scientific program was interrupted for several hours.

At 19:00 local time, a bathymetric survey (727SBM) was commenced. Mapping over Palinuro Seamount was conducted all night.

July 8th, 2006 - Saturday

At 09:00 local time, the next ROV operation (728ROV) was started, but had to be canceled due to a power failure in the system when the ROV reached a water depth of 350 m.

Four dredges (729DR-732DR) were towed over several targets at the caldera at Palinuro Seamount. The first dredge (729DR) yielded no recovery. The subsequent station (730DR) was successful and yielded half a load of pelagic sediments containing several dark-gray pieces of botryoidal massive sulfides and fragments of Fe-Mn-oxides. The following two dredges (731DR and 732DR) contained abundant hemipelagic, commonly calcareous mud and Fe-Mn-oxides.

At 18:00 local time, a mapping survey (733SBM) at Palinuro Seamount was commenced and continued over night.

July 9th, 2006 - Sunday

Due to power failure, the first ROV operation (734ROV) of the day had to be interrupted. Following this unsuccessful dive attempt, two further dredges were towed to sample the seafloor at Palinuro Seamount. The first dredge (735DR) returned empty and with a broken weak-link. The second dredge (736DR) recovered laminated sandstone fragments containing abundant black veins and discolorations, presumably caused by the presence of finely dispersed sulfides or sulfates.

After continuous testing of the ROV, the pilots suggested to undertake another dive attempt. Dive 737ROV was commenced at 13:30 local time, but had to be cancelled after a few minutes because of the persisting occurrence of a power failure at a water depth of ca. 300 m. The result was very discouraging and more exhausting hours of testing and repair for the two pilots had begun.

At 14:00 local time, the third dredge (738DR) of the day was towed over Palinuro Seamount and yielded calcareous mudstone, Mn-oxide coated green clay cobbles, Mn-oxide crusts including one chimney fragment, corals, and clam shells. The dredging was followed by a multibeam survey (739SBM) at Palinuro Seamount, which commenced at 18:45 local time and continued all night.

July 10th, 2006 - Monday

At 10:00 local time, the next ROV dive (740ROV) was attempted and reached the seafloor in a heavily sedimented area. However, the vehicle appeared to be too heavy and the thruster keeping the ROV afloat over the seafloor disturbed the sediment to a degree that hampered seafloor observations. The dive was stopped to bring the vehicle on board. Once on deck, additional floats were mounted on the ROV.

After installation of the floats and another system check, the ROV (741ROV) was launched again at 12:50 local time. This first successful dive of the cruise lasted over 5 hours. The seafloor observations revealed that the eastern summit of the caldera at Palinuro Seamount is covered by a thick layer of unconsolidated sediment. Rare outcrops of Mn-stained corals as well as Fe-Mn-oxide crusts and chimneys protruding the sediment were discovered. During the night, the mapping survey (742SBM) was continued.

July 11th, 2006 - Tuesday

The day started with another very successful ROV dive (743ROV) at Palinuro Seamount. An area of diffuse low-temperature venting was discovered hosting vestimentiferan tube worm colonies, previously unknown to occur in the Tyrrhenian Sea.

Following a short transit to Marsili Seamount in the late evening, a CTD cast (744CTD) was conducted at 20:30 local time at a water depth of ca. 2400 m. A sound velocity profile was recorded, which was required to calibrate the SEABEAM system used for bathymetric mapping.

At 23:15 local time, a first multibeam survey at Marsili Seamount was commenced (745SBM) to acquire bathymetric data along three parallel lines over night, covering parts of the volcanic edifice.

July 12th, 2006 - Wednesday

At 8:45 local time, the ROV was launched (746ROV) at Marsili Seamount to conduct detailed mapping of a previously discovered field of low-temperature hydrothermal activity. Extensive topography was encountered with abundant outcrops of lava and extensive talus fields. The lava outcrops were not covered by pelagic sediments. The hydrothermal vent field consisted of hundreds of small chimney-like structures that mainly consisted of Fe-Mn-oxides. Diffuse low-temperature hydrothermal fluid flow was suggested by the presence of shimmering water and the abundance of bacterial mats covering orifices at the chimney-like structures.

Following the ROV dive, the bathymetric mapping (747SBM) of the northern part of Marsili Seamount was continued from 17:50 to 21:00 local time. Subsequently, the ship returned to Palinuro Seamount to allow continuation of the ROV operation at this volcanic edifice in the morning. During the transit, a multibeam survey (748SBM) was conducted at Palinuro.

July 13th, 2006 - Thursday

At 9:00 local time, the next ROV dive (749ROV) at Palinuro Seamount was performed. The dive focused on the most westerly part of the volcanic edifice, an area that has not been previously surveyed in detail. The southwestern summit of the caldera showed abundant Fe-Mn-oxide crusts and chimney-like structures containing green (nontronitic?) material when broken up with the ROV manipulator. Some of the chimneys were tipped by bacterial mats, possibly suggesting the presence of diffuse hydrothermal fluid flow.

Following completion of the seafloor survey at the southwestern summit, the ROV was heaved to a water depth of 450 m. The ship was then moved to a second location further to the north and the ROV dive was continued at 11:30 local time at the western summit of the caldera. Initially, abundant Fe-Mn-oxides were observed, whereas only sediments with rare outcrops of volcanic rocks were encountered during the remaining part of the dive.

Bathymetric surveying (750SBM) at Palinuro was conducted between 18:00 and 24:00 local time. Mapping was followed by the transit to Panarea Island.

July 14th, 2006 - Friday

After arrival in the working area near Panarea Island, a sound velocity profile was acquired (751CTD).

At 10:00 local time, a first ROV dive (752ROV) was conducted to map a small channel-like depression to the north of the islet of Lisca Bianca, where previous research established the occurrence of sulfides at a water depth of ca. 80 m. Within this channel, several distinctly circular depressions were observed that appear to represent hydrothermal explosion craters. Active degassing is widespread at the seafloor in the survey area.

Bathymetric mapping (753SBM) in the vicinity of Panarea commenced at 17:00 local time to complement the data provided by Dr. Marco Anzidai from INGV in Rome. However, due

to illegal fishing activities in the immediate surroundings of the vessel, the survey was stopped at 23:00 local time.

July 15th, 2006 - Saturday

At 9:00 local time, a second ROV dive (754ROV) was performed at Panarea, focusing on an area to the northwest of Lisca Bianca. This area is typified by the intersection of two major faults having throws of several meters. Several areas of active degassing were encountered. In addition, a small field of Fe-oxide chimneys was discovered.

At 18:00 local time, additional bathymetric mapping (755SBM) was conducted. However, illegal fishing again caused an interruption of the survey at ca. 20:00. The vessel was stationed near Stromboli over night.

July 16th, 2006 - Sunday

After returning to the working area off Panarea Island, the last dive (756ROV) was commenced at 9:00 local time. The dive area included several craters that presumably formed by hydrothermal explosions and/or collapse following intense degassing. A previously unknown dome of flow-foliated rhyolite was identified and mapped in detail.

Between 18:00 and 21:00 local time, the area between Panarea and Basiluzzo Islands was surveyed (757SBM). At 02:00 local time, the ship departed from Panarea and sailed towards Messina.

July 17th, 2006 - Sunday

The ship arrived at the port of Messina at 09:00 local time. Most of the day was dedicated to packing and unloading of the scientific equipment. The scientific crew disembarked the vessel.

6 Multibeam Bathymetry

N. Augustin and B. Melchert

Multibeam mapping was carried out with a mobile SEABEAM 1050 system provided by ELAC Nautik GmbH. The system consisting of two transmitter/receiver units, a motion sensor, and a CTD was installed in the moonpool of R/V Poseidon. A Garmin mobile GPS receiver was used to obtain geositional data. The system was set at 50 kHz, a 120° cover sector, and 108 beams per ping, allowing a swath width of about 3.5 times water depth. Data acquisition was conducted with the software Hydrostar 3.4. The program HDPedit was used for provisional data editing, whereas data post-processing was conducted using HDPpost. All programs were provided by ELAC Nautik GmbH. Final gridding and bathymetric map production was realized using GMT.

During the first survey (722SBM), severe problems with the setup of the mobile system were noted (Fig. 6-1). All swath data showed a discontinuity at the centre of the swath, presumably due to a wrong calibration. In the generated bathymetric maps, this resulted in an artificial depression and a doubling effect in the topography. The influence of the erroneous calibration is most pronounced in areas characterized by steep slopes, but it also occurs in flat terrain.

Based on our observations, it must be assumed that bathymetric data acquired during all cruises following installation of the mobile system on R/V Poseidon in Heraklion require post-processing to correct for the erroneous calibration. Selected files from previous cruises were checked and the same artificial effects were encountered in the generated bathymetric maps. Using the original XSE-files, recorded with the Hydrostar software, post-processing of the data at IFM-GEOMAR may allow production of more accurate maps.

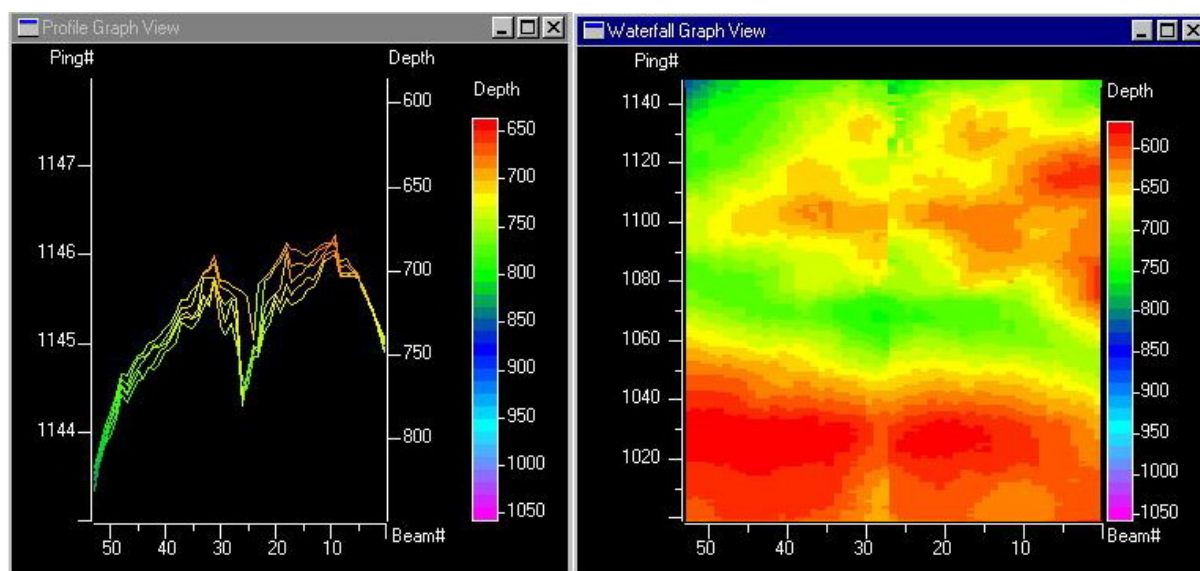


Fig. 6-1: Screenshot of the Hydrostar software during the first bathymetric survey (722SBM) illustrating problems in the calibration of the mobile system. The images show an artificial discontinuity at the centre of the swath (left) and a doubling effect in the topography (right).

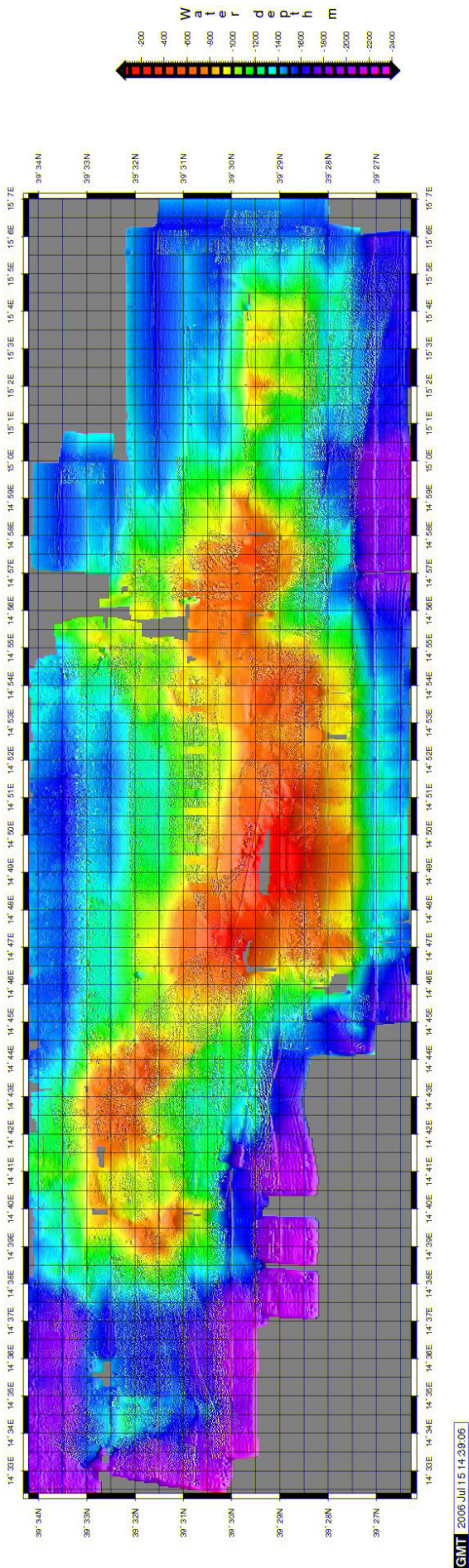


Fig. 6-2: Preliminary bathymetric map of Palinuro Seamount.

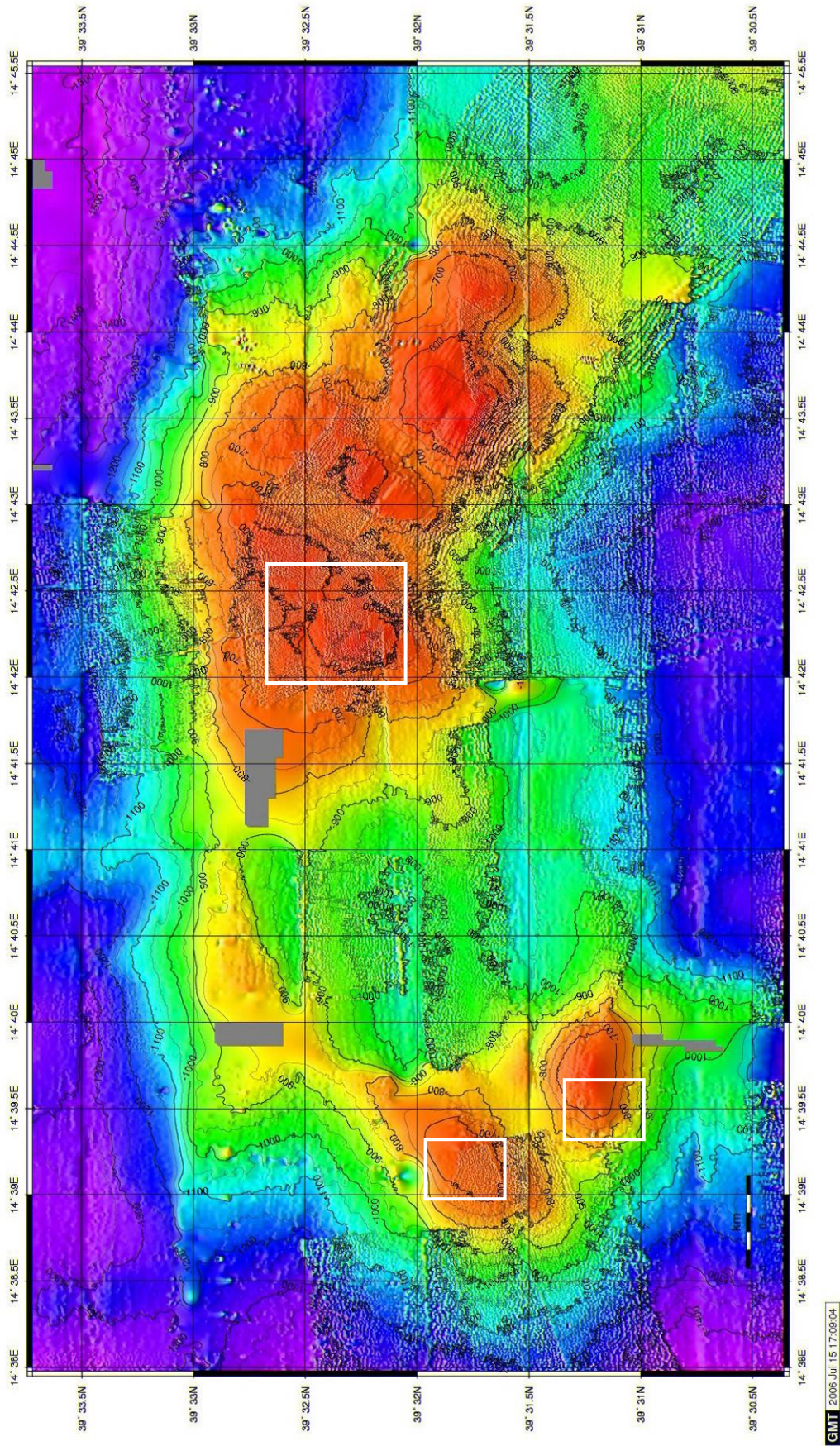


Fig. 6-3: Preliminary bathymetric map of the western portion of Palinuro Seamount. The ROV dive areas are indicated by the white boxes.

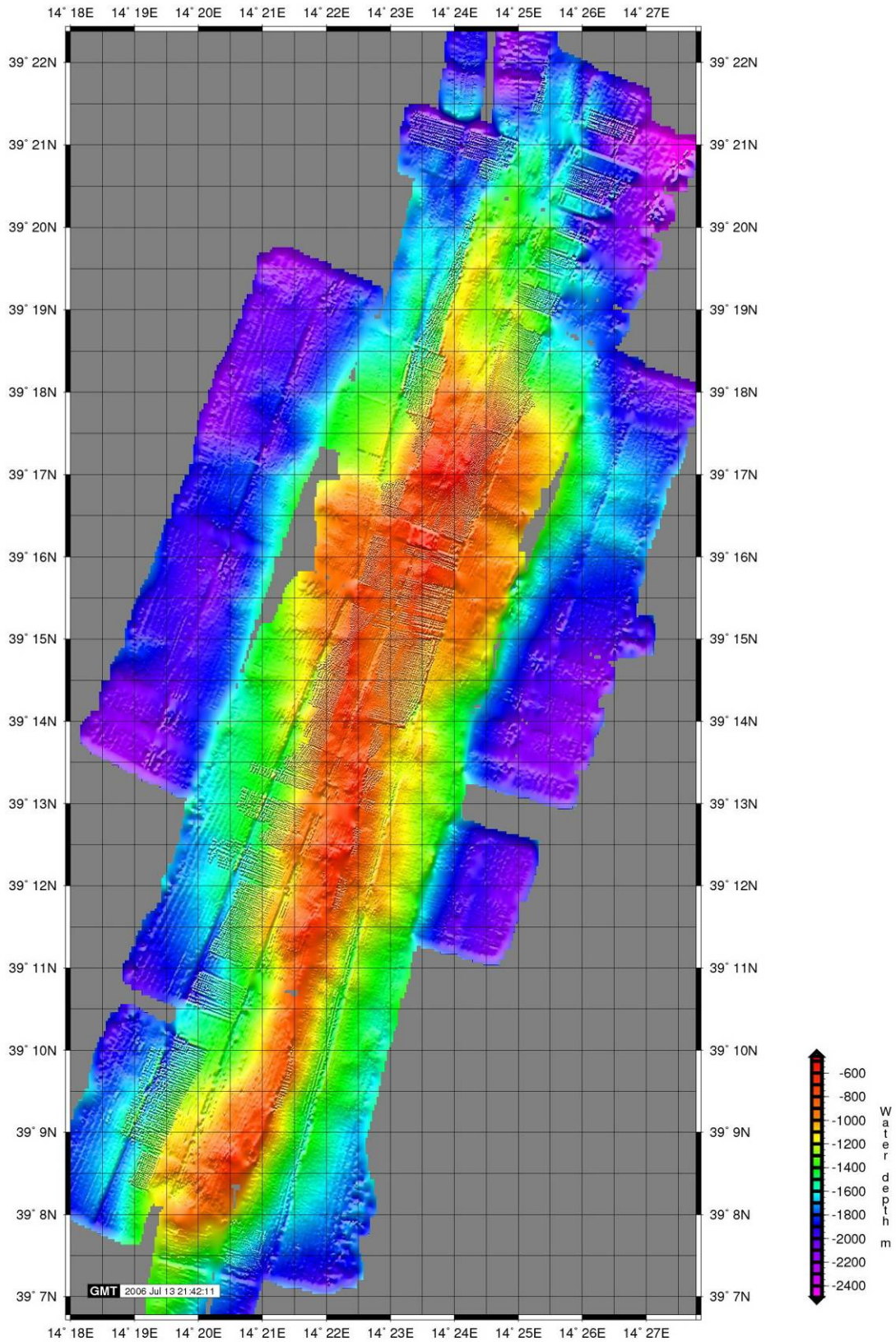


Fig. 6-4: Preliminary bathymetric map of Marsili Seamount.

During the cruise, numerous crashes of the multibeam system occurred that could only be overcome by restarting the mobile unit. These system failures were most likely related to overheating of the power supply during pinging with high power and occurred surprisingly only during data recording. No system failures occurred while mapping off Panarea Island, presumably because of the low power required for the pinging at low water depths.

In total, 12 multibeam surveys with a total profile length of ca. 530 nautical miles were conducted during the cruise at water depths ranging from 100 to 3,000 m. Figures 6-2 to 6-5 show preliminary maps produced during cruise P340. Mapping was mainly carried out to identify bathymetric highs at the Palinuro and Marsili volcanic edifices, which were likely to host sulfide mineralization. Bathymetric surveying off Panarea Island aimed to provide complementary information to the bathymetry previously recorded by Dr. Marco Anzidai from INGV in Rome.

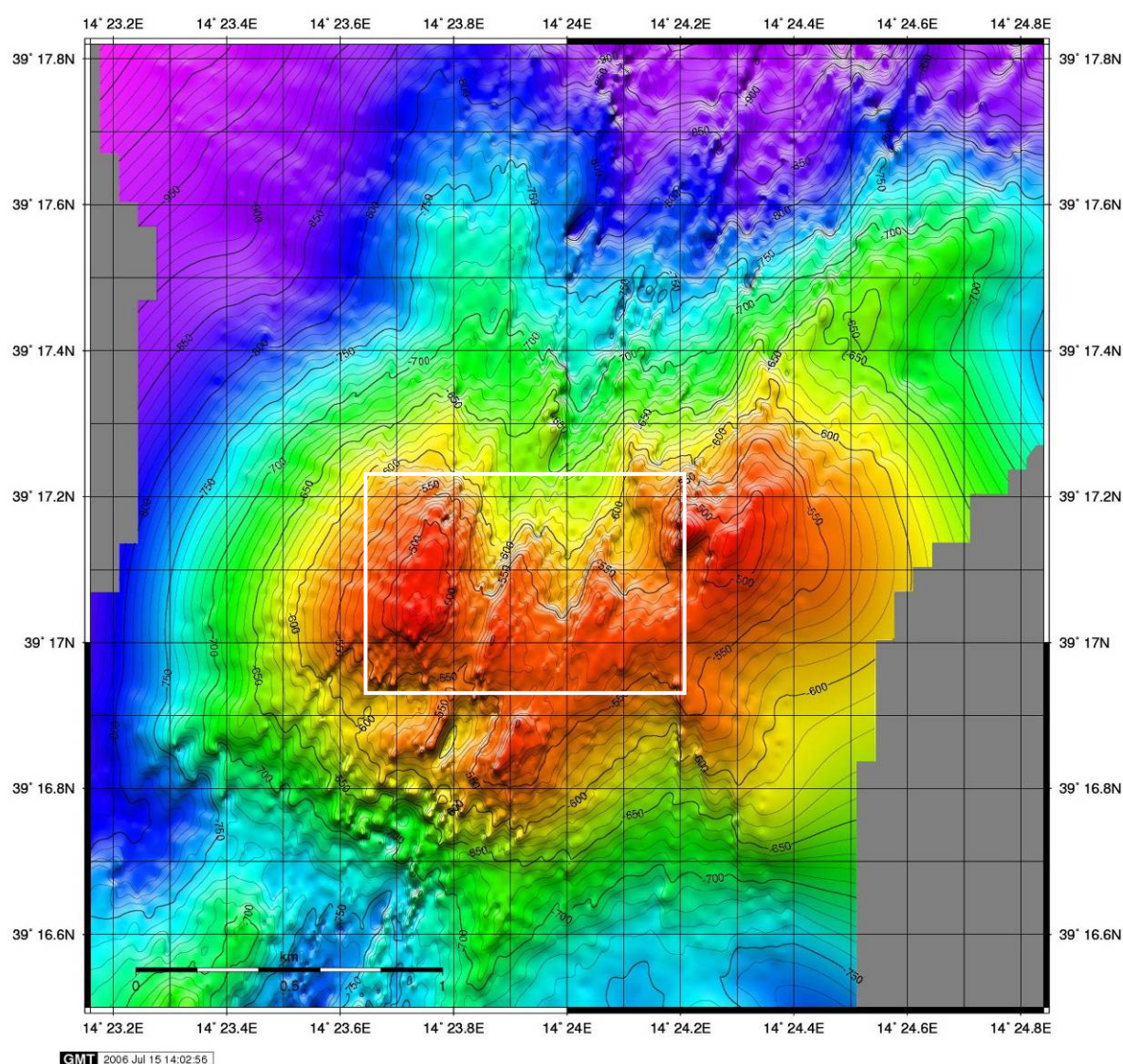


Fig. 6-5: Preliminary bathymetric map of the northern summit of Marsili Seamount. The ROV dive area is indicated by the white box.

6.1 Palinuro Seamount

Mapping at Palinuro Seamount revealed that the western part of the volcanic edifice is characterized by the occurrence of a large subsidence structure, assumed to be a caldera (Figs. 6-2 and 6-3). The previously discovered massive sulfide mineralization is located at a bathymetric height to the east of the caldera (Tufar, 1991). Due to the length of the cable, ROV operation was restricted to depths of less than 800 m and therefore only the three larger summits surrounding the caldera were studied during P340. The caldera floor is located at a water depth of >900 m.

6.2 Marsili Seamount

Bathymetric mapping of Marsili Seamount was conducted along three track lines. The bathymetric characteristics of Marsili Seamount are strikingly similar to mid-ocean ridge spreading centers. Based on the preliminary map, the ROV dive was targeted at the peak occurring at the shallowest water depth (Figs. 6-4 and 6-5).

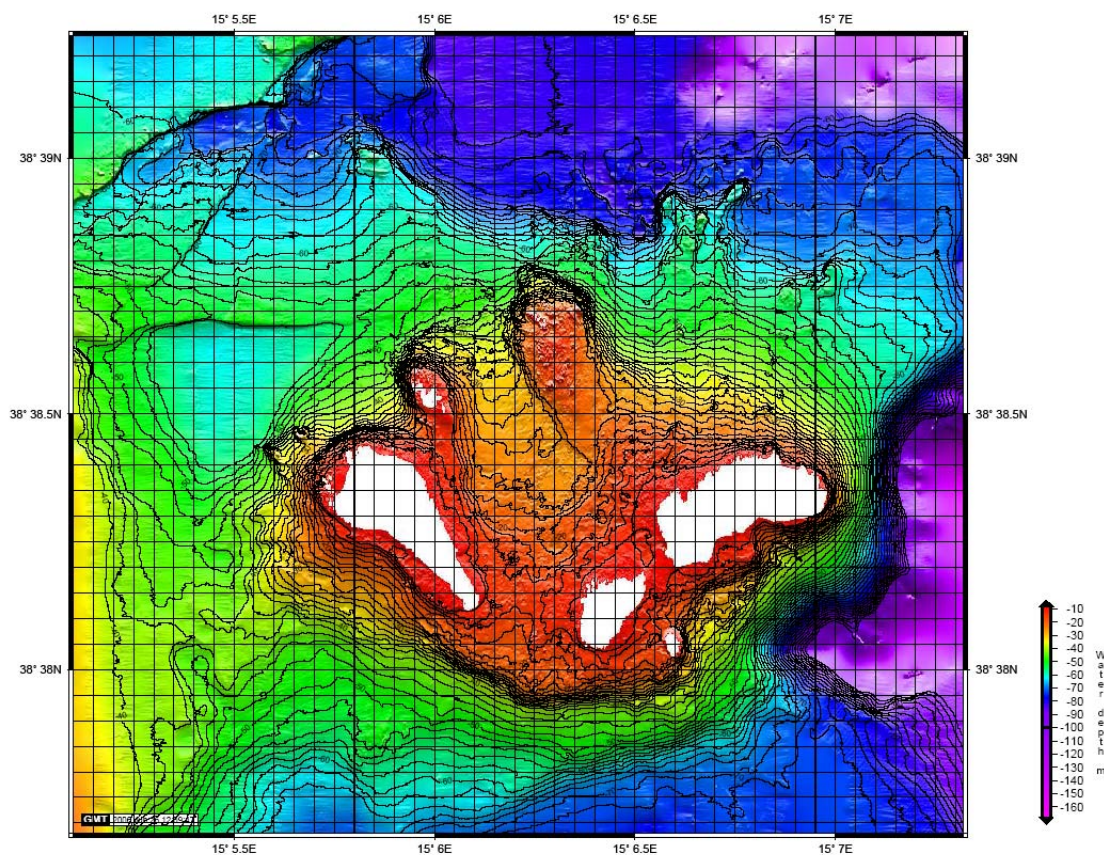


Fig. 6-6: Detailed bathymetry of the area of the central islets off Panarea Island (map and data courtesy of Dr. M. Anzidei).

6.3 Panarea

A high-resolution bathymetric map of the shallow water area (<70 m) surrounding the central islets off Panarea Island was provided by Dr. Marco Anzidei from INGV in Rome prior to the cruise (Fig. 6-6). This map was essential for the planning of the dives. Mapping during P340 was performed to collect information at greater water depths (Fig. 6-7).

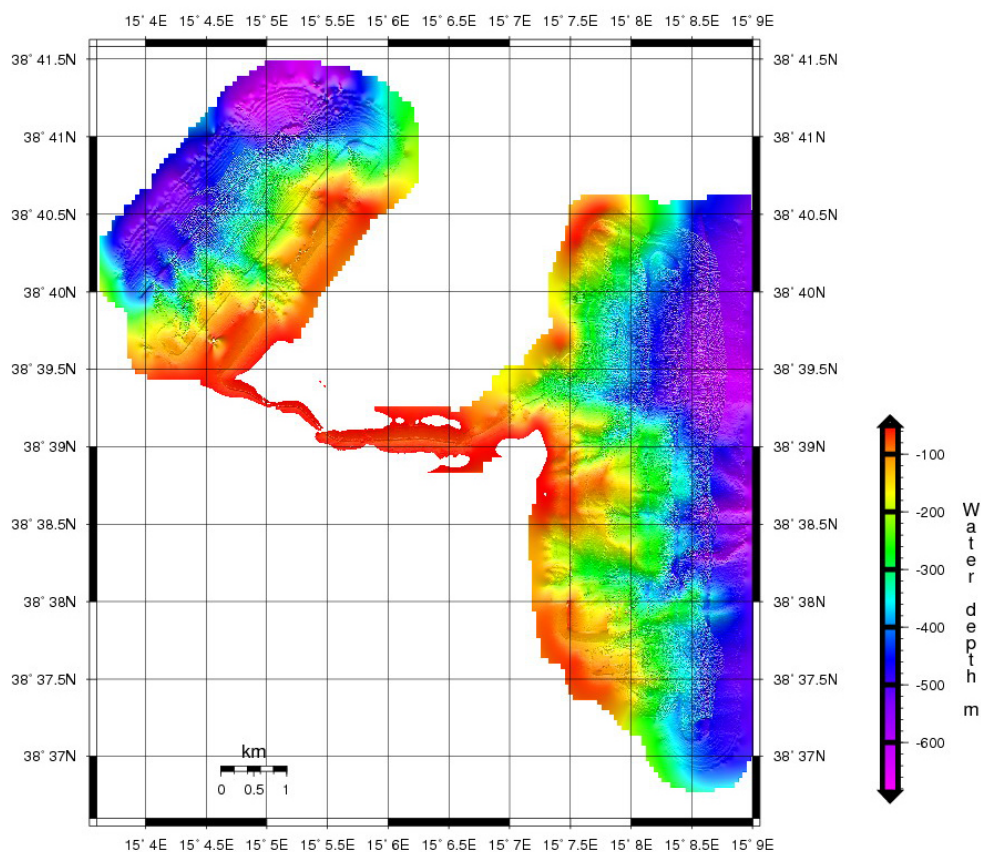


Fig. 6-7: Preliminary bathymetric map of the areas to northwest and east of Lisca Bianca.

7 ROV Operations and Mapping

M. Hannington, T. Monecke, S. Petersen, D. Garbe-Schönberg, G. Giordano, A. Esposito, H. Schulz, and I. Suck

Initially, a total of ten dives was planned. However, technical difficulties hampered the use of the ROV during the first three work days. Following repair, seven successful dives totaling 45 hours of seafloor observation were conducted.

A sub-positioning system was not available during cruise P340. The dive maps were, therefore, constructed using the ship's position and the estimated horizontal deviation of the ROV from the ship. Because mini-filming and high-resolution imaging could not be performed simultaneously, it was decided to conduct the latter recording method during the dives. Headings given for the high-resolution images represent a combination of the ROV heading and the camera pan and, therefore, correspond to the true direction.

7.1 Palinuro Seamount

The first four dives at Palinuro (723ROV, 728ROV, 734ROV, and 737ROV) failed due to an earth fault caused by penetration of water into the main power supply. Although the fifth dive (740ROV) reached bottom, it was rapidly deduced that the ROV was too heavy hampering maneuvering of the vehicle at the seafloor. The dive was canceled. To increase buoyancy, additional floats were mounted on ROV Cherokee. Subsequently, two successful dives (741ROV and 743ROV) were performed at the eastern summit of the caldera (Fig. 7-1). The southwestern and western topographic highs of the caldera were investigated during the next dive (749ROV).

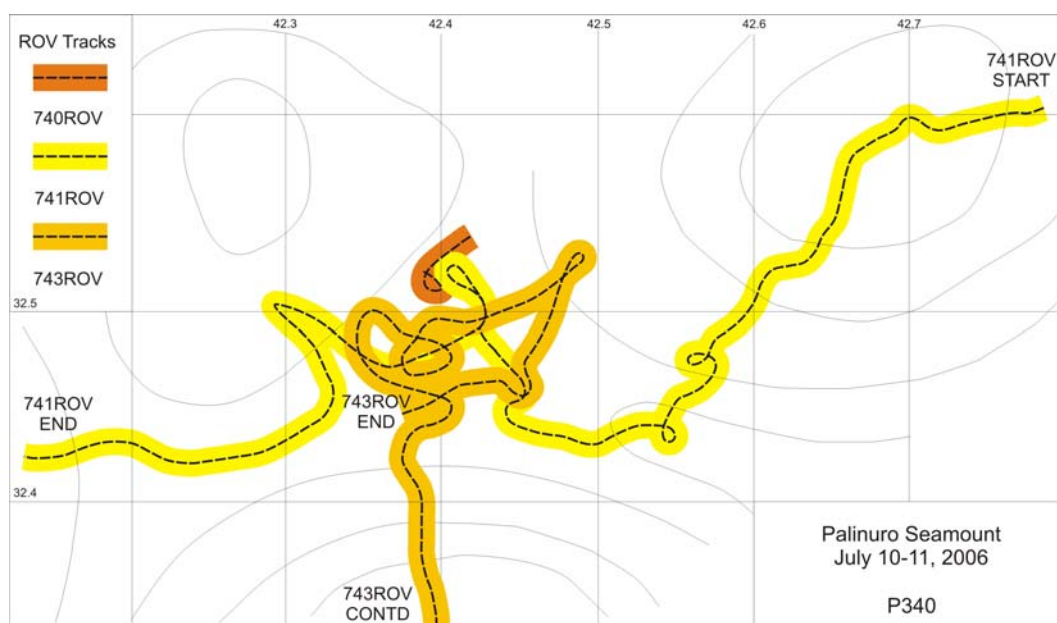


Fig. 7-1: ROV dive tracks at the eastern summit of the caldera of Palinuro Seamount.

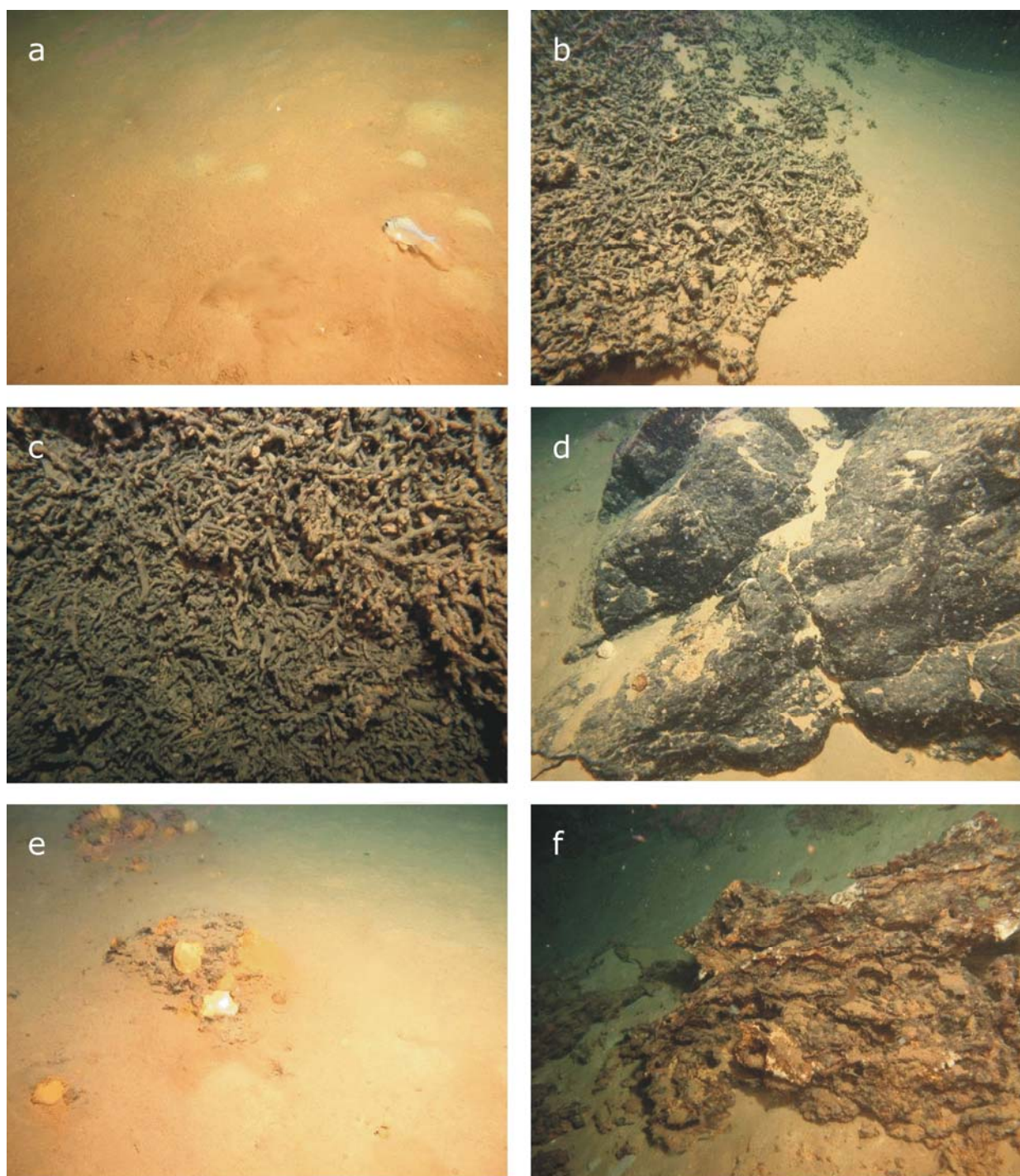


Fig. 7-2: Seafloor images obtained during dive 741ROV at Palinuro Seamount (Date: 10 July 2006). a. Thick sediment cover showing characteristic red discoloration (Depth: 650 m; Heading: 271°; Time: 13:50:46 UTC). b. Outcrops of corals that are coated by Mn-oxides (Depth: 626 m; Heading: 324°; Time: 14:35:56 UTC). c. Close-up of corals coated by Mn-oxides (Depth: 625 m; Heading: 003°; Time: 14:34:57 UTC). d. Outcrop of basaltic lava (Depth: 620 m; Heading: 062°; Time: 14:43:11 UTC). e. Isolated patches of Fe-oxides protruding through pelagic mud. The flocculent, orange caps are interpreted to represent bacterial colonies (Depth: 608 m; Heading: 254°; Time: 15:13:18 UTC). f. Exposure of Fe-oxides (Depth: 638 m; Heading: 218°; Time: 14:05:13 UTC).

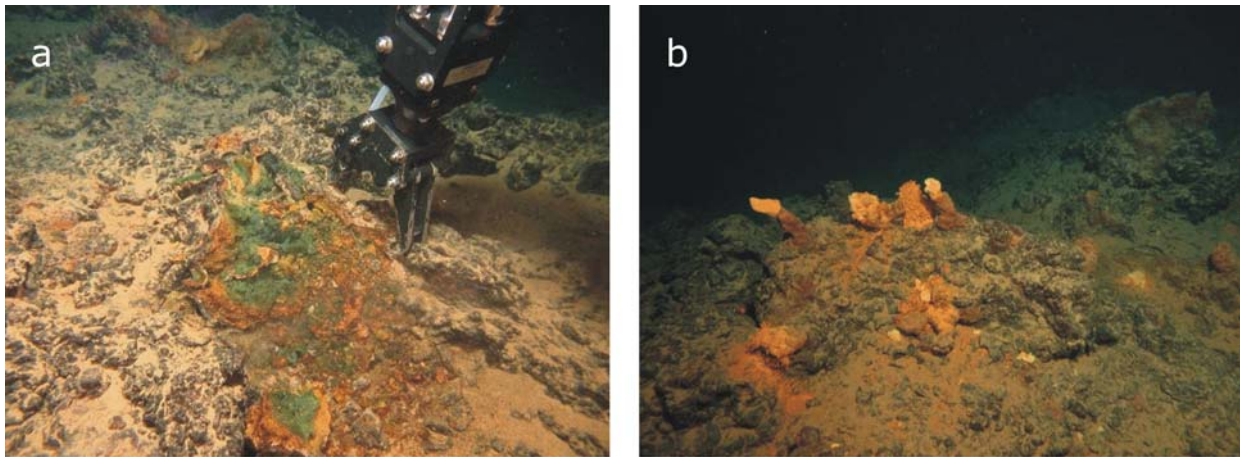


Fig. 7-3: Seafloor images obtained during dive 741ROV at Palinuro Seamount (Date: 10 July 2006). a. Operation of the ROV manipulator reveals that the Mn- and Fe-oxides cover green, possibly nontronitic material (Depth: 595 m; Heading: 265°; Time: 15:23:44 UTC). b. Fe-oxide chimneys. Active fluid venting is indicated by the presence of bacterial colonies at the orifices of the chimneys (Depth: 593 m Heading: 167°; Time: 15:26:29 UTC).

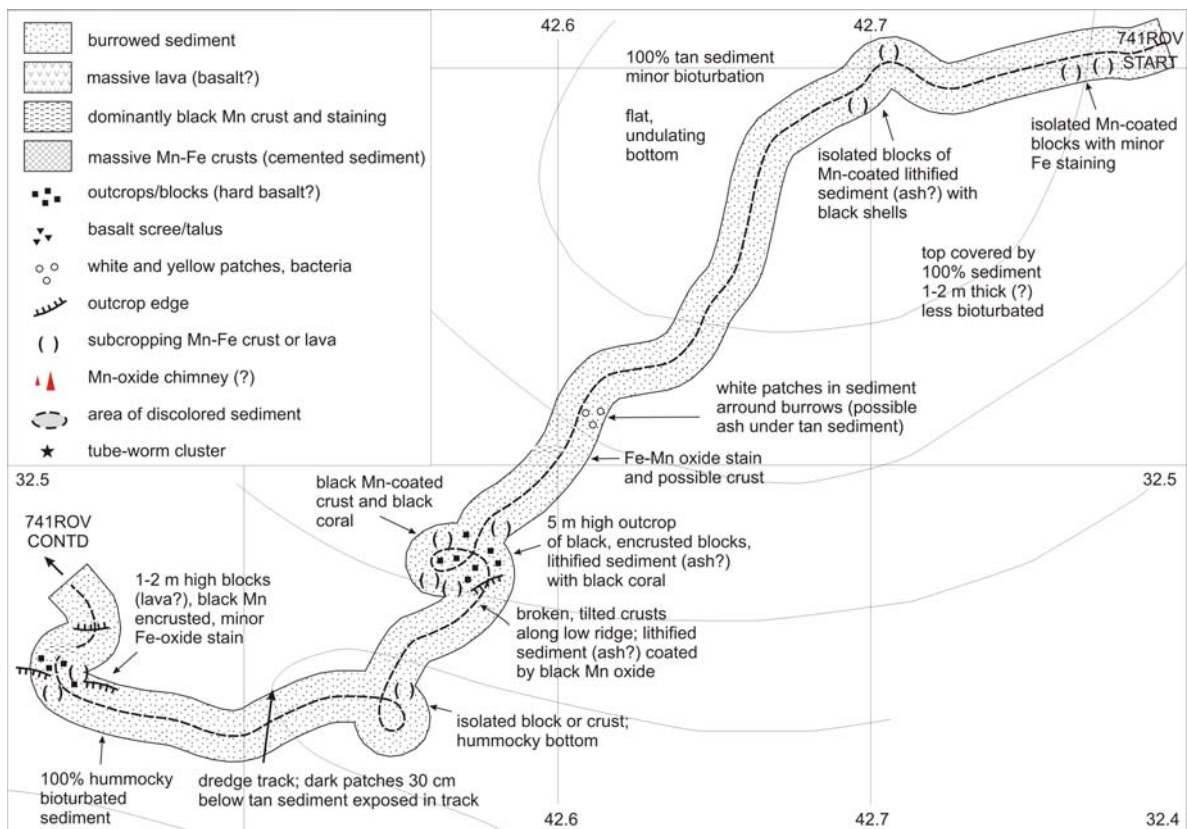


Fig. 7-4: Geological map of the first part of dive 741ROV at Palinuro Seamount.

Dive 741ROV

The eastern summit of the caldera at Palinuro Seamount is typified by three small knolls. Dive 741ROV started at the top of the eastern most knoll and proceeded towards increasing water depth into the area enclosed by the three knolls. Seafloor observations revealed that most of the area is covered by unconsolidated mud. Exposures of lava and Mn-coated corals were only locally observed (Fig. 7-2). Towards the end of the dive, an area characterized by the occurrence of Mn- and Fe-oxides forming chimney-like structures was identified (Fig. 7-3). Based on the seafloor observations, geological summary maps were constructed (Figs. 7-4 and 7-5).

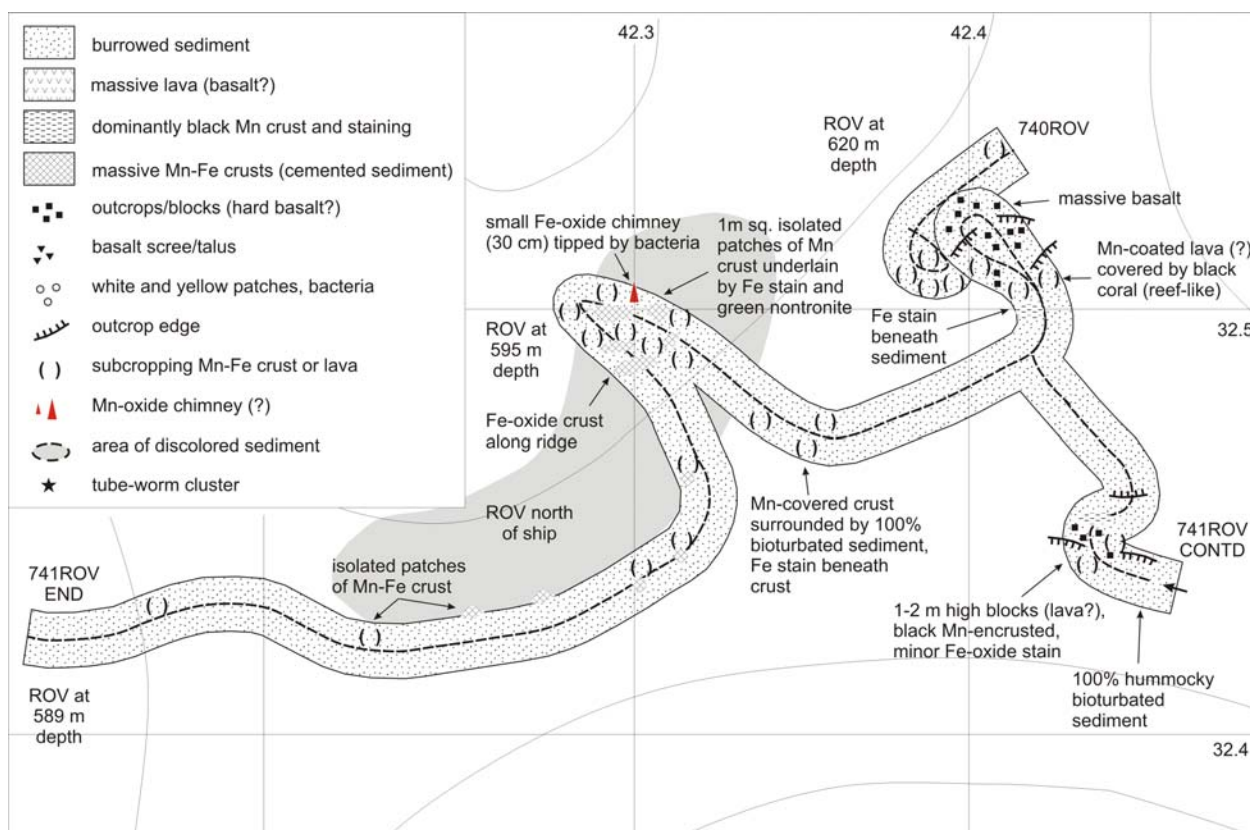


Fig. 7-5: Geological map of the second part of dive 741ROV at Palinuro Seamount.

Dive 743ROV

Dive 743ROV followed dredge track 730DR, during which massive sulfide samples have been recovered. Due to the limited cable length, the dive was commenced at a water depth of only 750 m. The ROV was targeted in an easterly direction towards the depression enclosed by the three adjacent knolls. Abundant Mn-oxide crusts were observed (Fig. 7-6). In the small depression between the knolls, several tube worm colonies occurring on a substrate of altered sediment or hydrothermal precipitates were discovered (Fig. 7-6). The presence of tube worm colonies, diffuse fluid flow, and slight bottom water temperature anomalies (Fig. 7-7) are indicative for active venting at 39°32.43'N/ 14°42.38'E at a water depths of 640 m. Figures 7-8 and 7-9 show geological summary maps for dive 743ROV.

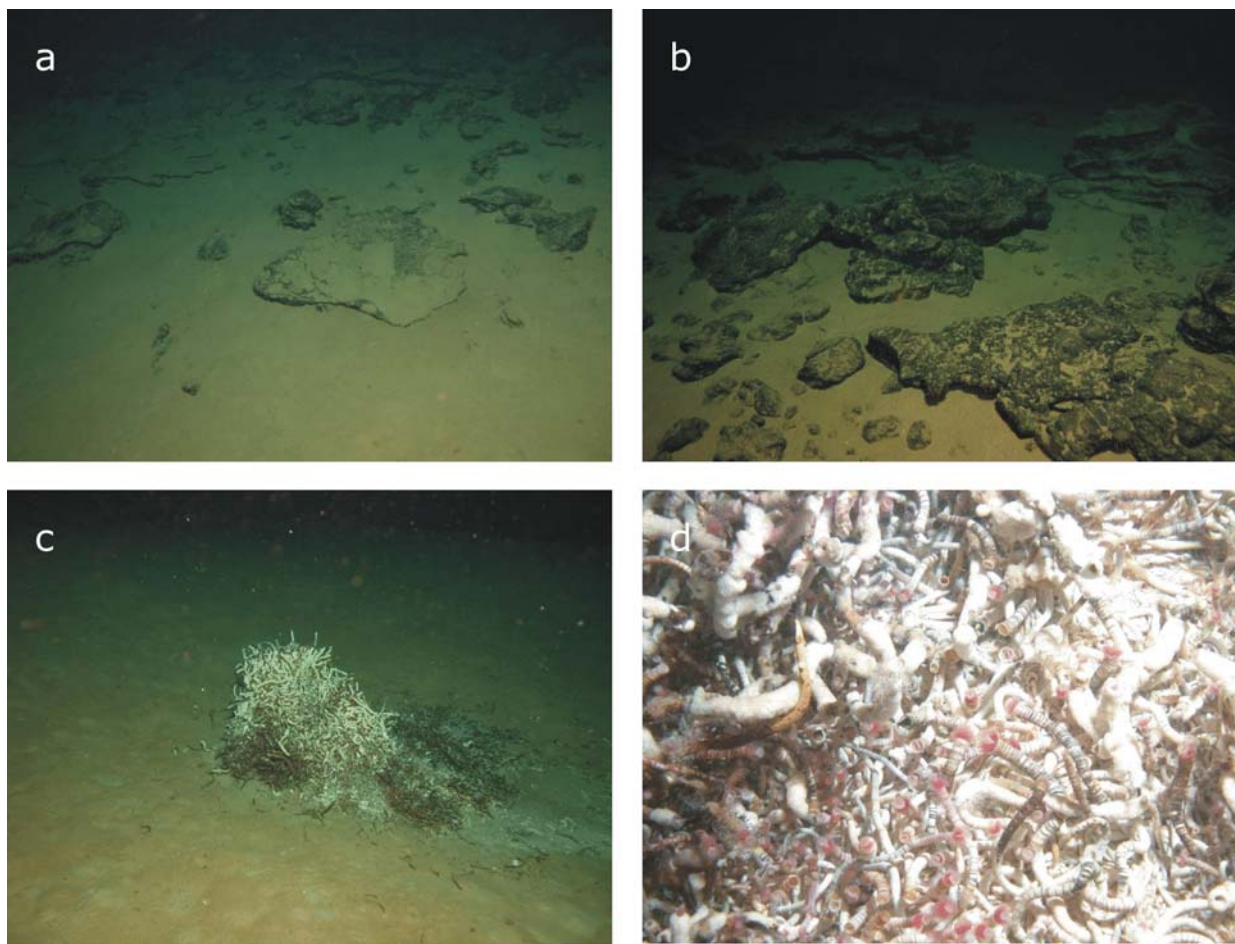


Fig. 7-6: Seafloor images obtained during dive 743ROV at Palinuro Seamount (Date: 11 July 2006). a. Mn-oxide crusts that are partially covered by mud (Depth: 564 m; Heading: 143°; Time: 09:37:52 UTC). b. Mn-oxide crusts (Depth: 563 m; Heading: 120°; Time: 09:38:58 UTC). c. Tube worm colony. Some tubes were recovered with the manipulator (Depth: 641 m; Heading: 101°; Time: 11:27:14 UTC). d. Close-up of living tube worms (Depth: 641 m; Heading: 030°; Time: 12:07:07 UTC).

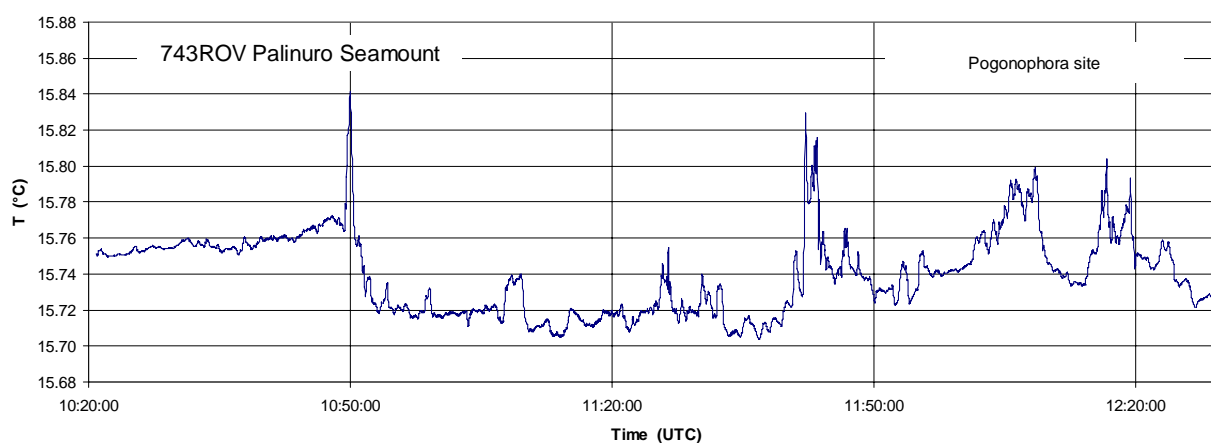


Fig. 7-7: Several temperature anomalies (up to 0.1°C) were recorded during dive 743ROV in an area typified by diffuse fluid flow and the presence of tube worm colonies.

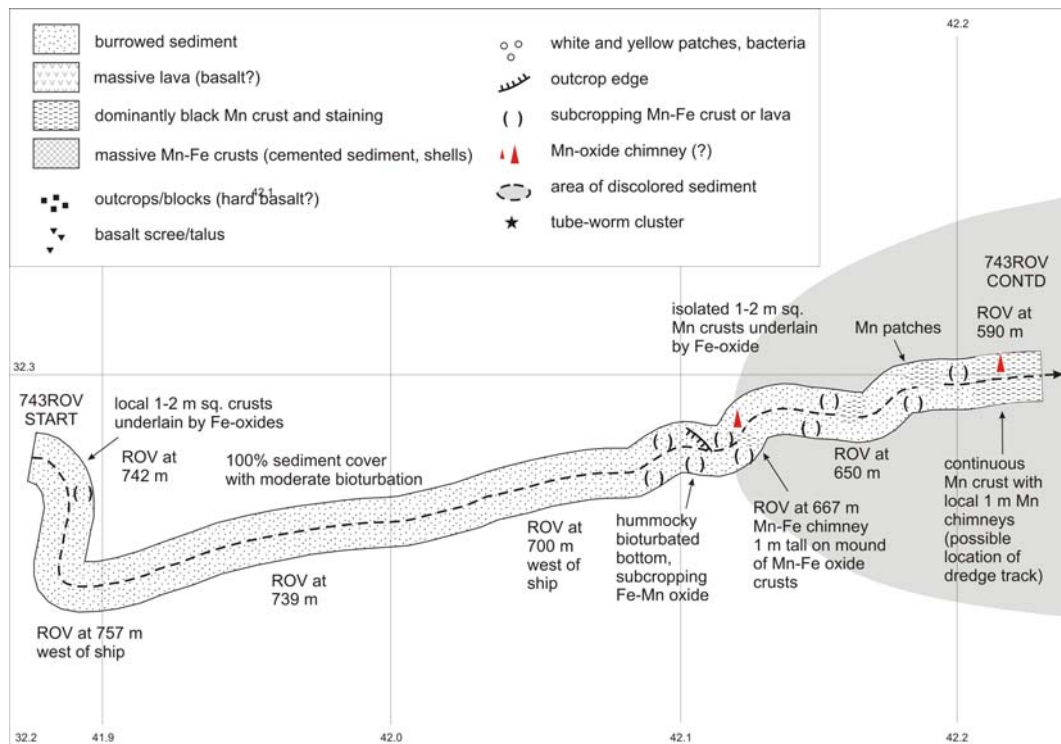


Fig. 7-8: Geological map of the first part of dive 743ROV at Palinuro Seamount.

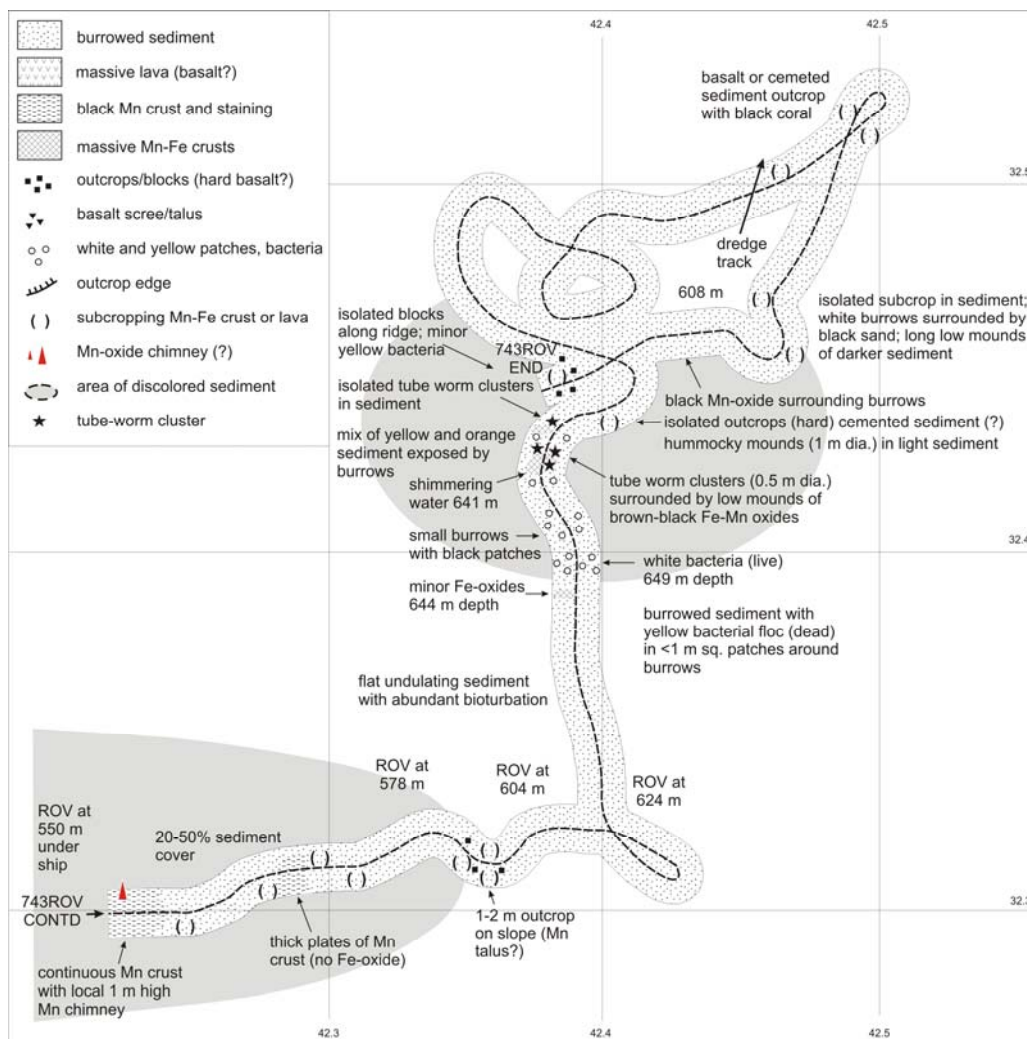


Fig. 7-9: Geological map of the second part of dive 743ROV at Palinuro Seamount.

Dive 749ROV

Dive 749ROV was targeted on the southwestern and western summits of the caldera at Palinuro Seamount (Figs. 7-10 to 7-12). The first part of the dive focused on the southwestern topographic high where abundant Fe-oxides were observed. Numerous Fe-chimneys tipped by bacterial colonies were discovered (Fig. 7-13). During the second part of the dive, the western summit of the caldera was investigated. A thick sediment cover with only limited Fe-oxide occurrences was noted (Fig. 7-14).

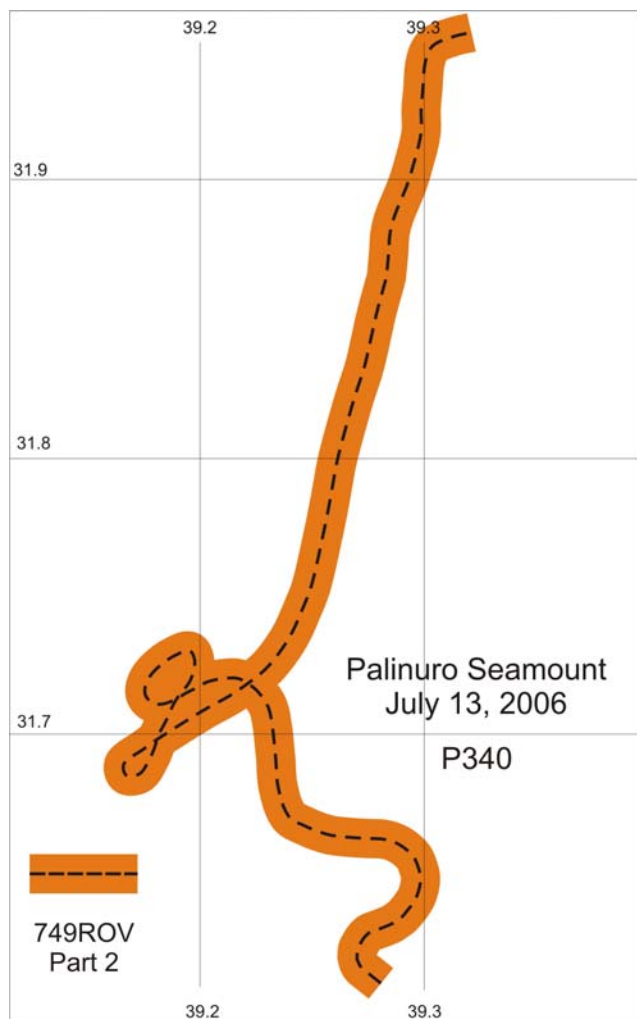
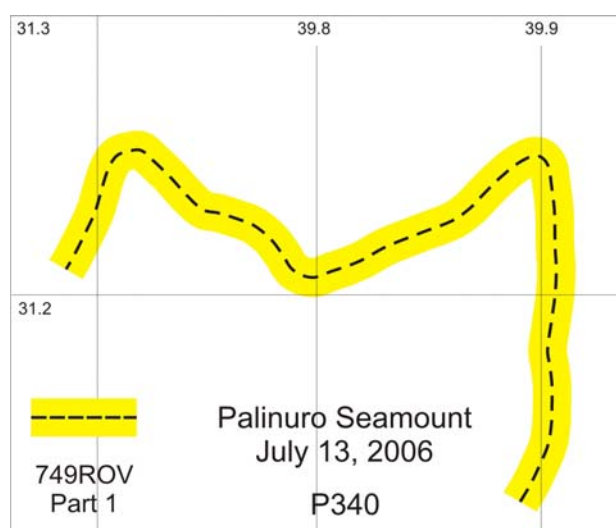


Fig. 7-10: ROV dive tracks at the southwestern and western summits of the caldera at Palinuro.



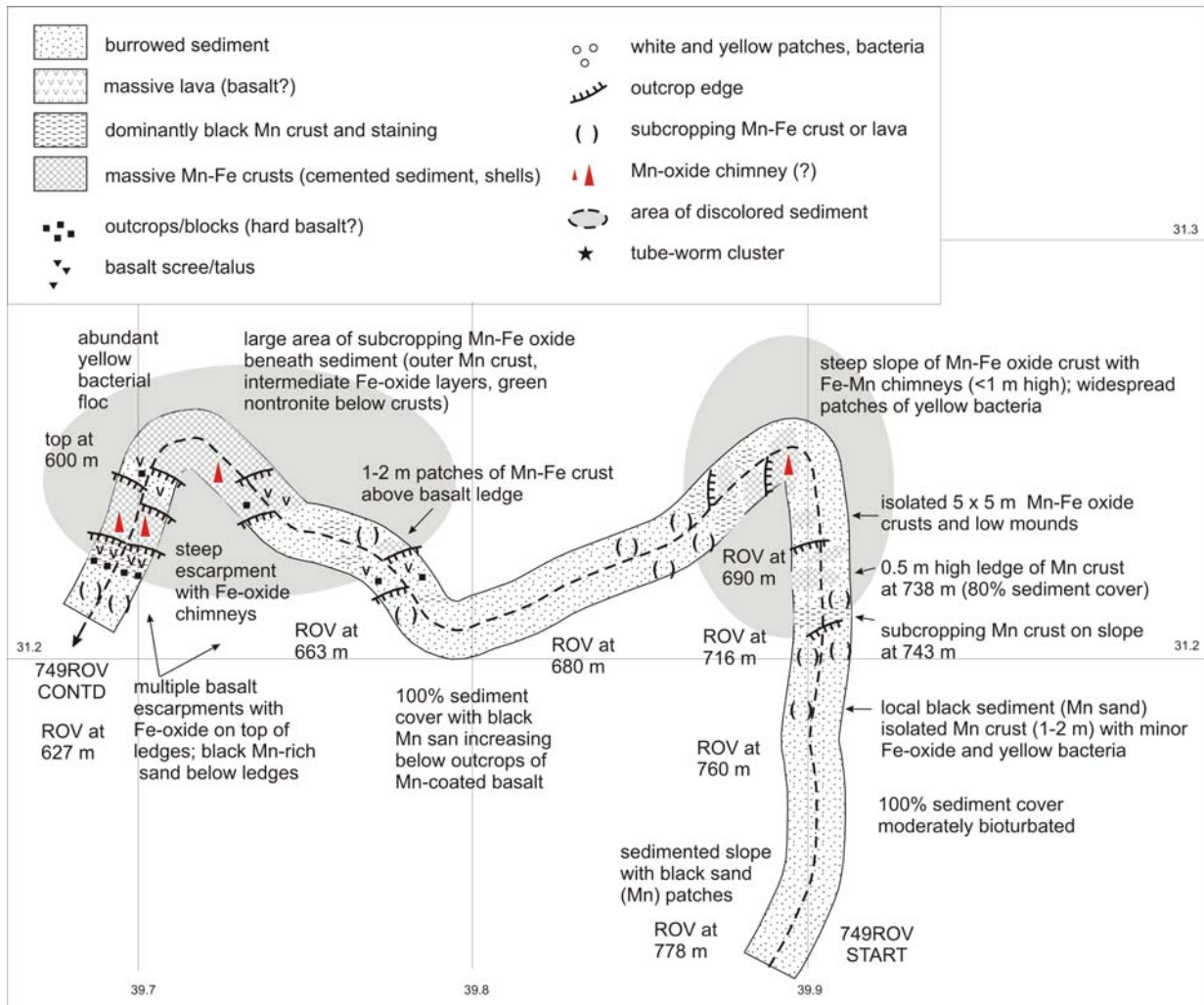


Fig. 7-11: Geological map of the first part of dive 749ROV at Palinuro Seamount.

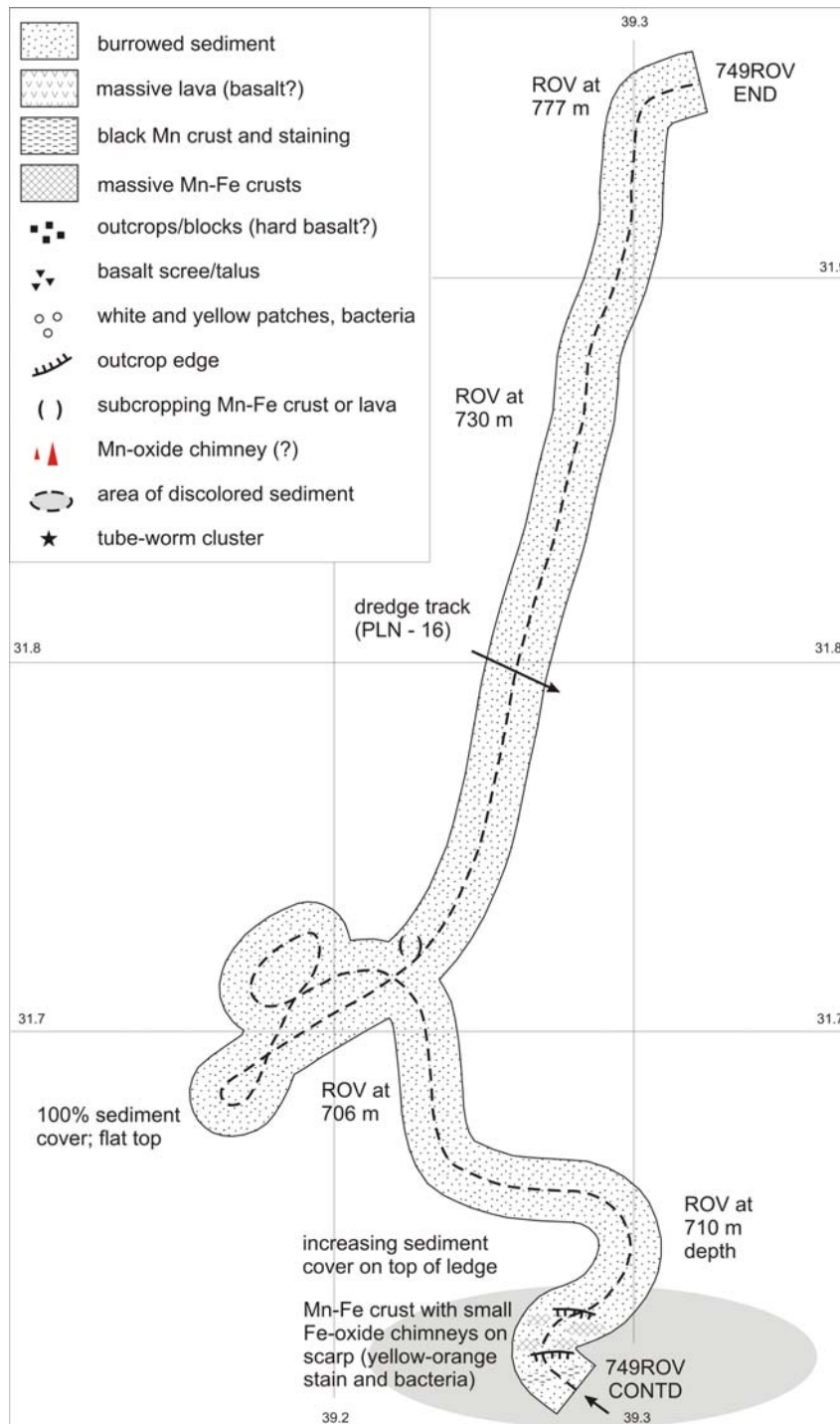


Fig. 7-12: Geological map of the second part of dive 749ROV.

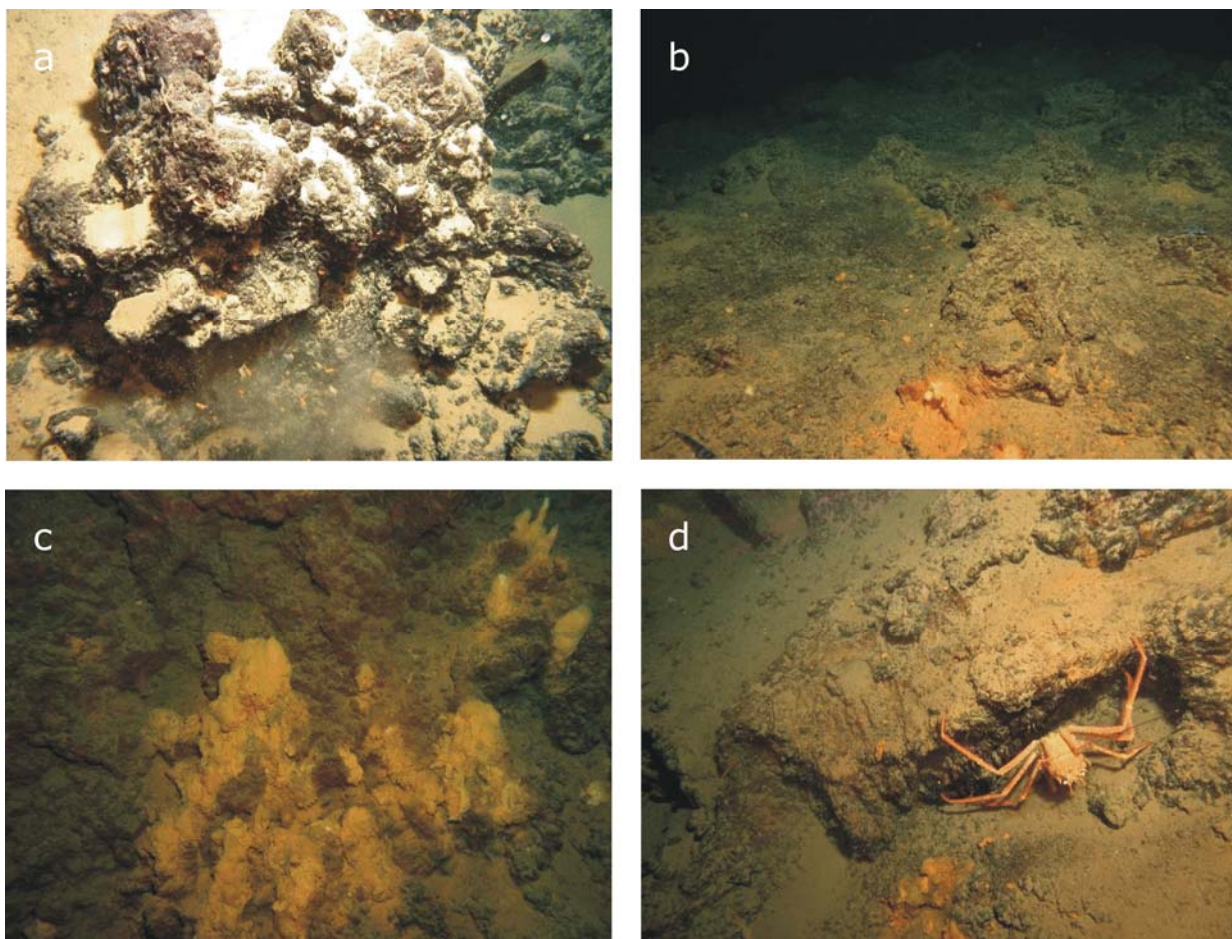


Fig. 7-13: Seafloor images obtained during the first part of dive 749ROV at Palinuro Seamount (Date: 13 July 2006). a. Hydrothermally cemented shells and shell fragments (Depth: 694 m; Heading: 337°; Time: 08:49:48 UTC). b. Mn-Fe-oxides at the summit (Depth: 601 m; Heading: 045°; Time: 09:22:55 UTC). c. Fe-oxide chimneys tipped by bacterial colonies (Depth: 610 m; Heading: 250°; Time: 09:48:04 UTC). d. Spider crab at an exposure of Fe-oxides near the summit (Depth: 623 m; Heading: 286°; Time: 09:58:49 UTC).

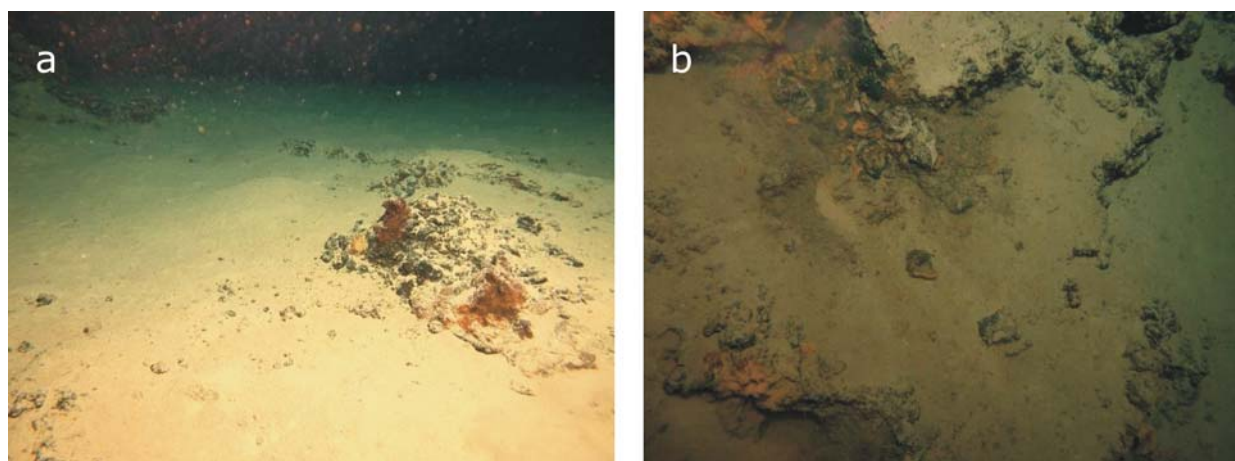


Fig. 7-14: Seafloor images obtained during the second portion of dive 749ROV at Palinuro Seamount (Date: 13 July 2006). a. Thick sediment cover with scattered Fe-oxide crusts (Depth: 716 m; Heading: 333°; Time: 12:00:47 UTC). b. Fe-oxide occurrence at the flank of the summit (Depth: 725 m; Heading: 050°; Time: 11:52:12 UTC).

7.2 Marsili Seamount

The central summit of Marsili Seamount was investigated during dive 746ROV (Fig. 7-15) to locate and map a previously discovered area of low-temperature hydrothermal precipitates (Uchupi and Ballard, 1989). The dive revealed that the geology at Marsili Seamount differed substantially from that observed at Palinuro Seamount. The seafloor at Marsili Seamount is characterized by abundant basalt exposures, large talus fields, and limited sediment cover. A large area with Fe-oxide chimneys and crusts was examined in detail during the second part of the dive (Figs. 7-16 and 7-17).

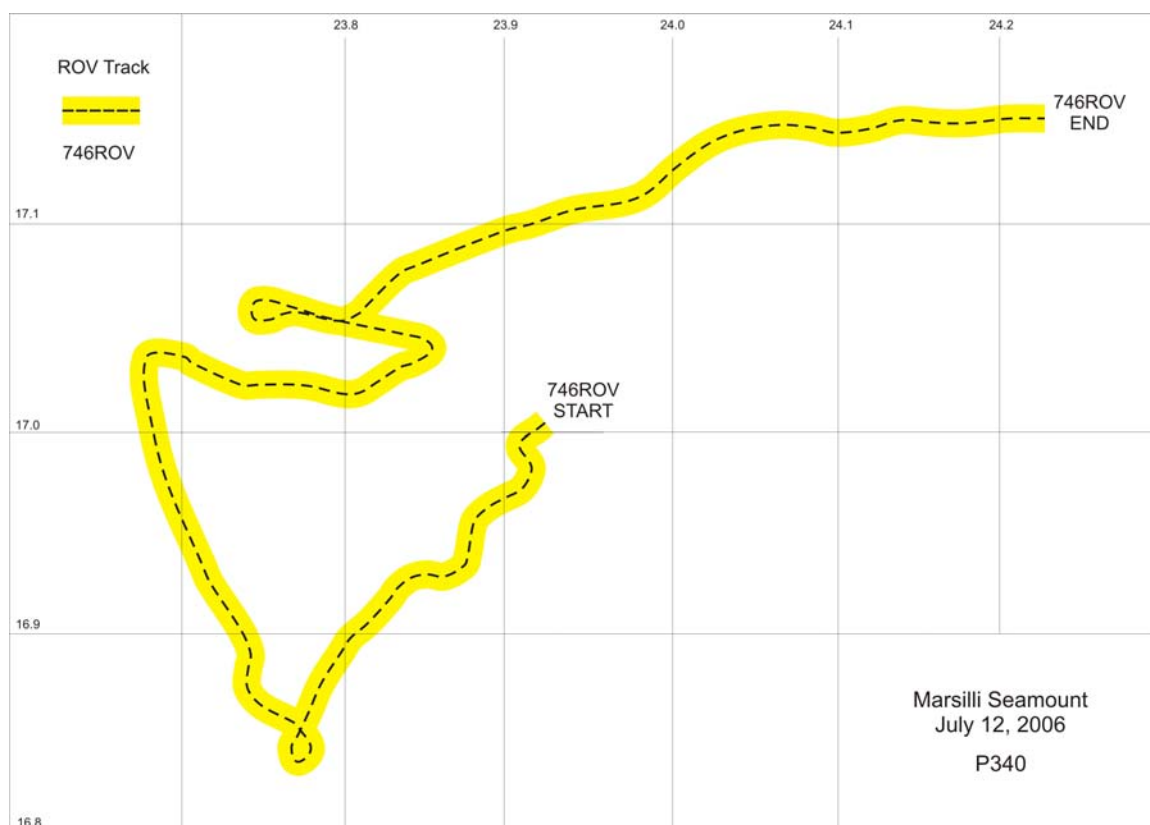


Fig. 7-15: ROV dive track at Marsili Seamount.

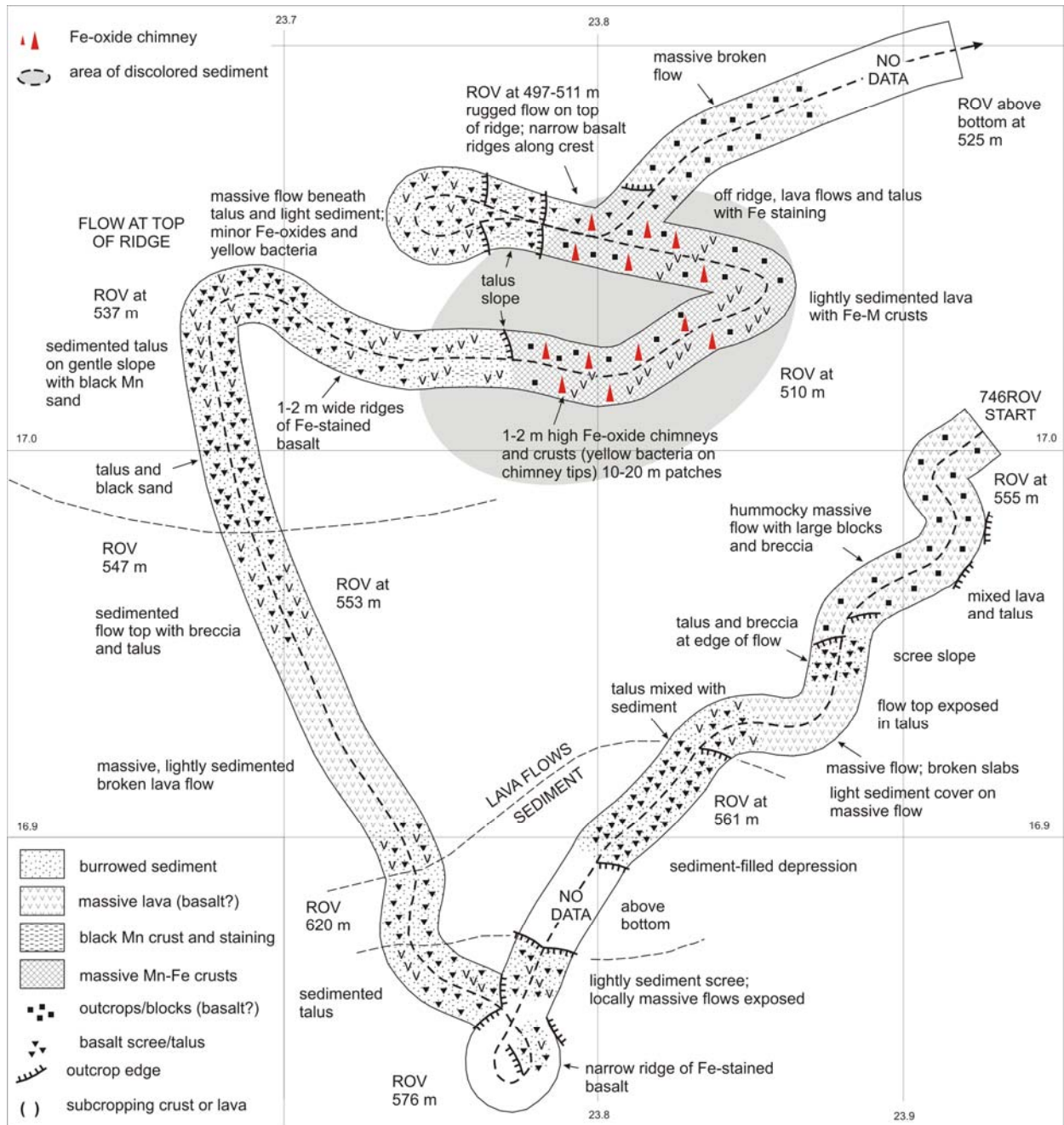


Fig. 7-16: Geological map of dive 746ROV at Marsili Seamount.

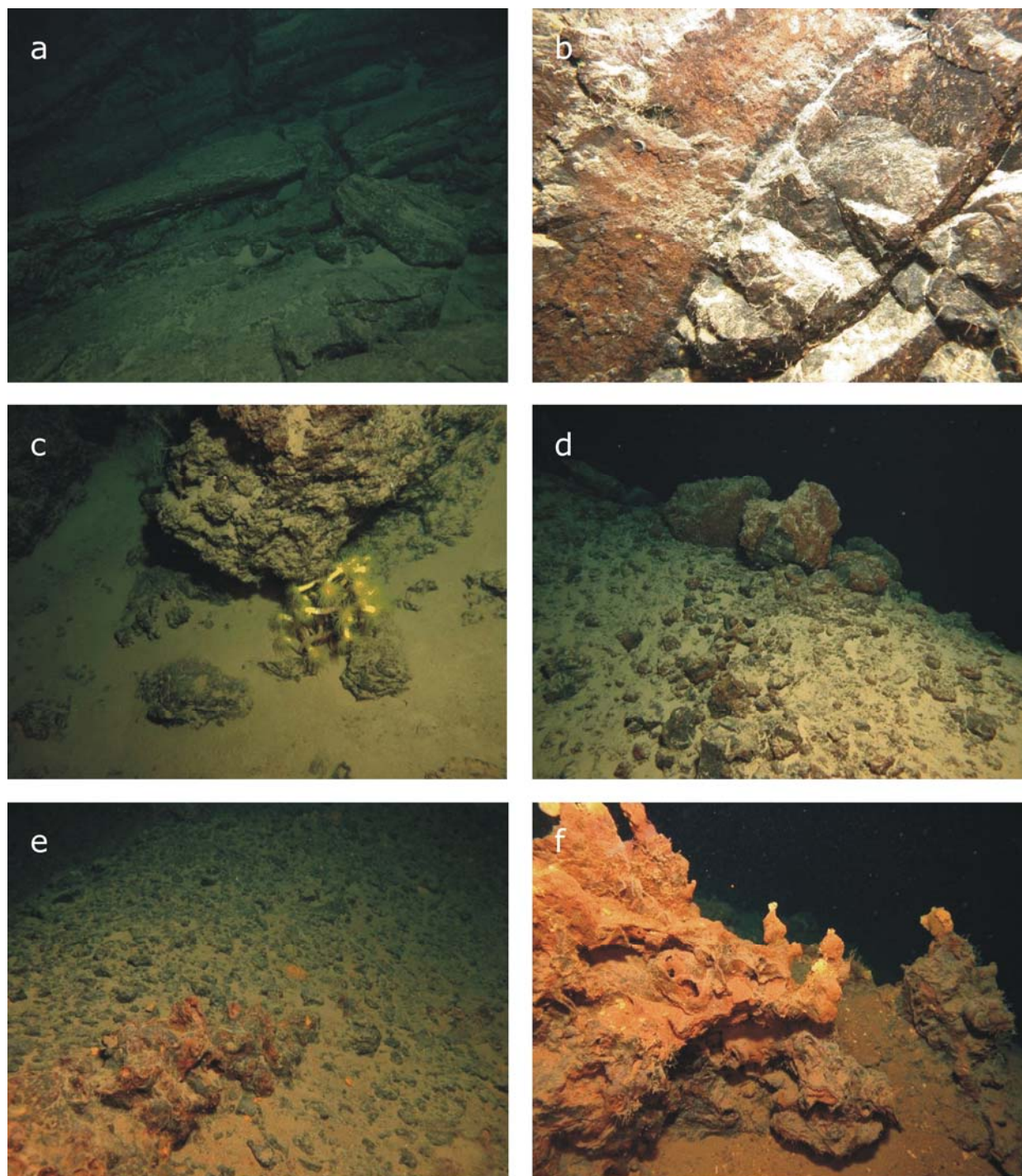


Fig. 7-17: Seafloor images obtained during dive 746ROV at Marsili Seamount (Date: 12 July 2006). a. Massive basalt flow (Depth: 546 m; Heading: 310°; Time: 07:26:28 UTC). b. Basaltic dike (Depth: 552 m; Heading: 300°; Time: 07:30:48 UTC). c. Anemones attached to an exposure of Fe-oxide coated volcanic rocks (Depth: 560 m; Heading: 039°; Time: 08:17:00 UTC). d. Fe-oxide coated volcanic rocks at a small ridge (Depth: 573 m; Heading: 157°; Time: 08:43:39 UTC). e. Top of the small ridge showing basalt talus and Fe-oxide precipitates aligned along a fracture (Depth: 494 m; Heading: 089°; Time: 10:32:22 UTC). f. Fe-oxide chimneys topped by bacterial colonies (Depth: 495 m; Heading: 315°; Time: 10:38:47 UTC).

7.3 Panarea

Three dives (752ROV, 754ROV, and 756ROV) were performed at Panarea to document the distribution of submarine gas venting and to map the seafloor to the north of Lisca Bianca. These dives complement previous mapping carried out in the area of the central islets (Esposito et al., 2006) and focused on several circular depressions interpreted to have formed during submarine gas explosions or collapse following intense gas venting.

Dive 752ROV

Dive 752ROV was targeted on a small channel-like depression to the north of Lisca Bianca (Fig. 7-18) where sulfide samples have previously been recovered by box-coring (Marani et al., 1997). The seafloor in the depression is dominated by sandy to pebbly, unconsolidated sediments and boulder fans. Only few exposures of volcanic rocks have been observed (Figs. 7-19 and 7-20). Gas venting at the seafloor is widespread and commonly intense within the circular seafloor depressions. The dive also documented the abundant occurrence of small sediment cones that formed in response to gas venting. Fe-oxide chimneys and chimney-like structures have been observed during the second part of the dive (Fig. 7-21).

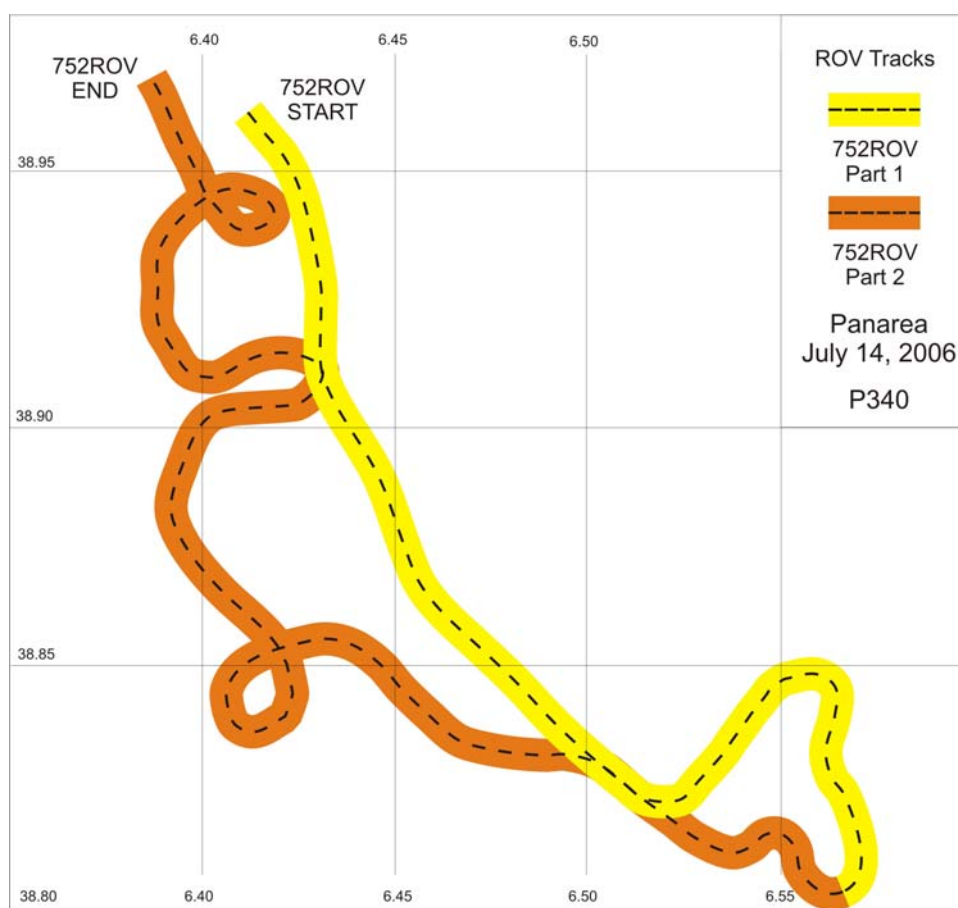


Fig. 7-18: Track of dive 752ROV to the north of Lisca Bianca.

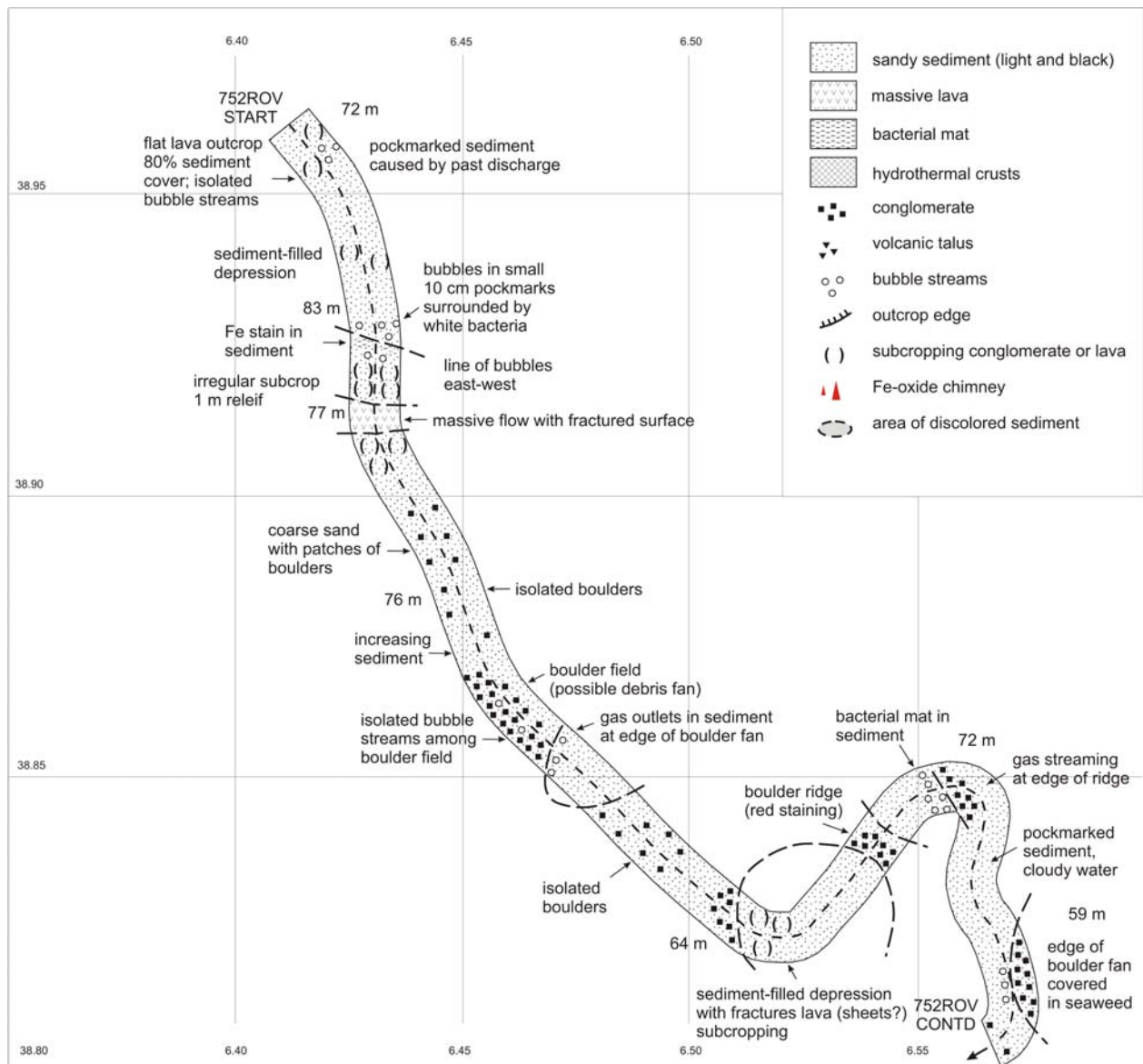


Fig. 7-19: Geological map of the first part of dive 752ROV to the north of Lisca Bianca.

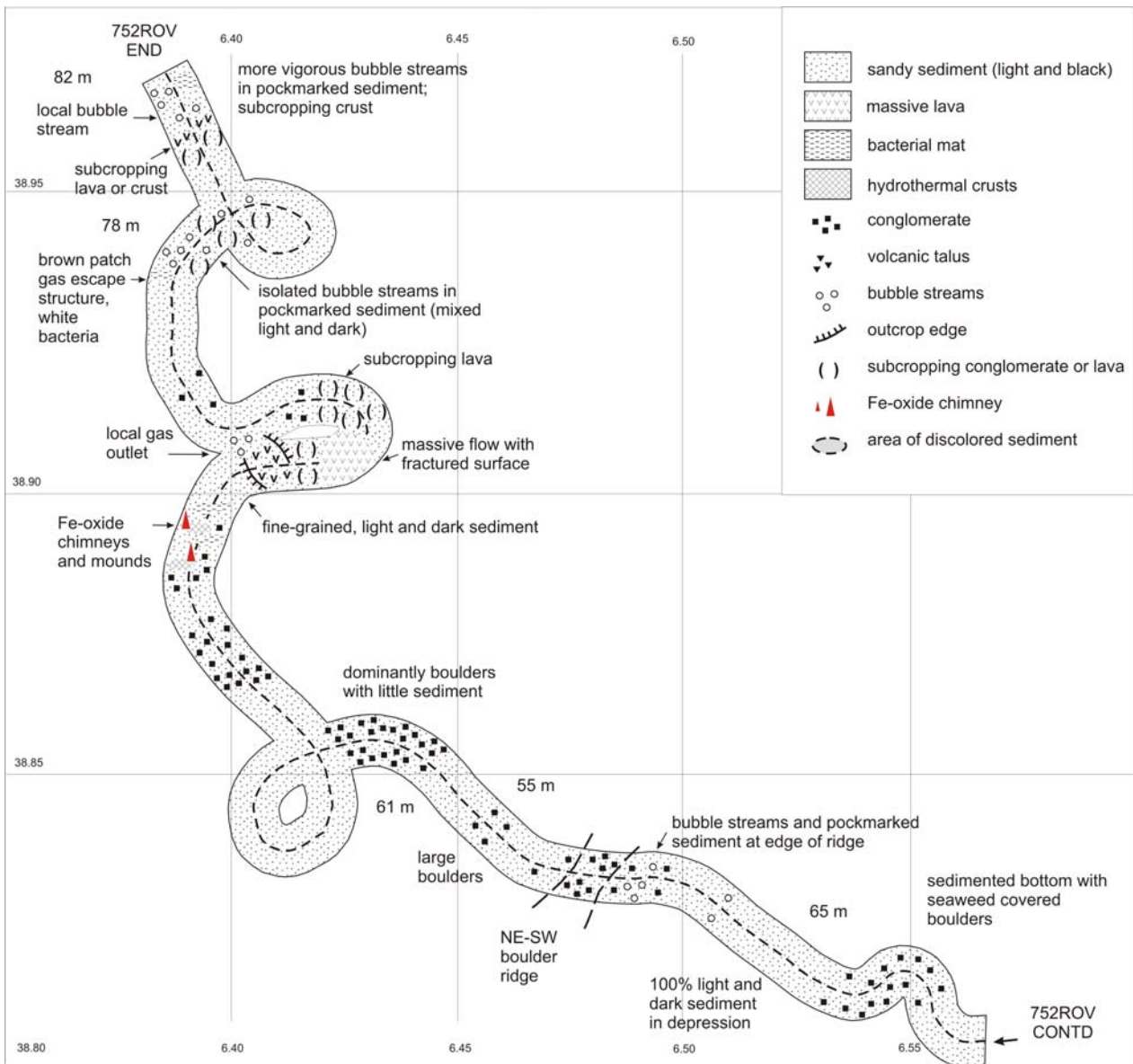


Fig. 7-20: Geological map of the second part of dive 752ROV to the north of Lisca Bianca.

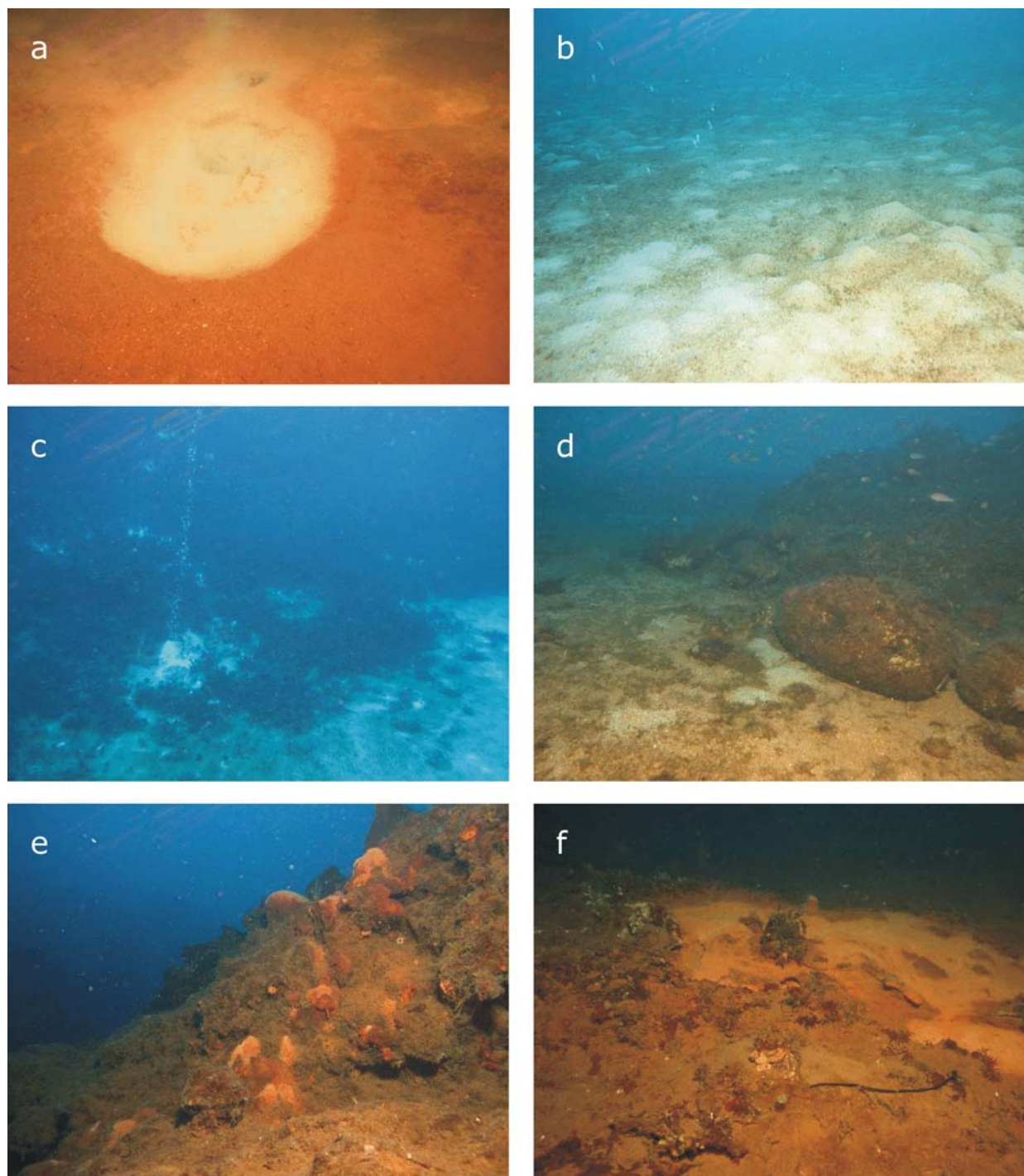


Fig. 7-21: Seafloor images obtained during dive 752ROV to the north of Lisca Bianca (Date: 14 July 2006). a. Small circular depressions characterized by gas venting and diffuse fluid flow. Note the staining of the sediment and the presence of bacterial colonies (Depth: 84 m; Heading: 135°; Time: 08:43:26 UTC). b. Sediment cones formed as a result of former gas discharge. Ascending gas bubbles can be seen in the left part of the image (Depth: 71 m; Heading: 124°; Time: 09:44:56 UTC). c. Gas venting at the rim of a circular depression (Depth: 59 m; Heading: 138°; Time: 11:02:42 UTC). d. Base of boulder fan that is covered by seafloor organisms (Depth: 67 m; Heading: 285°; Time: 11:55:25 (UTC)). e. Lower portion of a ca. 5 m large Fe-oxide chimney. Intense overgrowth by seafloor organisms (Depth: 77 m; Heading: 226°; Time: 12:38:06 UTC). f. Seafloor covered by Fe-oxide precipitates. Bacterial mats are stained by Fe-oxides (Depth: 78 m; Heading: 017°; Time: 13:55:23 UTC).

Dive 754ROV

The dive focused on the area to the northwest of Lisca Bianca where a fault with a throw of ca. 10 m (Figs. 7-22 to 7-24). During the dive, numerous Fe-oxide chimneys were observed. The presence of associated bacterial colonies suggests that low temperature hydrothermal fluid flow is ongoing. Another remarkable observation is the occurrence of large fans of rounded boulders that may represent former beach deposits. During the second part of the dive, a light gray, flow-banded, coherent rhyolite unit was discovered (Figs. 7-25 and 7-26).



Fig. 7-22: Track of dive 754ROV to the northwest of Lisca Bianca.

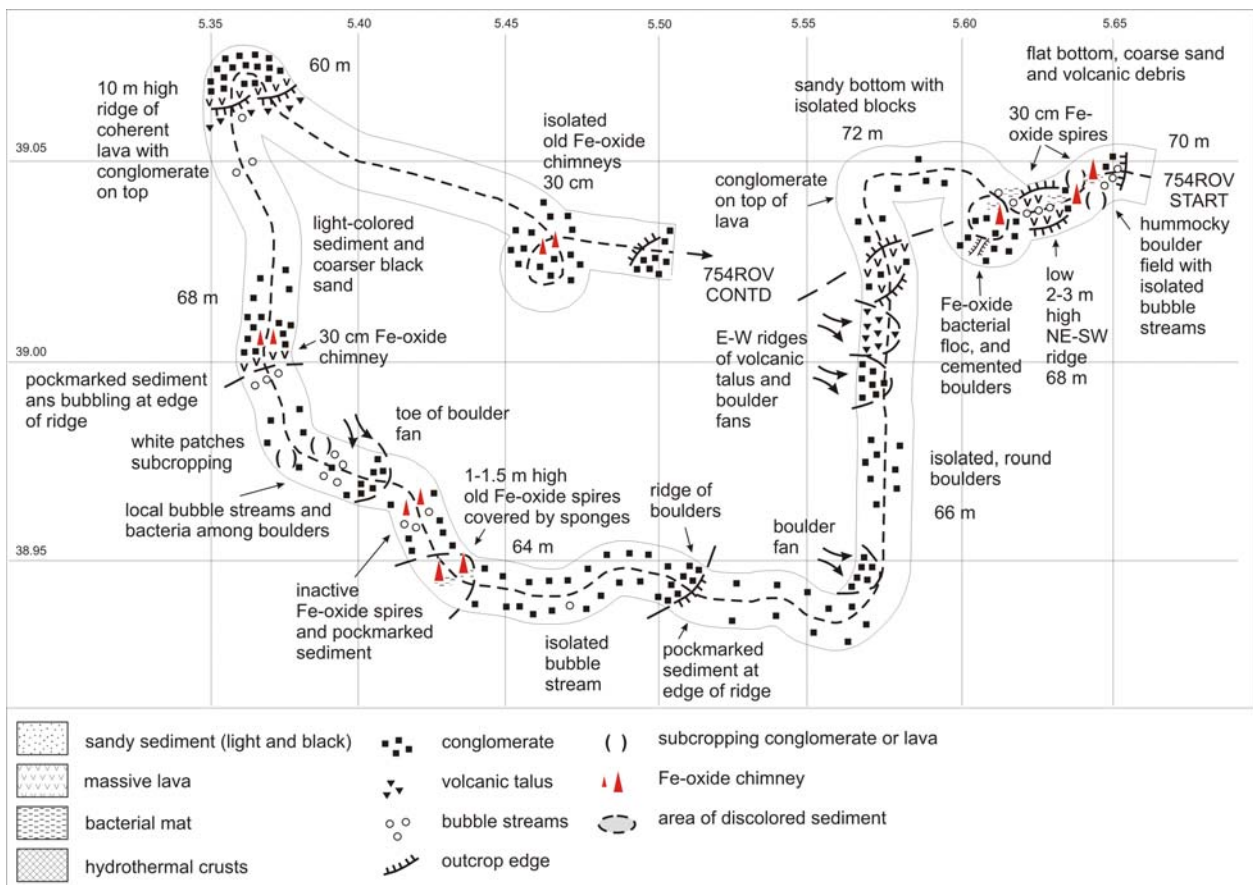


Fig. 7-23: Geological map of the first part of dive 754ROV to the northwest of Lisca Bianca.

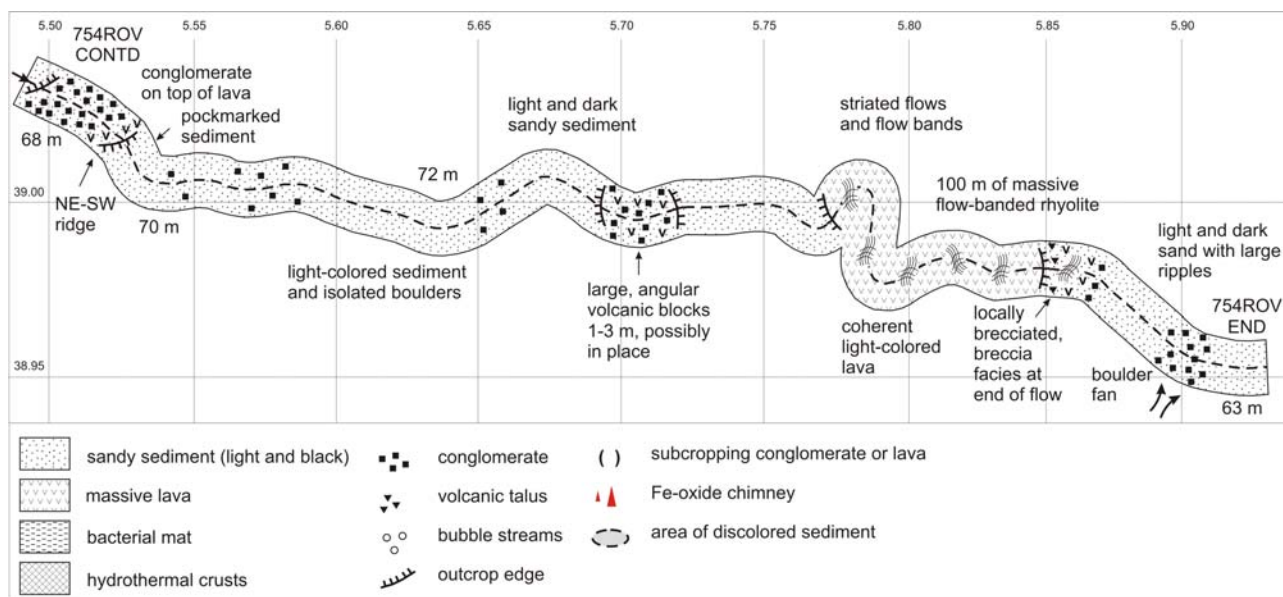


Fig. 7-24: Geological map of the second part of dive 754ROV to the northwest of Lisca Bianca.

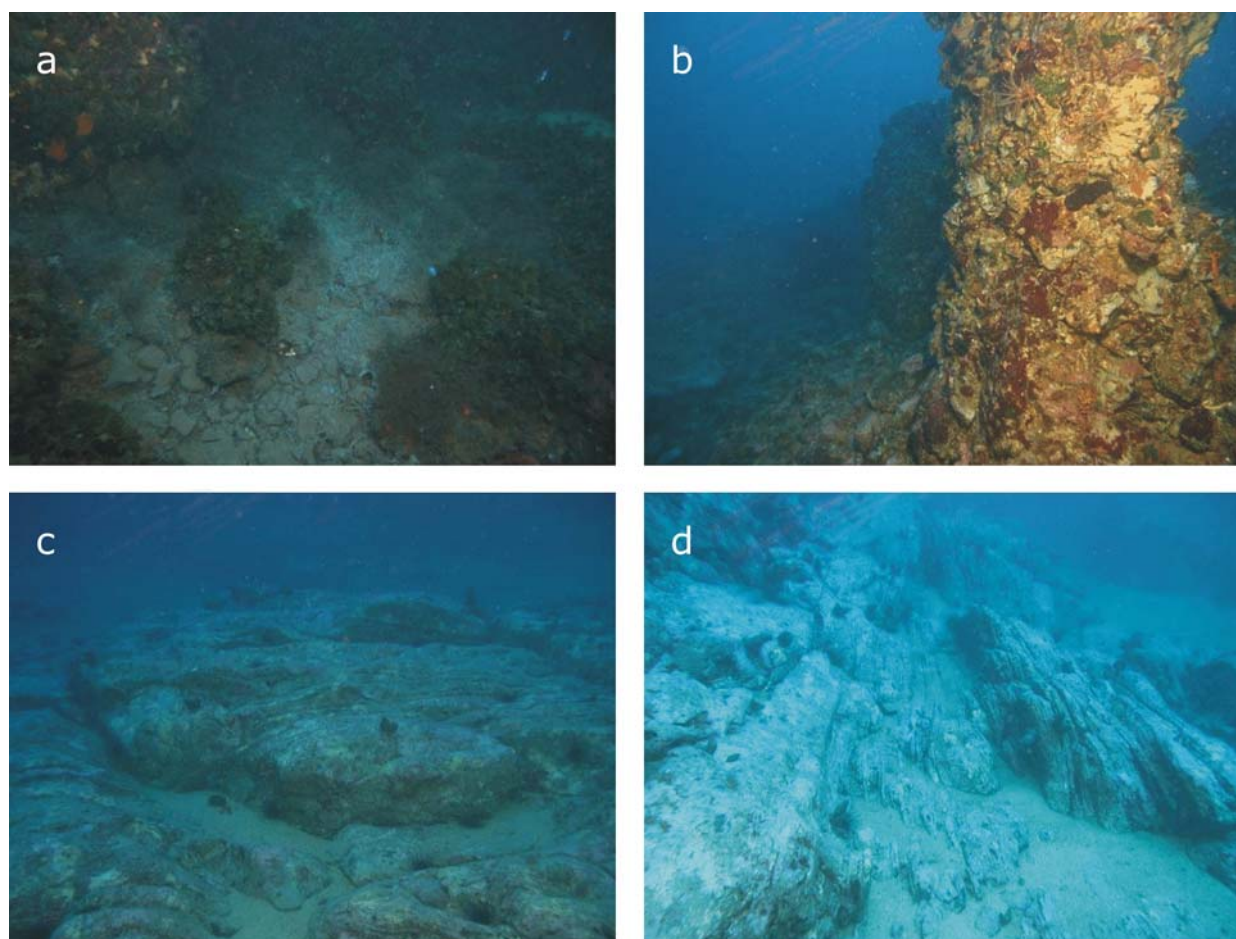


Fig. 7-25: Seafloor images obtained during dive 754ROV to the northwest of Lisca Bianca (Date: 15 July 2006). a. Gas venting and associated bacterial mat in proximity to a Fe-oxide chimney (Depth: 64 m; Heading: 310°; Time: 10:32:33 UTC). b. Pillar composed of volcanic breccia (Depth: 68 m; Heading: 231°; Time: 11:06:28 UTC). c. Flow-banded rhyolite unit (Depth: 61 m; Heading: 356°; Time: 12:59:55 UTC). d. Prominent flow-banding of rhyolite (Depth: 59 m; Heading: 095°; Time: 13:12:56 UTC).

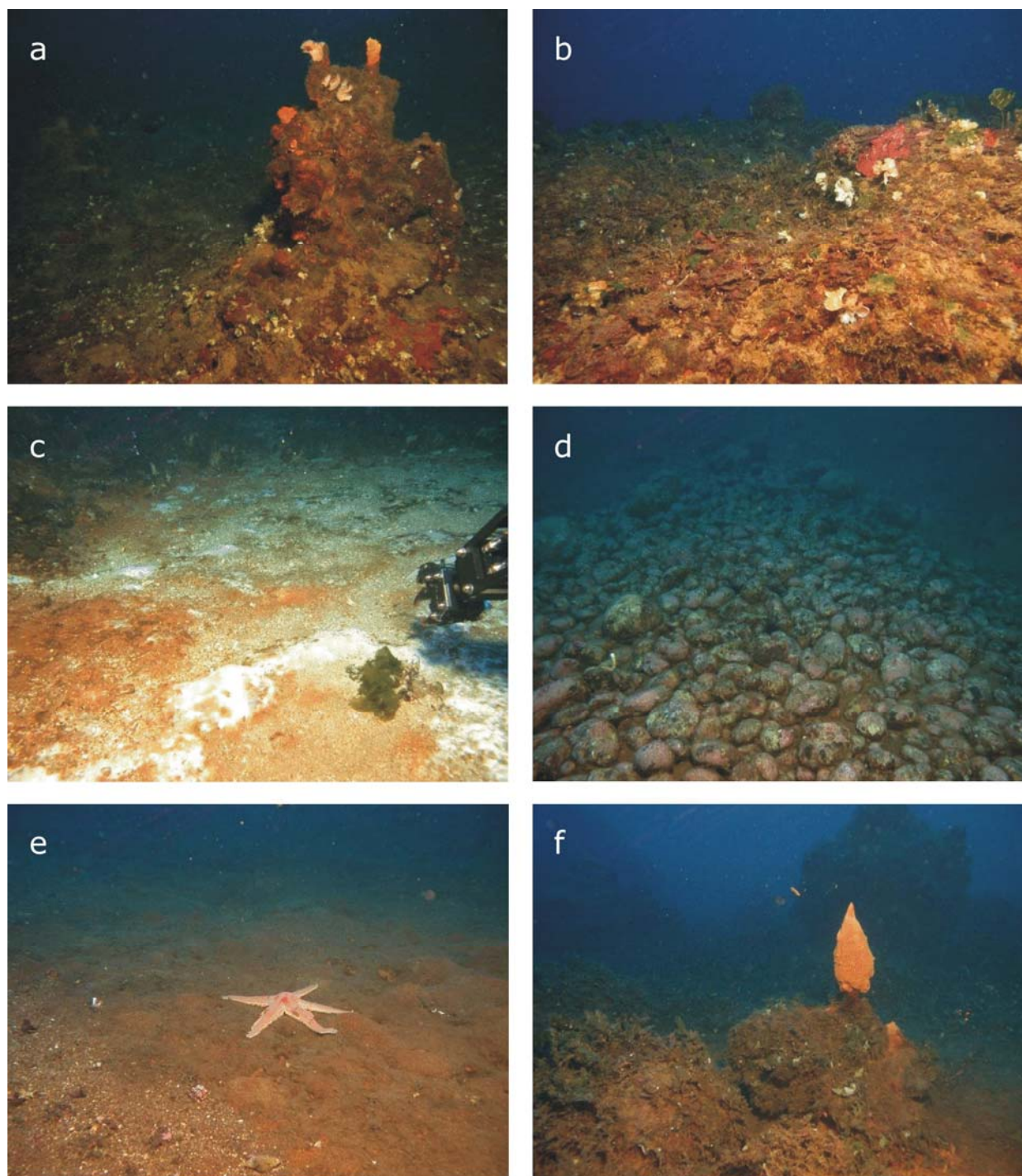


Fig. 7-26: Seafloor images obtained during dive 754ROV to the northwest of Lisca Bianca (Date: 15 July 2006). a. Isolated Fe-oxide chimney (Depth: 72 m; Heading: 285°; Time: 07:23:04 UTC). b. Small ridge covered by seafloor fauna (Depth: 72 m; Heading: 329°; Time: 07:27:55 UTC). c. Area of active venting with bacterial mats. Site of fluid sample 754ROV-1 (Depth: 77 m; Heading: 330°; Time: 07:41:32 UTC). d. Boulder fan that probably represents an old beach deposit (Depth: 69 m; Heading: 213°; Time: 08:37:59 UTC). e. Brittle star in an area typified by abundant sediment cones (Depth: 66 m; Heading: 287°; Time: 09:13:23 UTC). f. Fe-oxide chimney tipped by a bacterial community. Note the occurrence of a larger chimney in the background (Depth: 64 m; Heading: 339°; Time: 09:47:27 UTC).

Dive 756ROV

The dive focused on an area to the northeast of Lisca Bianca that is typified by the occurrence of several circular depressions (Figs. 7-27 to 7-29). The seafloor observations revealed that the walls surrounding these depressions are several meters in height and con-

sist of material of local derivation. No juvenile volcanic debris was observed. Gas venting was abundant in the depressions, but also occurred outside these topographic lows. Sediments cemented by native sulfur were observed in one depression (Figs. 7-30 and 7-31).

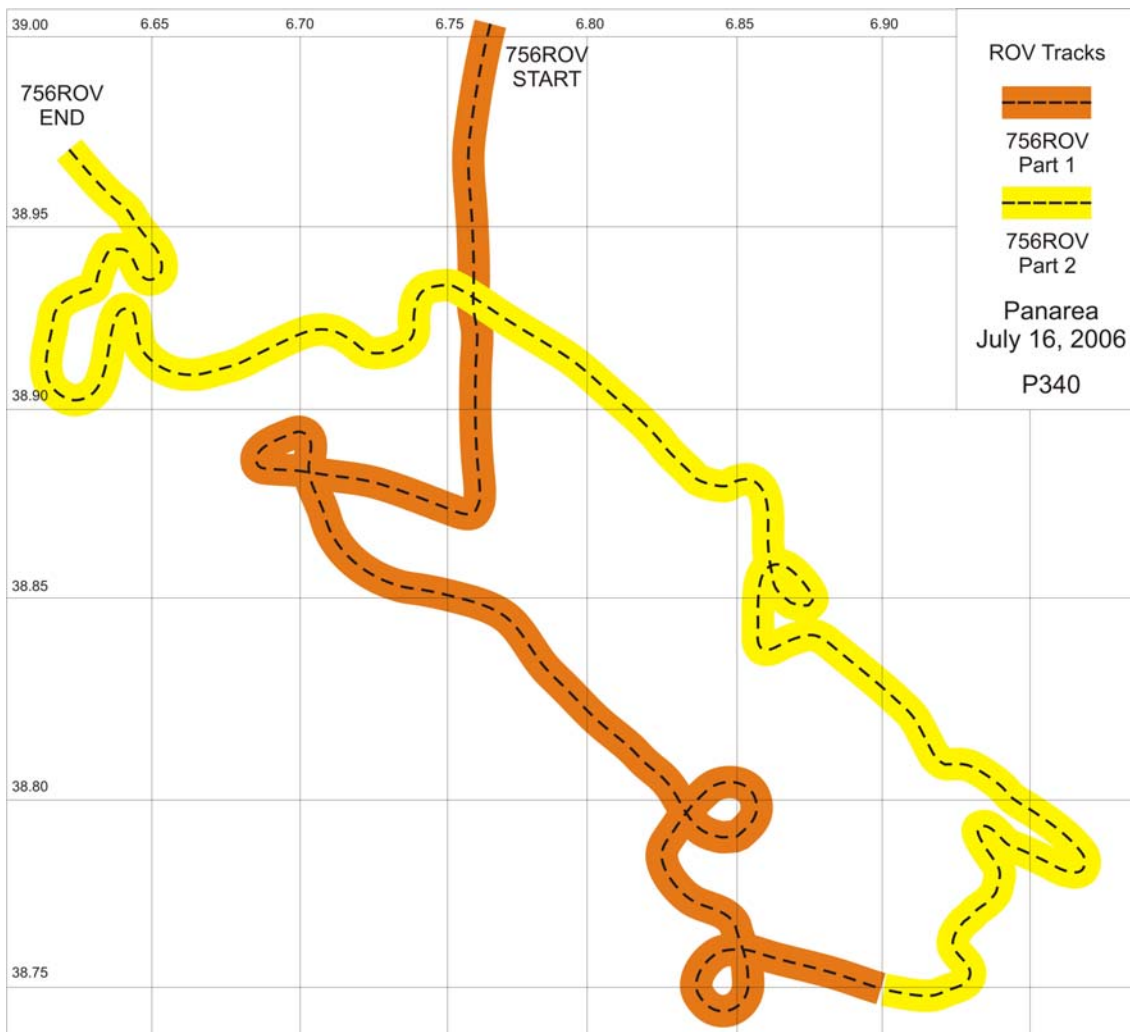


Fig. 7-27: Track of dive 756ROV to the northeast of Lisca Bianca.

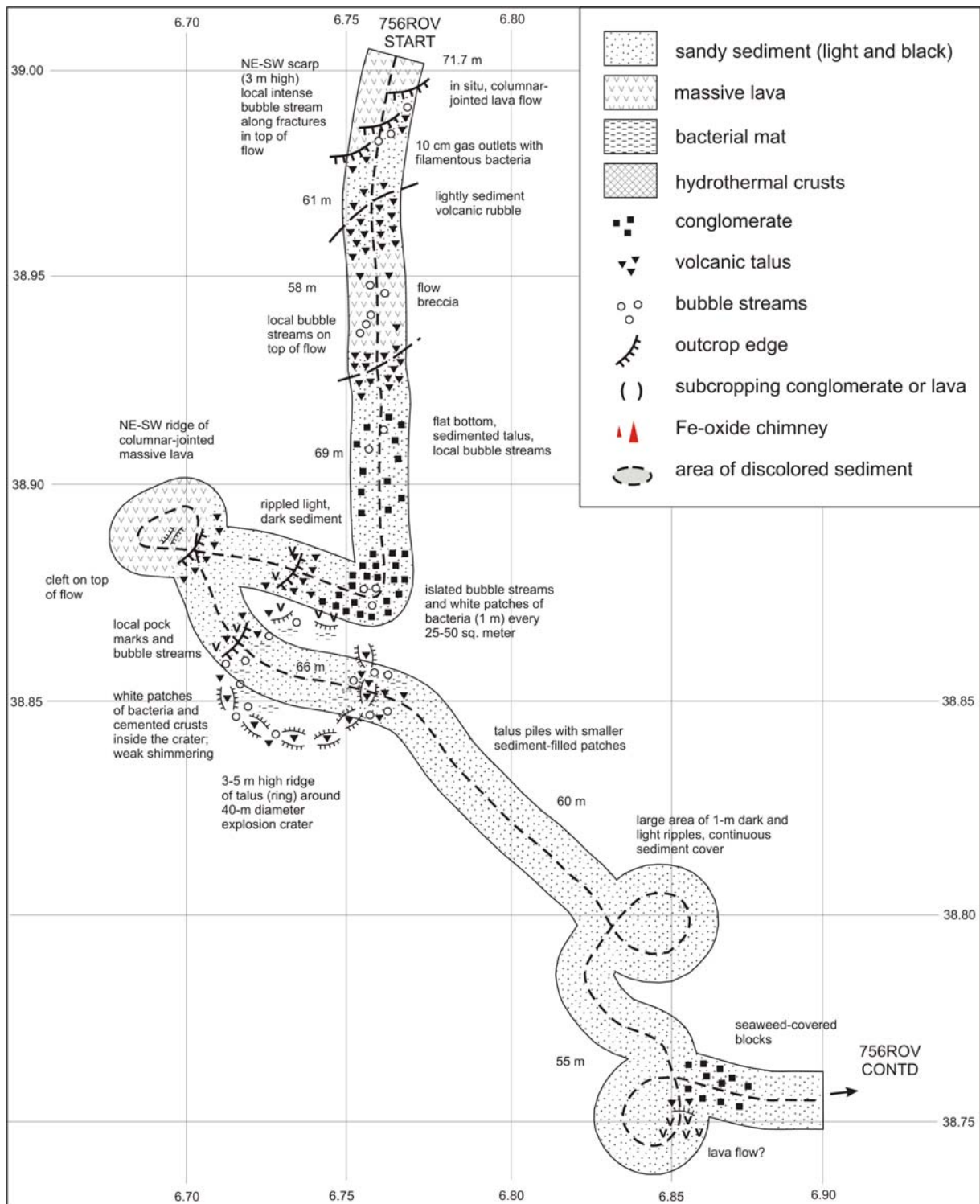


Fig. 7-28: Geological map of the first part of dive 756ROV to the northeast of Lisca Bianca.

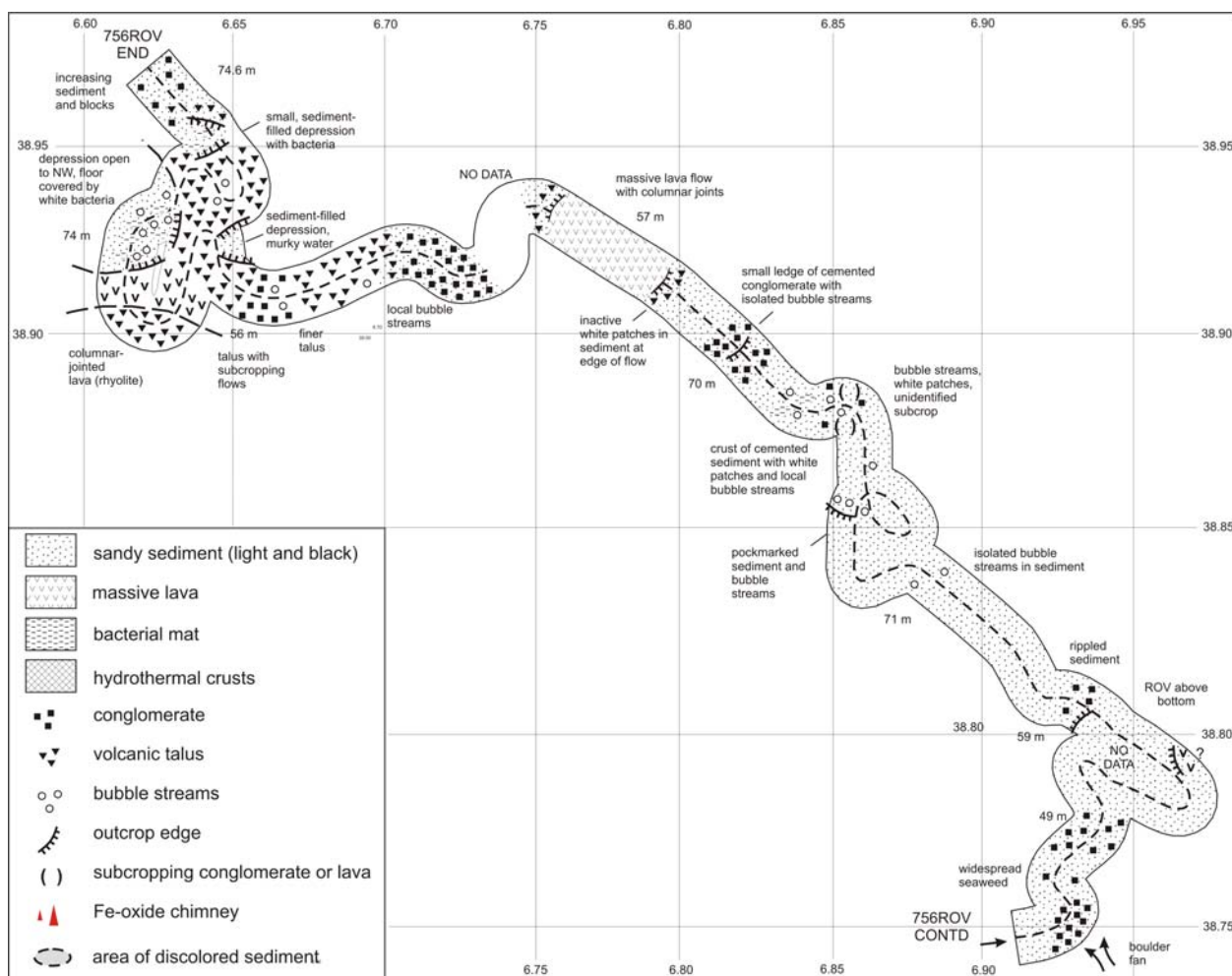


Fig. 7-29: Geological map of the second part of dive 756ROV to the northeast of Lisca Bianca.

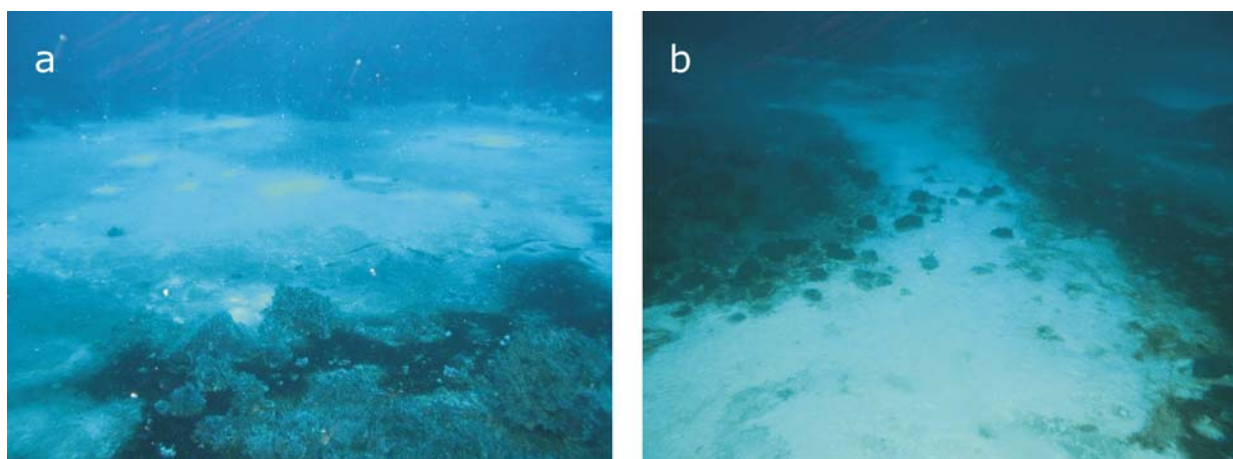


Fig. 7-30: Seafloor images obtained during dive 756ROV to the northeast of Lisca Bianca (Date: 16 July 2006). a. Abundant gas venting in an area typified by variably colored bacterial mats (Depth: 64 m; Heading: 136°; Time: 11:14:05 UTC). b. White bacterial mats in an area of limited gas venting (Depth: 76 m; Heading: 001°; Time: 14:11:27 UTC).

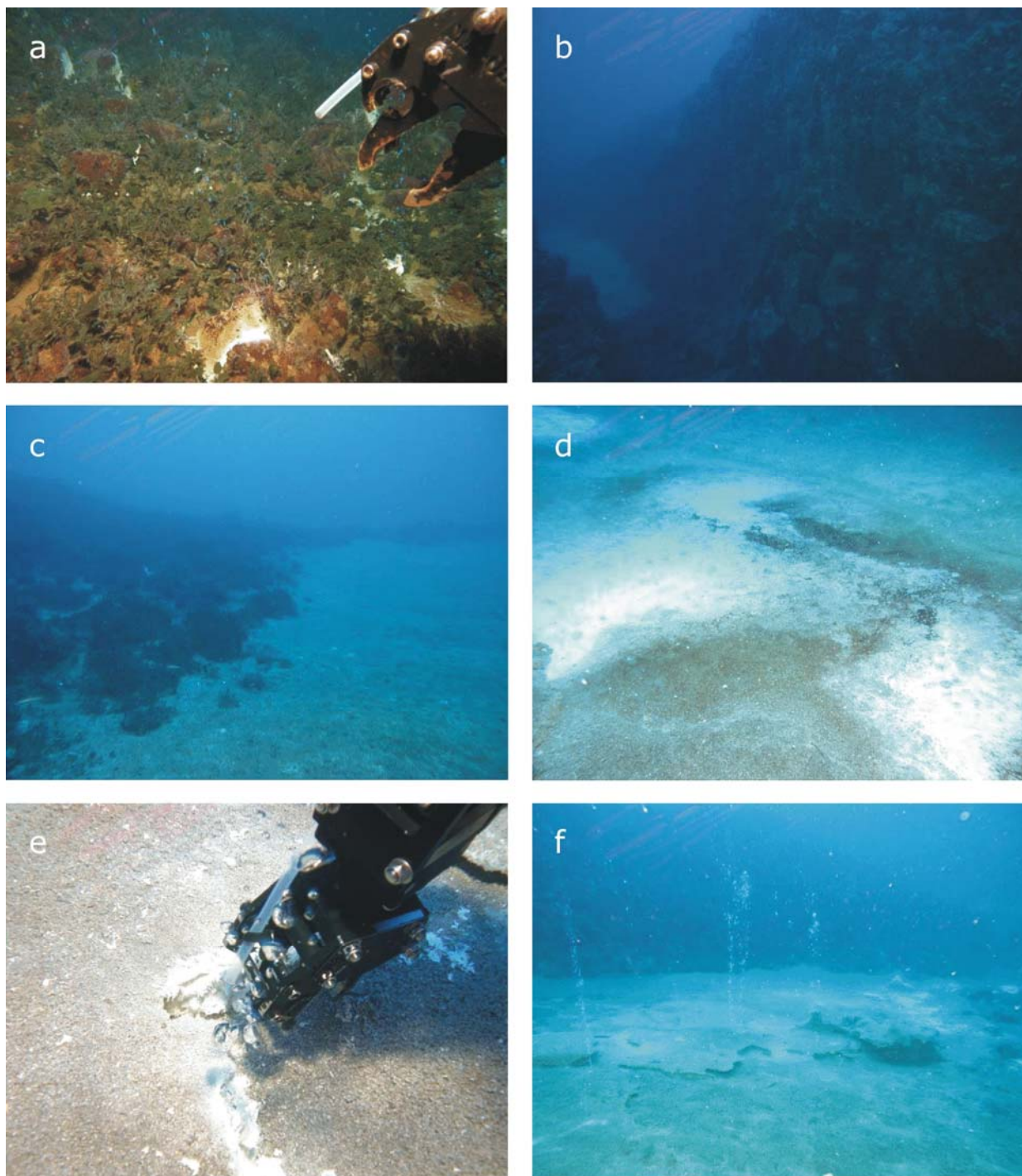


Fig. 7-31: Seafloor images obtained during dive 756ROV to the northeast of Lisca Bianca (Date: 16 July 2006). a. Gas venting in an area covered by seaweed (Depth: 75 m; Heading: 091°; Time: 08:10:22 UTC). b. Eastern wall of a topographic high at 38°38.88'N / 15°06.70'E that is composed of mafic volcanic rocks (Depth: 53 m; Heading: 240°; Time: 09:25:58 UTC). c. Inner wall of a circular seafloor depression representing an explosion crater or a collapse structure following intense gas venting. Note that the crater floor is covered by a thick layer of sediment (Depth: 63 m; Heading: 135°; Time: 09:33:07 UTC). d. Bacterial mats in the center of the same circular seafloor depression (Depth: 66 m; Heading: 149°; Time: 09:35:56 UTC). e. Fluid sampling (756ROV-3) at an active vent site. The site is characterized by the presence of a bacterial mat and native sulfur (Depth: 67 m; Heading: 346°; Time: 10:18:15 UTC). f. Abundant gas venting at the floor of the seafloor depression. Note that the sediments are cemented by native sulfur (Depth: 66 m; Heading: 191°; Time: 10:47:14 UTC).

8 Chemistry of hydrothermal fluids

D. Garbe-Schönberg

8.1 Fluid sampling and temperature measurements

To obtain *in-situ* fluid samples in areas of hydrothermal fluid flow, a remotely controlled flow-through system, the Kiel Pumping System KIPS-3 (Garbe-Schönberg et al., 2006), was mounted on the tool sled at the backside of the ROV Cherokee. The system consists entirely of inert materials including perfluoralkoxy (PFA) and polytetrafluorethylene (PTFE). Sampled fluids entered the system through PFA tubing attached to the claw of the manipulator (Fig. 8-1). The tubing is connected to a remotely controlled multi-port valve that is driven by a stepper motor (Schilling, U.S.A.). Opening and closing of the multi-port valve were controlled by RS232 communication using software provided by Marum Soft, Bremen. A thermistor sensor with a data logger was used to monitor *in-situ* temperatures.



Fig. 8-1: PFA sampling tube attached to the manipulator claw of ROV Cherokee.

Due to limited space availability on ROV Cherokee, the KIPS-3 system was modified to collect a maximum of 5 fluid samples only (Figs. 8-2 and 8-3). The multi-port valve was set accordingly to allow the use of five ports, each connected to a 550 ml PFA flask (Savillex, USA). Each bottle was equipped with check valves at the inlet and outlet. The five flasks were mounted on a single rack, facilitating the transfer of the sample flasks to the laboratory. A remotely controlled 24 VDC mechanical gear pump was positioned downstream from the sample flasks to avoid sample contamination. The outlet of the pump was re-directed to the front of the ROV to monitor the fluid flow during sampling using the video system of the ROV. The pumping time per sample was set to 3 min to ensure that the flask volume was exchanged at least four times prior to final sampling. Unfortunately, the remote control of the multi-port valve failed entirely during the cruise due to problems with the RS232 communication. Consequently, only the flask directly connected to the fluid pump could be used.

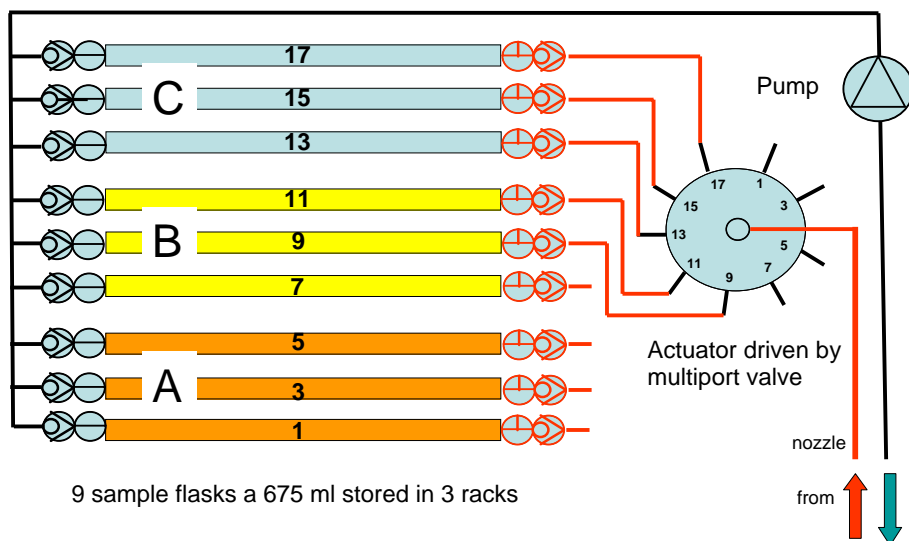


Fig. 8-2: Schematic configuration of the KIPS-3 fluid sampling system. Fluids entering PFA tubing at the manipulator claw are distributed by a motorized multi-port valve to the sample flasks, each with check valves and stopcocks. The pump is positioned downstream. The shown configuration was modified for cruise P340 to collect five fluid samples into 550 ml flasks.

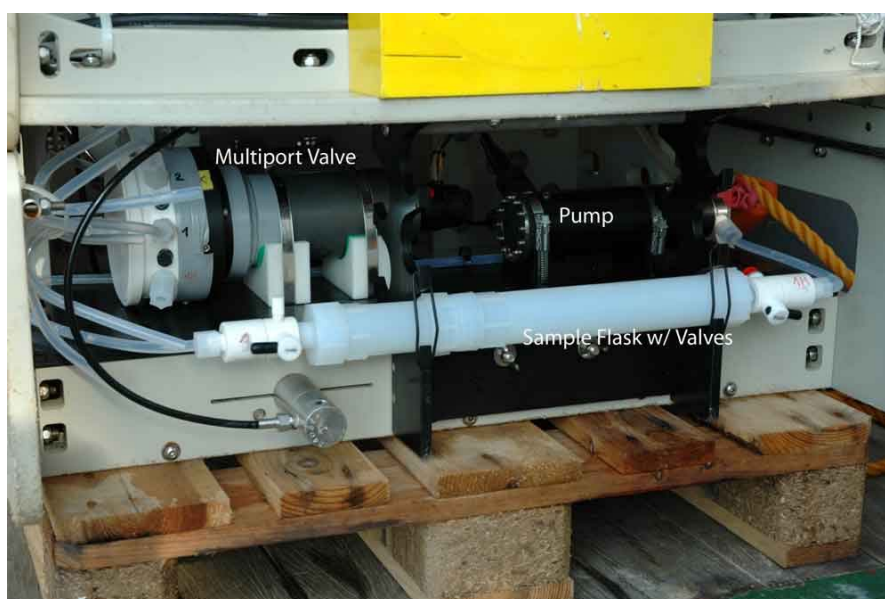


Fig. 8-3: KIPS-3 system mounted on the tool sled at the back side of ROV Cherokee.

Following each dive, the recovered water sample was sub-sampled for subsequent geochemical analyses at the University of Kiel by ICP-OES and ICP-MS. An aliquot of 2 ml was treated with 100 μ l of ZnAc (10.4 g/l ZnAc) to determine the concentration of dissolved sulfide. Aliquots for the analysis of nutrients were stored in polypropylene bottles, sealed and kept refrigerated at 4°C. Aliquots for cation and trace element analysis were pressure-filtrated through 0.2 μ m Nuclepore polycarbonate (PC) membrane filters using Sartorius PC filtration units and high purity nitrogen. The samples were acidified with sub-boiled

nitric acid to a pH<2 and stored in perfluoralkoxy (PFA) bottles. Measurements of the fluid pH were performed immediately after sample recovery using a pH 196 instrument (WTW, Germany) with calibration standards for pH 7.00 and 10.00, respectively. The error of the measurement was ±0.01 pH.

Monitoring of *in-situ* temperatures was conducted during the dives with a thermistor-based temperature sensor that was mounted portside at the inside of the drawer, ca. 30 cm above the base of the ROV. The sensor was connected to the RBR 1050 data logger and to a RS232 port for real-time temperature readings. Due to technical problems with the RS232 connection, real-time temperature readings were not possible during the cruise. However, the temperature data could be extracted from the data logger following each dive.

Table 8-1 lists the sites of fluid sampling carried out during P340. The measured pH values of the collected fluids and temperature anomalies encountered during fluid sampling are also given. At several sites characterized by the presence of hydrothermal precipitates and bacterial mats, a small rise of temperature above ambient seawater was observed.

Table 8-1: List of fluid samples collected during P340.

<i>Sample</i>	<i>Area</i>	<i>Water depth (m)</i>	<i>Site description</i>	<i>Time (UTC)</i>	<i>pH</i>	<i>Temperature anomaly (°C)</i>
743ROV-1	Palinuro Seamount	641	tube worm site, above bacterial mat	12:06	7.62	+ 0.1
749ROV-1	Palinuro Seamount	696	ambient seawater	11:50	8.16	ambient
752ROV-1	Panarea	71	above sediment/ abundant gas bubbles	13:13	7.55	+ 0.3
754ROV-1	Panarea	77	10 cm above bacterial mat	07:37	7.63	+ 0.3
756ROV-3	Panarea	57	5 cm above bacterial mat and cemented sediment, shimmering water	10:17	7.24	(+ 0.4)

At Palinuro Seamount, a fluid sample (743ROV-1) was collected several centimeters above a bacterial mat, which was located adjacent to a tube worm colony. Shimmering water was observed at a nearby site. A rise of 0.1 °C above the ambient temperature of 15.7 °C (Figs. 8-4 and 8-5) and a fluid pH of 7.62 (ambient seawater has a pH of 8.12) clearly indicate that active fluid discharge occurs at the sample site. During the dive at the southwestern and western summits (749ROV), no indications for active hydrothermal fluid flow were observed (Fig. 8-6). However, a sample of ambient seawater was collected (749ROV-1).

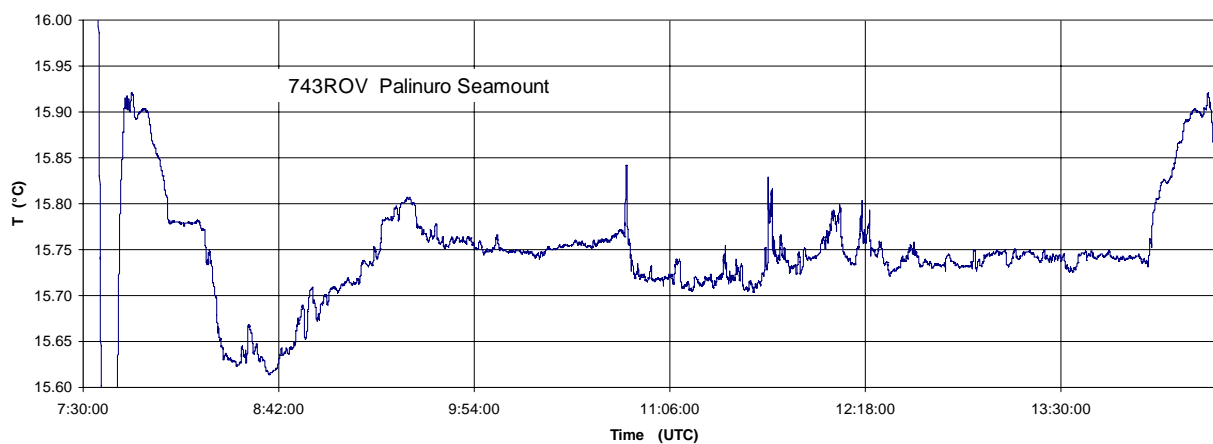


Fig. 8-4: Temperature profile collected during dive 743ROV.

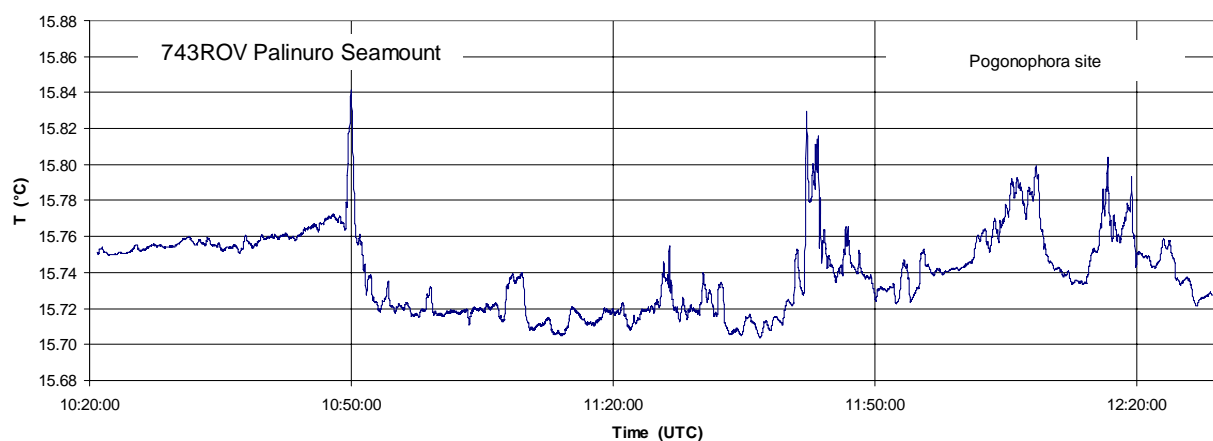


Fig. 8-5: Temperature profile collected at the tube worm site during dive 743ROV.

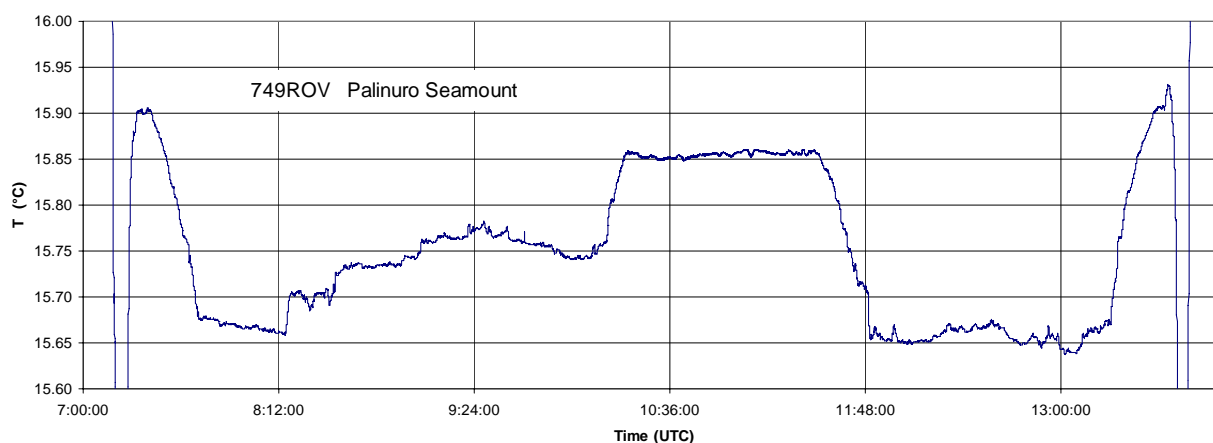


Fig. 8-6: Temperature profile collected during dive 749ROV.

In contrast to Palinuro Seamount, no bottom temperature anomaly was observed during dive 746ROV at Marsili Seamount (Fig. 8-7).

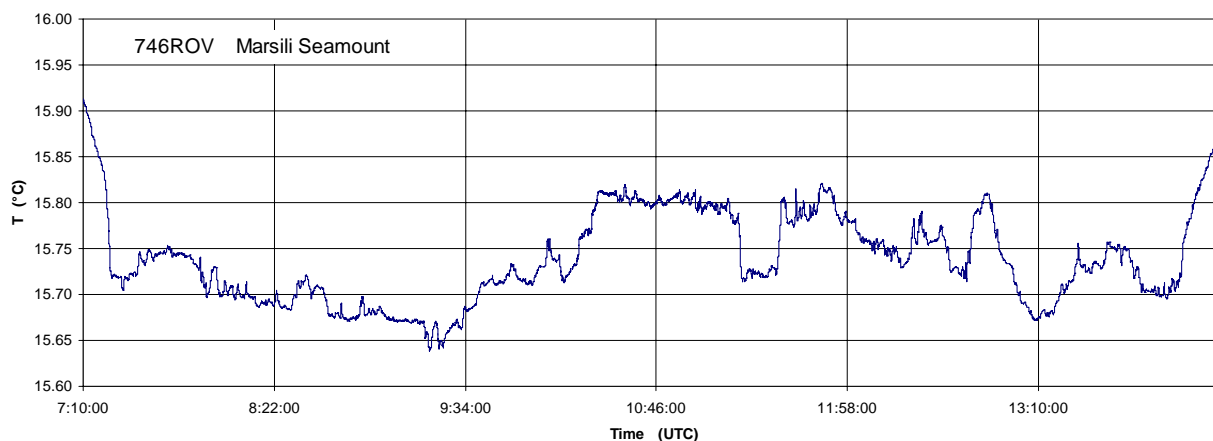


Fig. 8-7: Temperature profile collected during dive 746ROV.

The seafloor in the area off Panarea Island is characterized by widespread gas discharge. At several sites, shimmering water was observed. Bottom water samples taken immediately above gas vents (Fig. 8-8) showed pH values ranging from 7.24 to 7.65 (752ROV-1, 754ROV-1, and 756ROV-3). The relatively low pH values of the bottom water can be explained by the reaction of seawater with the CO₂-dominated gas venting at these sites or the presence of oxidized sulfur species.

Temperature readings during the ROV dives off Panarea Island indicate that temperature anomalies occur at many sites (Figs. 8-9 to 8-11). The maximum recorded bottom water temperature was 1.1 °C above the ambient value of 15.6-15.7 °C (756ROV). This finding indicates that the discharge of thermal water is widespread at Panarea.



Fig. 8-8: KIPS-3 fluid sampling above a bacterial mat off Panarea Island (754ROV).

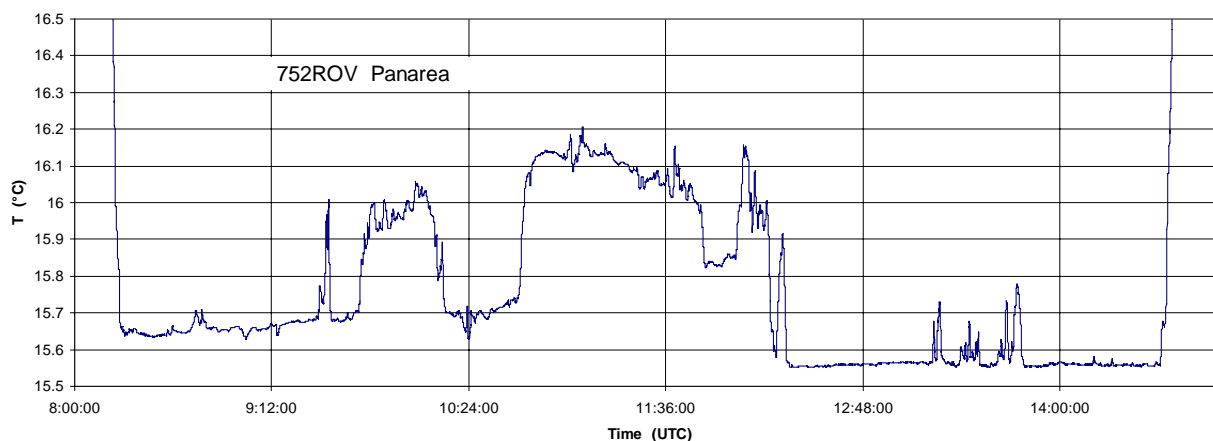


Fig. 8-9: Temperature profile collected during dive 752ROV.

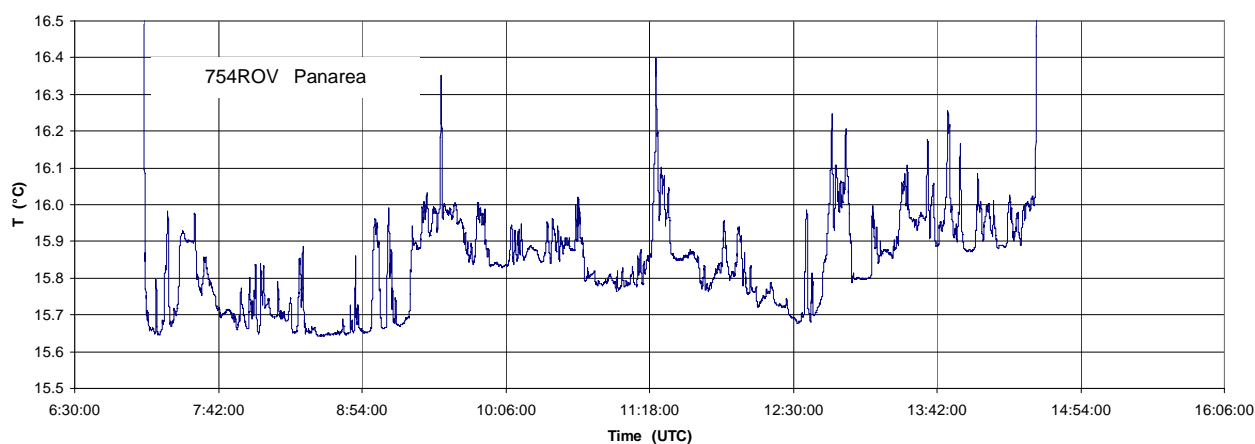


Fig. 8-10: Temperature profile collected during dive 754ROV.

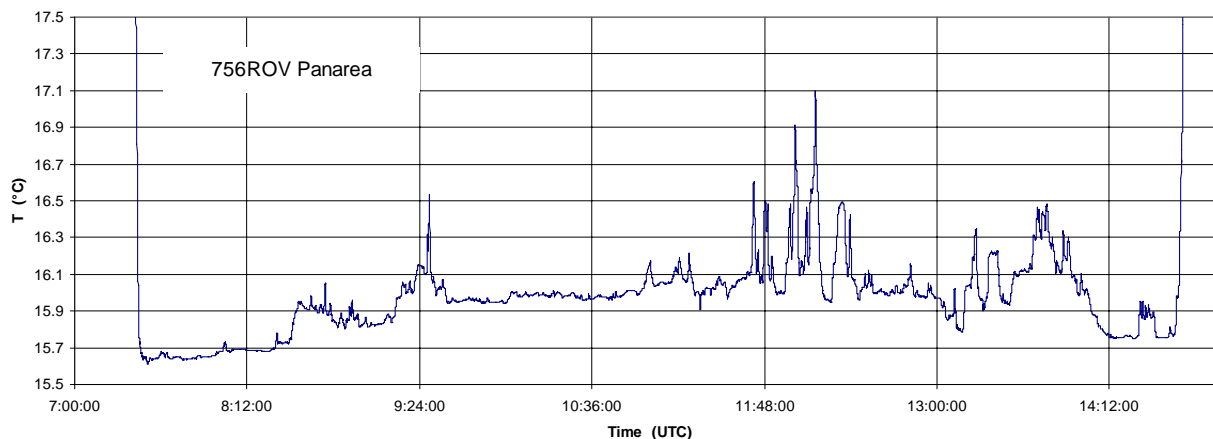


Fig. 8-11: Temperature profile collected during dive 756ROV.

8.2 Analytical procedure and composition of fluids

Multi-element analysis of the major ions (Cl, Br, B, Si, Na, K, Ca, and Mg) of the water samples was performed at the University of Kiel using a SPECTRO Ciros SOP ICP-OES spectrometer. Three independent replicate analyses were performed to evaluate the precision of the data. Precision was better than 1 RSD% for all elements except Si (10 RSD%), which was difficult to measure due to concentrations close to detection limit.

The concentrations of the trace elements were determined by ICP-MS using an Agilent 7500cs mass spectrometer. The calibration strategy followed Garbe-Schönberg (1993). However, a weak signal suppression originating from the seawater matrix was noted and corrected during the ICP-MS analysis. The certified reference materials IAPSO and NASS-5 were measured as unknowns along with the water samples to evaluate the calibration and to constrain the accuracy of the measurements (Table 8-2). Close agreement between the measured concentrations and the certified values indicates that the analyses were performed at high accuracy.

Table 8-2: Composition of fluid samples collected during P340. Concentrations represent averages of three independent replicate analyses.

		IAPSO	NASS-5	Palinuro 743ROV-1	Palinuro 749ROV-1	Panarea 752ROV-1	Panarea 754ROV-1	Panarea 756ROV-3
Cl	(mM)	567		628	626	615	617	618
Br	(mM)	0.83		0.92	0.92	0.90	0.90	0.91
B	(mM)	0.44		0.48	0.46	0.45	0.46	0.46
Si	(μ M)	57		15	9.2	7.1	7.5	3.6
Na	(mM)	474		526	528	516	521	517
K	(μ M)	10.5		11.7	11.7	11.5	11.6	11.6
Ca	(mM)	10.4		11.8	11.6	11.4	11.5	11.4
Mg	(mM)	56.8		63.4	63.4	60.9	62.5	61.7
Li	(μ M)	26.8	22.0	42.2	29.2	27.9	28.2	29.1
Rb	(μ M)	1.5	1.2	2.1	1.6	1.6	1.6	1.6
Cs	(nM)	2.3	2.0	156	2.6	3.3	2.8	6.8
Sr	(μ M)	87.9	75.1	100	97.8	97.7	96.6	96.7
Ba	(μ M)	0.73	0.04	0.09	0.31	0.21	0.09	0.06
Mo	(nM)	121	104	136	236	243	187	142
U	(nM)	13.1	11.2	14.5	14.0	14.3	14.2	14.4
W	(nM)	0.61	0.60	1.2	1.1	0.82	0.81	0.65
Sb	(nM)			2.8	2.1	2.1	2.0	1.9
Fe	(μ M)			< 0,2	< 0,2	< 0,2	< 0,2	< 0,2
Mn	(μ M)		0.01	1.7	0.04	0.25	0.12	1.1
Zn	(μ M)		< 10	2.7	0.48	1.4	0.09	0.09
As	(nM)		< 10	387	67	80	53	53
Pb	(nM)		< 0,5	21.2	7.2	8.7	< 0,5	< 0,5
Ag	(nM)		< 3	< 3	< 3	< 3	< 3	< 3





The chemical analysis showed that the fluid sample 743ROV-1 from Palinuro Seamount, although highly diluted with ambient seawater, has a clear hydrothermal component. The sample has a pH of only 7.62 whereas the ambient seawater sample 749ROV-1 has a value of 8.16. More significantly, the dissolved metals Mn (1.7 μ M), Zn (2.7 μ M), As (387 nM), Sb (2.8 nM), W (1.2 nM), and Pb (21.2 nM) are enriched. The hydrothermal fluid component also appears to be more saline and alkali-rich in composition as suggested by elevated Cs (156 nM), Li (42.2 μ M), Ca (11.8 mM), and Rb (2.1 μ M) concentrations when compared to the seawater sample.




In contrast to Palinuro, the three samples from Panarea have compositions similar to ambient seawater, at least in respect to most cations. There are, however, some significant deviations in sample 756ROV-3. The concentrations of Mn (1.1 μ M) and As (53 nM) are slightly elevated, but dissolved silica (3.6 μ M) and Ba (0.06 μ M) are depleted. The range of pH values exhibited by the three samples (7.24 to 7.63) is significantly lower than normal seawater.

9 Rock Sample Descriptions

M. Hocking, M. Hannington, and T. Monecke

	<p><u>P340-724DR-1</u></p> <p>Irregularly shaped and subangular Fe-Mn-oxide crust (25 x 25 x 20 cm, ca. 4 kg). The surface shown is covered in orange-red Fe-oxide whereas other surfaces are covered in dull dark gray, Mn-oxide. Beneath the coating are bands of hard, dark red, Fe-oxide-rich silica, laminated with layers of soft, powdery, orange Fe-oxide. Ca. 30 % of the surface is covered with <2 cm long, bivalve shells and tube fossils that are Mn-Fe-oxide-coated. Rare siliceous sponges are present. Fauna is not present on the Fe-oxide stained side, indicating it was face down on the seafloor.</p>
	<p><u>P340-724DR-2</u></p> <p>Rounded to sub-angular Fe-Mn-oxide pebbles (up to 4 x 4 x 2 cm, ca. 0.5 kg) that are dull black with variable orange-red Fe-oxide. Some pebbles consist of a thin, black, Mn-oxide crust on the outer surface with thin orange Fe-oxide laminations within. One 3 cm long chimney with an internal diameter of <1.5 cm and <1 cm thick walls was recovered. It is dominantly dull dark gray, with moderate orange-red Fe-oxide on the outer surface. In cross-section, laminations of Mn-oxide occur on the outer surfaces of the chimney with internal layers of orange-red Fe-oxide.</p>
	<p><u>P340-730DR-1</u></p> <p>Calcareous mud. Large vial of light brown, likely calcareous, mud. Mud filled dredge bucket and cemented rock fragments.</p>

	<p><u>P340-730DR-2</u></p> <p>Fe-Mn-oxide stained calcareous mudstone. 20 fragments totaling ca. 1 kg were recovered. The largest sample measures 13 x 8 x 5 cm. Fragments are beige colored mud-siltstone, likely a product of hydrothermal baking of pelagic marine sediment. Outer surfaces are very soft. Internally the sample is much harder. Orange-brown to yellow-orange Fe-oxide covers >50 % of the samples. Black Mn-oxide is a subordinate phase. Dark Mn-oxide coating is slightly harder than orange-red Fe-oxides and soft mudstone surface.</p>
	<p><u>P340-730DR-3</u></p> <p>Mn-Fe-oxide stained calcareous mudstone (ca. 2 kg). Sample is similar to P340-730DR-2. The largest piece measures 15 x 15 x 8 cm. Samples are lithified, irregular shaped, beige siltstone with up to 80 % of the outer surface coated in dull black Mn-Fe-oxide. 50 % of the surface area of some samples is covered by orange Fe-oxide. Worm burrows and possible gas conduit structures are observed. The outer surface is soft, but Mn-Fe-oxide coating is slightly harder.</p>
	<p><u>P340-730DR-4</u></p> <p>Fe-Mn-oxide stained calcareous mudstone (ca. 1 kg). The largest piece measures <6 cm. Samples are rounded and very light pieces of possibly calcareous mud-siltstone. Orange-dark brown Fe-Mn-oxides coat the outer surfaces. Worm burrows up to 1 cm in diameters are observed. Laminations of fine-grained powdery orange and near vitreous, red, Fe-oxide are observed locally.</p>
	<p><u>P340-730DR-5</u></p> <p>Massive Mn-Fe-oxide. In total, 25 rounded pieces with an approximate weight of ≤ 1 kg were recovered. The largest cobble has a maximum diameter of 8 cm. The average diameter is 4 cm. Samples are black, crumbly, massive Mn-Fe-oxide, laminations are rare. Minor green and yellow coating, possibly consisting of nontronite, is observed on outer surfaces.</p>

	<p><u>P340-730DR-6</u></p> <p>Massive hydrothermal sulfide crust. In total, 8 angular massive sulfide fragments were recovered. The largest sample is 9 x 8 x 6 cm. The smallest piece measures ca. 2 cm³. Samples are dull black, fine-grained masses with a crumbly, porous, internal texture. Outer surfaces are smooth. A botryoidal texture is observed on the largest sample (shown). Patchy red-brown to pink coloration occurs over up to 30 % of the sample, possibly representing sulfosalts. A high specific density is indicative of significant barite content. Rare pyrite is observed.</p>
	<p><u>P340-730DR-7</u></p> <p>Green clay-rich pebbles that possibly consist of nontronite. In total, 12 soft green clay-rich pebbles were recovered that were ≤5 cm in diameter. Several samples are entirely composed of green clay and lack an internal structure. A single pebble consists of green clay coating on orange-red Fe-oxide-rich layers with tightly packed white clasts that possibly represent shell fragments.</p>
	<p><u>P340-730DR-8</u></p> <p>Clay-altered, basaltic to andesitic hyaloclastite. In total, 4 pebbles were recovered. The largest sample measures 6 x 3 x 3 cm. Fragments are soft, have a green coloration, and a blocky, fragmental texture. A strong yellow coating covers most surfaces and grades into a green or orange-red/brown veneer. Coating may consist of nontronite.</p>
	<p><u>P340-730DR-9</u></p> <p>Assorted Fe-Mn-oxide pebbles (ca. 2 kg of pebbles with a diameter of <5 cm). The sample color ranges from red-orange to dull gray. The content of calcareous mudstone is variable. One small, rounded, pumice fragment. One chimney structure measures 3 cm long with an internal diameter of <1 cm. The fragment is coated with Fe-Mn-oxide.</p>



P340-731DR-1

Large vial of light brown, likely calcareous, mud. Mud filled dredge bucket and cemented rock fragments.



P340-731DR-2

Calcareous mudstone that is coated by Mn-Fe-oxides. Single piece measuring 30 x 15 x 10 cm with an approximate weight of 4 kg. The sample has a beige color and is hard and lithified. Numerous sponge spicules and bivalve shells are located on outer surfaces. Some sponge spicules are also observed in the inner portion of the sample. The entire outer surface, including shells, is coated with a dull black, and locally orange-brown, Mn-Fe-oxide veneer.







P340-731DR-3


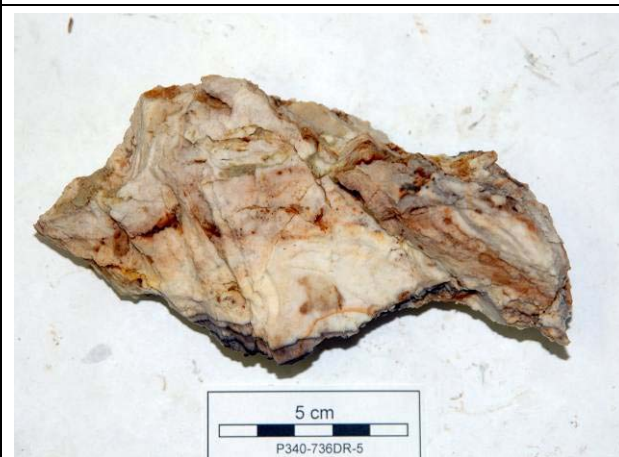


Mn-Fe-oxide coated agglomeration of bivalve shells, sponges, and calcareous mudstone. Single piece measuring 15 x 10 x 8 cm (ca. 1 kg). Bivalve shells, shell fragments, and sponge spicules are cemented by a lithified calcareous mudstone. The outer surface is coated with dull black to locally orange-brown Mn-Fe-oxide. Sample is similar to P340-731-DR2 but contains more abundant shells and shell fragments and a smaller percentage of mudstone. Few millimeter-scale, black, Mn-oxide veins are observed in the beige mudstone.



P340-731DR-4

Rounded pebbles (ca. 0.5 kg) that have a maximum dimension of 8 cm. Three different pebble types were observed. Most pebbles consist of soft red-orange Fe-Mn-oxide that has a low specific density. In addition, bivalves and sponge fragments were recovered that are cemented by beige, calcareous mudstone and coated by dull black Mn-Fe-oxide. A third type of pebbles consists of green clay-altered hyaloclastite that has a blocky texture. The outer surface is coated with a yellow-green clay veneer that possibly consists of nontronite.

	<p><u>P340-732DR-1</u></p> <p>One laminated Mn-Fe-oxide crust (6 x 5 x 3 cm). The sample is typified by millimeter-scale laminations of black Mn-oxide, orange Fe-oxide, and soft beige, likely calcareous mud. A single Mn-Fe-oxide coated worm burrow 3 cm long, with an internal diameter of <1 cm, is preserved on one surface.</p>
	<p><u>P340-736DR-1</u></p> <p>Thinly laminated sandstone (ca. 10-15 kg). The largest piece measures 30 x 15 x 10 cm. Sample is comprised of fine- to medium-grained, white, sub-rounded to elongate clasts. Some grains may be detrital feldspar grains. Sample is well bedded with thin, flat to curvilinear, sub centimeter laminations. Minor red-brown Fe-oxide is present on outer surfaces. Sandstone possibly contains volcanically derived material.</p>
	<p><u>P340-736DR-2</u></p> <p>Thinly laminated sandstone with thin black veins (ca. 1-2 kg). Thinly laminated, light colored sandstone that is similar to P340-736DR-1. The sandstone contains thin black veins that crosscut bedding. Approximately 2-4 veins per 5 cm. Veins are likely Mn-Fe-oxide.</p>
	<p><u>P340-736DR-3</u></p> <p>Sandstone with yellow, green, and orange-red coloration (<0.5 kg). Sample is similar to P340-736DR-1. Zones of grayish color may be caused by fine sulfide impregnations. Rare orange-red coloration indicates possible arsenic sulfide or barite. Yellow and green coloration on outer surface may be caused by hydrothermally derived sulfur that is weathered and partially consumed by bacteria. Several of the recovered samples contain small veinlets and coatings of Mn-oxides.</p> <p>Sample stored at the University of Ottawa.</p>

	<p><u>P340-736DR-4</u></p> <p>Sandstone with abundant yellow coloration. The material is similar to P340-736DR-1. Fractures are lined with yellow to greenish-yellow material, interpreted to be weathered native sulfur or organic material. Mn-oxide stained patches and small veins are present.</p> <p>Sample stored at the University of Ottawa.</p>
	<p><u>P340-736DR-5</u></p> <p>Laminated sandstone. Similar to P340-736DR-1. Sample is a lithified, thinly laminated, white to grayish sandstone with few dark Mn-Fe-oxide laminations interbedded with wavy, distorted sand beds. Individual beds are defined by subtle variations in grain size and color, some approximately 1 mm thick beds are quite siliceous.</p> <p>Sample stored at the University of Ottawa.</p>
	<p><u>P340-736DR-6</u></p> <p>Laminated sandstone. Similar to P340-736DR-1. Sample is a lithified, thinly laminated, sandstone with few dark Mn-Fe-oxide laminations interbedded with wavy, distorted sand beds. Sandstone is relatively fine-grained and slightly yellowish green in color.</p> <p>Sample stored at the University of Ottawa.</p>
	<p><u>P340-736DR-7</u></p> <p>Fe-Mn-oxide coated mudstone (ca. 2-3 kg). The largest piece measures 20 x 20 x 8 cm. Moderately well lithified brown mud coated with red-brown to black Fe-Mn-oxide.</p>



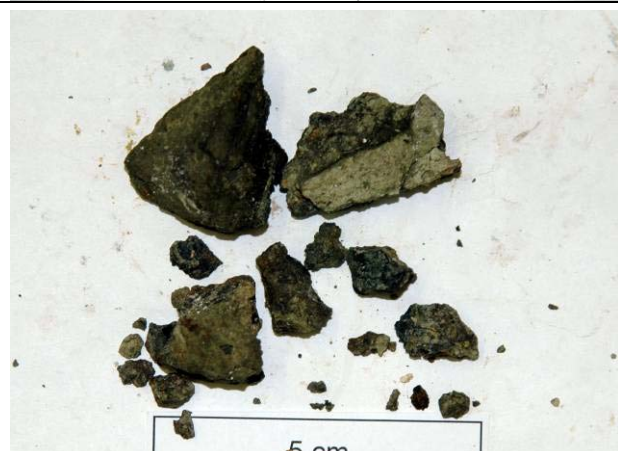
P340-736DR-8

Weakly lithified, beige mud cobbles with minor Fe-oxide coating (ca. 1 kg). The largest piece measures 10 x 8 x 4 cm. The samples are similar to P340-736DR-7. Brown mudstone is partially coated with red-brown Fe-Mn-oxide.



P340-736DR-9

Small Fe-oxide coated mudstone pebbles (<2 kg). The largest piece has a maximum dimension of 6 cm. Moderately well lithified, beige mud with few small clasts. The pebbles have a red-brown to black Fe-Mn-oxide coating. In addition, a few pieces of Fe-Mn crust were recovered.







P340-736DR-10

Green clay pebbles (<100 g). The largest piece measures 3 cm. Pebbles are moderately well lithified green clay, with millimeter scale banding defined by color variation. Samples are probably clay-altered mafic to intermediate volcanic rocks.



P340-736DR-11

Silicified fossil corals with black Mn-Fe-oxide coating (<0.5 kg). Sample was cemented by pelagic mud in dredge.

	<p><u>P340-736DR-12</u></p> <p>Fe-Mn crust pebbles. Large vial of pebbles. Sample was cemented by pelagic mud in dredge bucket.</p>
	<p><u>P340-738DR-1</u></p> <p>Fe-Mn-oxide coated, calcareous mudstone (ca. 10 kg). The largest piece measures 65 x 12 x 35 cm, whereas most of the smaller pieces are 18 x 18 x 6 cm in size. The calcareous mudstone is hard and beige in color. Samples have irregular shapes, possibly reflecting contorted bedding. Numerous centimeter-scale worm burrows are present. Red-brown Fe-Mn-oxide coats up to 60 % of the sample surface. Black Mn-Fe-oxide is a subordinate phase. Numerous bivalve shells are located on the outer surface.</p>
	<p><u>P340-738DR-2</u></p> <p>Calcareous mudstone with red-brown Mn-Fe-oxide (<2 kg). The largest piece measures 10 x 6 x 4 cm. Samples are subrounded cobbles of calcareous mudstone with red-brown Fe-Mn-oxide and minor black Mn-Fe-oxide. Sample is similar to P340-738DR-1 but is comprised of smaller pieces and contains fewer bivalve shells. Few silicified fossil corals are present.</p>
	<p><u>P340-738DR-3</u></p> <p>Calcareous mudstone with black and red-brown Mn-Fe-oxide coating (ca. 5 kg). The largest piece measures 30 x 25 x 6 cm. Calcareous mud was likely affected by hydrothermal baking. Sample is similar to P340-738DR-2 but is coated in dominantly black Mn-Fe-oxide, with subordinate red-brown Fe-Mn-oxide.</p>



P340-738DR-4

Rounded green clay cobbles (ca. 2-3 kg). Maximum dimension of largest piece is 8 cm. The cobbles consist of green, relatively homogenous, clay with minor black and red-brown Mn-Fe-oxides.



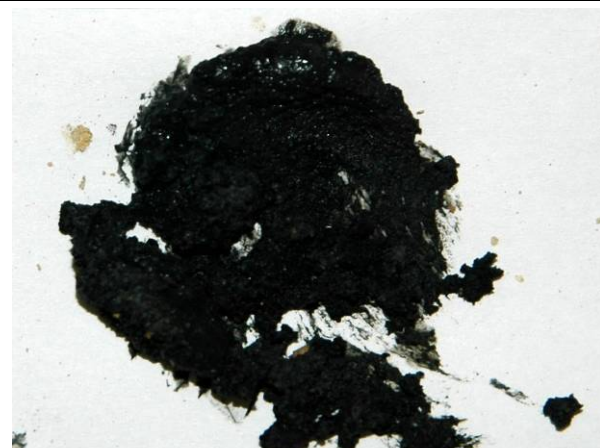
P340-738DR-5

Mn-oxide coated green clay cobbles (ca. 1-2 kg). One 3 cm long chimney structure is observed with an internal dimension of 3 x 1.5 cm. All surfaces are coated with greasy, black, Mn-oxide. A second 3 cm long chimney fragment was also recovered.







P340-738DR-6

Fossil corals cemented by beige, calcareous mud. Approximately 2 kg of rounded clay cobbles were recovered. The largest cobble has a diameter of 8 cm. Shell fragments are also present.



P340-738DR-7

Mn-oxide mud. One large vial of greasy black Mn-oxide mud. Large quantities of mud in dredge haul.

	<p><u>P340-738DR-8</u></p> <p>Mn-oxide mud and green clay. One large vial of greasy black Mn-oxide mud and green clay. Large quantities in dredge haul.</p>
	<p><u>P340-738DR-9</u></p> <p>Two clam shells recovered in dredge.</p>
	<p><u>P340-743ROV-1</u></p> <p>Worm tubes. Six empty worm tubes were collected with the ROV. Live tube worm clusters in the sample area were coated with white flocculent bacterial mats.</p>
	<p><u>P340-752ROV-1</u></p> <p>Silica-rich Fe-oxide chimney fragment. One 11 x 10 x 7 cm sized piece recovered from a chimney structure. Active venting was not observed. Sample is a contorted arrangement of <0.5 cm bands of Fe-oxide and silica. Banding is hard and has a near vitreous appearance. Soft, powdery, orange-red Fe-oxide is observed filling cavities. A green, locally pink, organic film with few sponges covers most of the weathered surfaces.</p>

	<p><u>P340-752ROV-2</u></p> <p>Silica-rich Fe-oxide chimney fragment. One 6 x 4 x 3 cm sized piece recovered from a chimney structure. Active venting was not observed. Sample is a contorted arrangement of <0.5 cm bands of Fe-oxide and silica. Banding is hard and has a near vitreous appearance. 30 % of the weathered surface area is covered with a yellow sponge, originally thought to be native sulfur during sampling.</p>
 <p>5Centimeters P340-756ROV-1</p>	<p><u>P340-756ROV-1</u></p> <p>Sulfur cemented sand. The single piece measures 12 x 5 x 3 cm. Cemented sand formed crust slightly elevated above surrounding bottom sediments. Weakly cemented collection of moderately well sorted, framework supported, sub-rounded, fine-medium grained sand grains. Grains are dominantly quartz with a smaller component of white clasts (kaolinite or feldspars), and few green mafic grains. Yellow native sulfur accounts for approximately 50 % of the sample by volume. Yellow, translucent sulfur cements the sand grains.</p> <p>Sample stored at the University of Ottawa.</p>
	<p><u>P340-756ROV-2</u></p> <p>Sulfur cemented sand. The single piece measures 4 x 4 x 3 cm. Very weakly cemented collection of moderately well sorted, framework supported, sub angular, medium grained sand grains. Grains are dominantly quartz with a smaller component of white clasts (kaolinite or feldspars), and few green mafic grains. Yellow native sulfur accounts for approximately 50 % of the sample by volume. Yellow, translucent sulfur cements the sand grains.</p> <p>Sample stored at the University of Ottawa.</p>

10 Station list

<i>Date / Time (UTC)</i>	<i>Station No.</i>	<i>Lat. / Long. (start)</i>	<i>Lat. / Long. (end)</i>	<i>Comment</i>
06.07.06/ 18:22 – 21:50	721CTD	39°32.50'N/ 14°30.00'E	-	sound velocity profile
06.07.06/07.07.06 22:00 – 06:30	722SBM	39°32.49'N/ 14°30.00'E	39°32.516'N/ 14°42.426'E	multibeam mapping
07.07.06/ 07:05 – 07:50	723ROV	(39°32.516'N/ 14°42.426'E)	-	power failure
07.07.06/ 09:20 – 10:20	724DR	39°32.55'N/ 14°42.40'E	39°32.20'N/ 14°42.45'E	Fe-Mn-oxides and pe- lagic sediment
07.07.06/ 11:25 – 12:15	725DR	39°32.50'N/ 14°42.35'E	39°32.20'N/ 14°42.40'E	empty
07.07.06/ 13:00 – 14:00	726DR	39°32.50'N/ 14°42.35'E	39°32.20'N/ 14°42.40'E	empty
07.07.06/08.07.06 17:10 – 06:30	727SBM	various courses		multibeam mapping
08.07.06/ 07:00 – 08:05	728ROV	(39°32.52'N/ 14°42.43'E)	-	power failure
08.07.06/ 08:40 – 09:40	729DR	39°32.45'N/ 14°42.30'E	39°32.60'N/ 14°42.70'E	empty
08.07.06/ 10:40 – 11:55	730DR	39°32.0'N/ 14°41.0'E ca. 1025 m	39°32.3'N/ 14°42.4'E ca. 560 m	half load of pelagic sediment with some nontronite-rich parts; several small pieces of massive sulfide and Fe- Mn-oxides
08.07.06/ 12:40 – 13:45	731DR	39°31.40'N/ 14°40.30'E ca. 1050 m	39°31.25'N/ 14°39.75'E 650 m	full load of pelagic sediment with two large pieces of Mn-Fe- oxides and Mn- Fe ce- mented carbonate shells
08.07.06/ 14:10 – 15:10	732DR	39°32.0'N/ 14°40.1'E ca. 1050 m	39°32.4'N/ 14°39.7'E 875 m	single piece (200 g) of Mn-oxides
08.07.06/09.07.06 16:00 – 05:00	733SBM	various courses		mapping at Palinuro Seamount
09.07.06/ 06:30 – 06:35	734ROV	39°32.49'N/ 14°42.39'E	-	power failure
09.07.06/ 07:15 – 08:45	735DR	39°31.6'N/ 14°41.0'E ca. 1050 m	39°32.3'N/ 14°42.4'E ca. 580 m	weak link broken
09.07.06/ 09:15 – 10:40	736DR	39°31.5'N/ 14°41.8'E ca. 1050 m	39°32.3'N/ 14°42.4'E ca. 580 m	baked sediment, Fe- oxides and dissemi- nated sulfides in sedi- ment
09.07.06/ 11:30 – 11:37	737ROV	39°32.53'N/ 14°42.39'E	-	power failure
09.07.06/ 12:05 – 13:35	738DR	39°32.5'N/ 14°41.2'E ca. 1050 m	39°32.5'N/ 14°42.5'E ca. 580 m	Mn-oxide mud, non- tronite in pelagic sedi- ment; Mn-oxide chim- neys
09.07.06/10.07.06 16:45 – 08:00	739SBM	various courses		mapping at Palinuro Seamount
10.07.06/ 08:15 – 09:00	740ROV (dive 57)	39°32.51'N/ 14°42.40'E ca. 600 m	39°32.60'N/ 14°42.45'E ca. 625 m	ROV on bottom, but too heavy
10.07.06/ 10:52 – 16:05	741ROV (dive 58)	39°32.60'N/ 14°42.67'E ca. 580 m	39°32.42'N/ 14°42.14'E ca. 600 m	mapping of the eastern summit of the caldera at Palinuro Seamount; thick sediment cover, low-T precipitates, Mn- oxide coated corals; lava outcrops

Cruise Report P340 (TYMAS) – Tyrrhenian Sea July 6th to 17th, 2006

10.07.06/11.07.06 17:40 – 06:25	742SBM	various courses		mapping at Palinuro Seamount
11.07.06/ 07:20 – 14:50	743ROV (dive 59)	39°32.24'N/ 14°42.670'E ca. 690 m	39°32.45'N/ 14°42.40'E ca. 595 m	mapping of the eastern summit of the caldera at Palinuro Seamount; low-T diffuse venting, tube worms and abundant Mn-oxide crusts
Transit to Marsili				
11.07.06/ 18:30 – 19:50	744CTD	39°14.02'N/ 14°26.96'E ca. 2400 m	-	sound velocity profile at Marsili Seamount
11.07.06/12.07.06 21:15 – 04:55	745SBM	various courses		mapping at Marsili Seamount
12.07.06/ 06:45 – 14:45	746ROV (dive 60)	39°16.967'N/ 14°23.909'E 545 m	39°17.160'N/ 14°24.239'E 481 m	mapping at Marsili Seamount
12.07.06/ 15:50 – 19:05	747SBM	various courses		mapping at Marsili Seamount
Transit to Palinuro				
12.07.06/13.07.06 22:20 – 01:30	748SBM	various courses		mapping at Palinuro Seamount
13.07.06/ 07:00 – 14:00	749ROV (dive 61)	39°31.135'N/ 14°39.889'E 777 m	39°31.942'N/ 14°39.736'E 780 m	mapping of the south-western and western summits of the caldera at Palinuro Seamount
13.07.06/ 15:55 – 22:00	750SBM	various courses	-	mapping at Palinuro Seamount
Transit to Panarea				
14.07.06/ 06:00 – 06:45	751CTD		-	sound velocity profile east of Panarea Island
14.07.06/ 08:05 – 14:55	752ROV (dive 62)	38°38.957'N/ 15°06.398 74 m	38°38.952'N / 15°06.352'E 79 m	mapping north of Lisca Bianca
14.07.06/ 15:20 – 20:55	753SBM	various courses	-	mapping to the east of Panarea Island
15.07.06/ 06:55 – 15:00	754ROV (dive 63)	38°39.046'N/ 15°05.656'E 73 m	38°38.962'N/ 15°05.929'E 52 m	mapping northwest of Lisca Bianca
15.07.06/ 16:10 – 18:10	755SBM	various courses	-	mapping to the east of Panarea Island
16.07.06/ 07:15 – 15:00	756ROV (dive 64)	38°39.001'N/ 15°06.760'E 70 m	38°38.929'N/ 15°06.649'E 73 m	seafloor mapping northeast of Lisca Bianca, locating of vent sites
16.07.06/ 15:55 – 18:55	757SBM	various courses	-	mapping to the north-east of Panarea Island

Note: Coordinates given in parenthesis represent the locations of the ship at the beginning and end of ROV dives where the vehicle did not reach the seafloor.

11 References

- Allen R.L., Weihed P., and Svenson S.Å. (1996) Setting of Zn-Cu-Au-Ag massive sulfide deposits in the evolution and facies architecture of a 1.9 Ga marine volcanic arc, Skellefte district, Sweden. *Econ. Geol.* 91, 1022-1053.
- Argnani A. and Savelli C. (1999) Cenozoic volcanism and tectonics in the southern Tyrrhenian Sea: space-time distribution and geodynamic significance. *J. Geodyn.* 27, 409-432.
- Bäcker H., Marchig V., Von Stackelberg U., Stoffers P., Puteanus D., and Tufar W. (1991) Hydrothermale Aktivität auf dem Meeresboden. *Geol. Jb.* D93, 103-197.
- Barberi F., Innocenti F., Ferrara G., Keller J., and Villari L. (1974) Evolution of Eolian Arc volcanism (Southern Tyrrhenian Sea). *Earth Planet. Sci. Lett.* 21, 269-276.
- Barberi F., Gandino A., Gioncada A., La Torre P., Sbrana A., and Zenucchini C. (1994) The deep structure of the Eolian arc (Filicudi-Panarea-Vulcano sector) in light of gravity, magnetic and volcanological data. *J. Volcanol. Geotherm. Res.* 61, 189-206.
- Bargossi G.M., Campos Venuti M., Gasparotto G., and Rossi P.M. (1989) Petrologia e stratigrafia delle successioni andesitiche I.s. di Lipari, Isole Eolie, Italia. *Mineral. Petrogr. Acta* 32, 295-326.
- Beccaluva L., Rossi P.L., and Serri G. (1982) Neogene to Recent volcanism of the Southern Tyrrhenian-Sicilian area: implications for the geodynamic evolution of the Calabrian Arc. *Earth Evol. Sci.* 3, 222-238.
- Beccaluva L., Gabbianelli G., Lucchini F., Rossi P.L., and Savelli C. (1985) Petrology and K/Ar ages of volcanics dredged from the Eolian seamounts: implications for geodynamic evolution of the southern Tyrrhenian basin. *Earth Planet. Sci. Lett.* 74, 187-208.
- Brusilovskiy Y.V. and Gorodnitskiy A.M. (1990) Evolution of basaltic volcanic activity and development of seamounts in the Tyrrhenian Basin as indicated by geomagnetic data. *Geotectonics* 24, 350-358.
- Butterfield D.A., Massoth G.J., McDuff R.E., Lupton J.E., and Lilley M.D. (1990) Geochemistry of hydrothermal fluids from Axial Seamount hydrothermal emission study vent field, Juan de Fuca Ridge: Subseafloor boiling and subsequent fluid-rock interaction. *J. Geophys. Res.* 95, 12895-12921.
- Calanchi N., Capaccioni B., Martini M., Tassi F., and Valentini L. (1995) Submarine gas-emission from Panarea Island (Aeolian Archipelago): distribution of inorganic and organic compounds and inferences about source conditions. *Acta Vulcanol.* 7, 43-48.
- Calanchi N., Tranne C.A., Lucchini F., Rossi P.L., and Villa I.M. (1999) Explanatory notes to the geological map (1:10,000) of Panarea and Basiluzzo islands (Aeolian arc, Italy). *Acta Vulcanol.* 11, 223-243.
- Calanchi N., Peccerillo A., Tranne C.A., Lucchini F., Rossi P. L., Kempton P., Barbier F., and Wu T.W. (2002) Petrology and geochemistry of volcanic rocks from the island of Panarea: implications for mantle evolution beneath the Aeolian island arc (southern Tyrrhenian sea). *J. Volcanol. Geotherm. Res.* 115, 367-395.
- Caliro S., Caracausi A., Chiodini G., Ditta M., Italiano F., Longo M., Minopoli C., Nuccio P.M., Paonita A., and Rizzo A. (2004) Evidence of a recent input of magmatic gases into the quiescent volcanic edifice of Panarea, Aeolian Islands, Italy. *Geophys. Res. Lett.* 31, L07619, doi: 10.1029/2003GL019359.
- Capaccioni B., Rossi P.M.L., Tassi F., Tedesco D., and Vaselli O. (2003) Risultati delle osservazioni geochimiche presso l'isola di Panarea in seguito all'evento di degassamento sottomarino del 3 novembre 2002. Abstract of the GNV General Assembly, 17.
- Caracausi A., Ditta M., Italiano F., Longo M., Nuccio P.M., Paonita A., and Rizzo A. (2005) Changes in fluid chemistry and physico-chemical conditions of geothermal systems caused by magmatic input: The recent abrupt outgassing off the island of Panarea (Aeolian Islands, Italy). *Geochim. Cosmochim. Acta* 69, 3045-3059.

- Carminati E., Wortel M.J.R. Spakman W., and Sabadini R. (1998) The role of slab detachment processes in the opening of the western-central Mediterranean basins: Some geological and geophysical evidence. *Earth Planet. Sci. Lett.* 160, 651-665.
- Colantoni P., Lucchini F., Rossi P. L., Sartori R., and Savelli C. (1981) The Palinuro volcano and magmatism of the southeastern Tyrrhenian Sea (Mediterranean). *Mar. Geol.* 39, 1-12.
- Cole D.R. and Drummond S.E. (1986) The effect of transport and boiling on Ag/Au ratios in hydrothermal solutions: A preliminary assessment and possible implications for the formation of epithermal precious-metal ore deposits. *J. Geochem. Expl.* 25, 45-79.
- De Astis G., Ventura G., and Vilardo G. (2003) Geodynamic significance of the Aeolian volcanism (Southern Tyrrhenian Sea, Italy) in light of structural, seismological, and geochemical data. *Tectonics* 22, doi: 10.1029/2003TC001506.
- De Rosa R., Mazzuoli R., Rossi P.L., Santacroce R., and Ventura G. (1989) Nuovi dati ed ipotesi per la ricostruzione della storia eruttiva dell'Isola di Salina (Isole Eolie). *Boll. GNV* 1989, 809-826.
- Dekov V.M. and Savelli C. (2004) Hydrothermal activity in the SE Tyrrhenian Sea: an overview of 30 years of research. *Mar. Geol.* 204, 161-185.
- Dekov V.M., Kamenov G.D., Savelli C., and Stummeyer J. (2006) Anthropogenic Pb component in hydrothermal ochres from Marsili Seamount (Tyrrhenian Sea). *Mar. Geol.* 229, 199-208.
- Del Monte M. (1972) Il vulcanesimo del Mar Tirreno: nota preliminare sui vulcani Marsili e Palinuro. *Giorn. Geol.* 38, 231-252.
- Drummond S.E. and Ohmoto H. (1985) Chemical evolution and mineral deposition in boiling hydrothermal systems. *Econ. Geol.* 80, 126-147.
- Eckhardt J.D., Glasby G.P., Puchelt H., and Berner Z. (1997) Hydrothermal manganese crusts from Enarete and Palinuro Seamounts in the Tyrrhenian Sea. *Mar. Georesour. Geotech.* 15, 175-208.
- Ellam R.M., Hawkesworth C.J., Menzies M.R., and Rogers N.W. (1989) The volcanism of southern Italy: role of subduction and the relationship between potassic and sodic alkaline magmatism. *J. Geophys. Res.* 94, 4589-4601.
- Esposito A., Giordano G., and Anzidei M. (2006) The 2002-2003 submarine gas eruption at Panarea volcano (Aeolian Islands, Italy): volcanology of the seafloor and implications for the hazard scenario. *Mar. Geol.* 227, 119-134.
- Fabbi A., Marabini F., and Rossi S. (1973) Lineamenti geomorfologici del Monte Palinuro e del Monte delle Baronie. *Giorn. Geol.* 29, 133-156.
- Faggioni O., Pinna E., Savelli C., and Schreider A.A. (1995) Geomagnetism and age study of Tyrrhenian seamounts. *Geophys. J. Int.* 123, 915-930.
- Favalli M., Karátson D., Mazzuoli R., Pareschi M.T., and Ventura G. (2005) Volcanic geomorphology and tectonics of the Aeolian archipelago (Southern Italy) based on integrated DEM data. *Bull. Volcanol.* 68, 157-170.
- Ferrari L. and Manetti P. (1993) Geodynamic framework of the Tyrrhenian volcanism: a review. *Acta Vulcanol.* 3, 1-10.
- Francalanci L., Manetti P., Peccerillo A., and Keller J. (1993) Magmatological evolution of the Stromboli volcano (Aeolian Arc, Italy): inferences from major and trace element and Sr isotopic composition of lavas and pyroclastic rocks. *Acta Vulcanol.* 3, 127-151.
- Gabbianelli G., Gillot P.Y., Lanzafame G., Romagnoli C., and Rossi P.L. (1990) Tectonic and volcanic evolution of Panarea (Aeolian Islands, Italy). *Mar. Geol.* 92, 313-326.
- Gamberi F., Marani M., and Savelli C. (1997) Tectonic, volcanic and hydrothermal features of a submarine portion of the Aeolian arc (Tyrrhenian Sea). *Mar. Geol.* 140, 167-181.
- Gamberi F., Marani M.P., Parr J.M., and Binns R.A. (1999) Sub-seafloor mineralisation at the Panarea shallow-water platform, Aeolian volcanic arc, Italy. In *Mineral deposits: processes to processing* (eds. C. J. Stanley et al.). Balkema, pp. 499-502.
- Garbe-Schönberg D. (1993) Simultaneous determination of 37 trace elements in 28 international rock standards by ICP/MS: *Geostandards Newslett.* 17, 81-97.
- Garbe-Schönberg D., Koschinsky A., Ratmeyer V., Jähmlich H., and Westernströer U. (2006) KIPS – a new multiport valve-based all-teflon fluid sampling system for ROVs. *Geophys. Res. Abstr.* 8, 07032.

- Gasparini C., Iannaccone G., Scandone P., and Scarpa R. (1982) Seismotectonics of the Calabrian arc. *Tectonophysics* 84, 267-286.
- Gasparotto G. and Savelli C. (1994) Mineral chemistry of the calcalkaline lavas from Marsili Seamount (Southeast Tyrrhenian Sea): some magmatological and geodynamic considerations. *Boll. Geof. Teor. Appl.* 36, 141-144.
- Gioncada A., Mazzuoli R., Bisson M., and Pareschi M.T. (2003) Petrology of volcanic products younger than 42 ka on the Lipari-Vulcano complex (Aeolian Islands, Italy): an example of volcanism controlled by tectonics. *J. Volcanol. Geotherm. Res.* 120, 191-220.
- Glasby G.P., Eckhardt J.D., and Puchelt H. (1995) Hydrothermal manganese crusts from the Tyrrhenian Sea. *Terra Abstr.* 7, 207.
- Halley S.W. and Roberts R.H. (1997) Henty: A shallow-water gold-rich volcanogenic massive sulfide deposit in western Tasmania. *Econ. Geol.* 92, 438-447.
- Hannington M.D., and Herzig P.M. (2000) Submarine epithermal deposits and the VMS-epithermal transition: A new exploration target. In: Gemmell J.B. and Pongratz J. (eds) *Volcanic Environments and Massive Sulfide Deposits*. CODES, University of Tasmania, Hobart, pp. 75-77.
- Hannington M.D., Poulsen K.H., Thompson J.F.H. and Sillitoe R.H. (1999) Volcanogenic gold in the massive sulfide environment. *Rev. Econ. Geol.* 8, 325-356.
- Herzig P.M., Petersen S., Kuhn T., Hannington M.D., Gemmell J.B., Skinner A.C., Becker K., Campbell N.C., Cavill-Jones J., Fensch M., Franz L., Gillespie E.J., Henkel E., Kidd R., Kim D., Ksienzyk F., Lancaster R., Lee J.H., Monecke T., Müller M., Smith D.J., and Strothmann F. (2003) Shallow drilling of seafloor hydrothermal systems using R/V Sonne and the BGS Rockdrill: Conical Seamount (New Ireland Fore-Arc) and Pacmanus (Eastern Manus Basin), Papua New Guinea. *InterRidge News* 12, 22-26.
- Hippolyte J., Angelier J., and Roure F. (1994) A major change revealed by Quaternary stress patterns in the Southern Apennines. *Tectonophysics* 230, 199-210.
- Honnorez J., Keller J., and Rittman A. (1968) Xenolithe in vulkanischen Gesteinen der Aeolischen Inseln (Sizilien). *Geol. Rundsch.* 57, 719-736.
- Hornig-Kjarsgaard I., Keller J., Koberski U., Stadlbauer E., Francalanci L., and Lenhart R. (1993) Geology, stratigraphy and volcanological evolution of the island of Stromboli, Aeolian arc, Italy. *Acta Vulcanol.* 3, 21-68.
- Huston D.L. and Cas R. (2000) Shallow water volcanic-hosted massive sulfide deposits: How common are they? In: Gemmell J.B. and Pongratz J. (eds) *Volcanic Environments and Massive Sulfide Deposits*. CODES, University of Tasmania, Hobart, pp. 93-95.
- Italiano F. and Nuccio P.M. (1991) Geochemical investigations of submarine volcanic exhalations to the east of Panarea, Aeolian Islands, Italy. *J. Volcanol. Geotherm. Res.* 46, 125-141.
- Kastens K., Mascle J., Auroux C., Bonatti E., Broglia C., Channell J., Curzi P., Emeis K. C., Glacon G., Hasegawa S., Hieke W., Mascle G., McCoy F., McKenzie J., Mendelson J., Müller C., Réhault J.P., Robertson A., Sartori R., Sprovieri R., and Torii M. (1986) A microcosm of ocean basin evolution in the Mediterranean. *Nature* 321, 383-384.
- Kastens K., Mascle J., Auroux C., Bonatti E., Broglia C., Channell J., Curzi P., Emeis K. C., Glacon G., Hasegawa S., Hieke W., Mascle G., McCoy F., McKenzie J., Mendelson J., Müller C., Réhault J.P., Robertson A., Sartori R., Sprovieri R., and Torii M. (1988) ODP Leg 107 in the Tyrrhenian Sea: insights into passive margin and back-arc basin evolution. *Geol. Soc. Amer. Bull.* 100, 1140-1156.
- Kidd R.B. and Ármannsson H. (1979) Manganese and iron micronodules from a volcanic seamount in the Tyrrhenian Sea. *J. Geol. Soc. London* 136, 71-76.
- Lanzafame G. and Rossi P.L. (1984). Evidenze di attivita' tettonica recente a Panarea (Eolie): implicazioni vulcanologiche. *Geol. Rom.* 23, 131-139.
- Marani M.P. and Trua T. (2002) Thermal constriction and slab tearing at the origin of a superinflated spreading ridge: Marsili volcano (Tyrrhenian Sea). *J. Geophys. Res.* 107, 2188, doi: 10.1029/2001JB000285.
- Marani M.P., Gamberi F., and Savelli C. (1997) Shallow-water polymetallic sulfide deposits in the Aeolian island arc. *Geology* 25, 815-818.

- Marani M.P., Gamberi F., Casoni L., Carrara G., Landuzzi V., Musacchio M., Penitenti D., Rossi L., and Trua T. (1999) New rock and hydrothermal samples from the southern Tyrrhenian Sea: the MAR-98 research cruise. *Giorn. Geol.* 61, 3-24.
- Milano G., Vilardo G., and Luongo G. (1994) Continental collision and basin opening in southern Italy: a new plate subduction in the Tyrrhenian Sea? *Tectonophysics* 230, 249-264.
- Minniti M. and Bonavia F.F. (1984) Copper-ore grade hydrothermal mineralization discovered in a seamount in the Tyrrhenian Sea (Mediterranean): is the mineralization related to porphyry-coppers or base metal lodes? *Mar. Geol.* 59, 271-282.
- Minniti M., Bonavia F.F., Dacquino C., and Raspa G. (1986) Distribution of Mn, Fe, Ni, Co, and Cu in young sediments on the Palinuro Seamount in the southeast Tyrrhenian Sea (Mediterranean). *Mar. Mining* 5, 277-305.
- Morelli C., Giese P., Cassinis R., Colombi B., Guerra I., Luongo G., Scarascia S., and Schutte K.G. (1975) Crustal structure of Southern Italy: a seismic refraction profile between Puglia, Calabria, Sicily. *Boll. Geof. Teor. Appl.* 17, 183-210.
- Nadaraju G.D. (1993) Triassic-Jurassic biochronology of the eastern Iskut River map area, northwestern British Columbia. M.Sc. thesis at the University of British Columbia, Vancouver, 268 p.
- Petersen S., Herzig P.M., Kuhn T., Franz L., Hannington M.D., Monecke T., and Gemmill J.B. (2005) Shallow drilling of seafloor hydrothermal systems using the BGS Rockdrill: Conical Seamount (New Ireland Fore-Arc) and Pacmanus (Eastern Manus Basin), Papua New Guinea. *Marine Georesour. Geotechnol.* 23, 175-193.
- Puchelt H. and Laschek D. (1986) *Fahrtbericht Forschungsfahrt Sonne 41 (HYMAS I)*. Universität Karlsruhe, 331 p.
- Puchelt H. and Laschek D. (1987) Massive sulphide and oxide ores in the Tyrrhenian Sea from Sonne cruise 41. *Terra Cognita* 7, 188.
- Santo A.P., Jacobsen S.B., and Baker J. (2004) Evolution and genesis of calc-alkaline magmas at Filicudi Volcano, Aeolian Arc (Southern Tyrrhenian Sea, Italy). *Lithos* 72, 73-96.
- Savelli C. (1988) Late Oligocene to recent episodes of magmatism in and around the Tyrrhenian Sea: implications for the processes of opening in a young inter-arc basin of intra-orogenic (Mediterranean) type. *Tectonophysics* 146, 163-181.
- Savelli C. (1992) Il rifting del vulcano Marsili (Mar Tirreno): aspetti morfo-tettonici osservati da bordo del sottomarino "MIR 2". *Giorn. Geol.* 54, 215-227.
- Savelli C. (2001) Two-stage progression of volcanism (8–0 Ma) in the central Mediterranean (southern Italy). *J. Geodyn.* 31, 393–410.
- Savelli C. and Gasparotto G. (1994) Calc-alkaline magmatism and rifting of the deep-water volcano of Marsili (Aeolian back-arc, Tyrrhenian Sea). *Mar. Geol.* 119, 137-157.
- Savelli C. and Schreider A.A. (1991) The opening processes in the deep Tyrrhenian basins of Marsili and Vavilov, as deduced from magnetic and chronological evidence of their igneous crusts. *Tectonophysics* 190, 119-131.
- Savelli C., Marani M., and Gamberi F. (1999) Geochemistry of metalliferous, hydrothermal deposits in the Aeolian arc (Tyrrhenian Sea). *J. Volcanol. Geotherm. Res.* 88, 305-323.
- Sborshchikov I.M. and Al´mukhamedov A.I. (1992) Submarine volcanoes of the Tyrrhenian Sea - testaments to the opening of a backarc basin. *Int. Geol. Rev.* 34, 166-177.
- Sborshchikov I.M., Savelli C., and Dukov N. (1989) Side-scan sonar survey on the summit of Marsili volcano: rifting morphology of an active axial zone in the Tyrrhenian Sea. *Giorn. Geol.* 51, 109-116.
- Sborshchikov I.M., Savelli C., and Dukov N. (1991) Side-scan sonar and submersible surveys on the Marsili Volcano: rifting morphology of an active axial zone in the Southern Tyrrhenian Sea. *Terra Abstr.* 3, 386.
- Selli R., Lucchini F., Rossi P.L., Savelli C., and Del Monte M. (1977) Dati geologici, petrochimici e radiometrici sui vulcani centro-tirrenici. *Giorn. Geol.* 42, 221-246.
- Sherlock R.L., Roth T., Spooner E.T.C., and Bray C.J. (1999) Origin of the Eskay Creek precious metal-rich volcanogenic massive sulfide deposit: Fluid inclusion and stable isotope evidence. *Econ. Geol.* 94, 803-824.

- Stüben D., Sedwick P., Savelli C., and Shipboard Scientific Party (1993) Cruise report Poseidon 200-4 MIPAMEHR-MAST 1 - investigations on hydrothermalism in the Tyrrhenian and Aeolian Sea. Geologisch-Paläontologisches Institut der Universität Kiel, 91 p.
- Trua T., Serri G., Marani M., Renzulli A., and Gamberi F. (2002) Volcanological and petrological evolution of Marsili Seamount (southern Tyrrhenian Sea). *J. Volcanol. Geotherm. Res.* 114, 441-464.
- Tufar W. (1991) Paragenesis of complex massive sulfide ores from the Tyrrhenian Sea. *Mitt. österr. geol. Ges.* 84, 265-300.
- Uchupi E. and Ballard R. D. (1989) Evidence of hydrothermal activity on Marsili Seamount, Tyrrhenian Basin. *Deep Sea Res.* 36, 1443-1448.
- Ventura G., Vilardo G., Milano G., and Pino N.A. (1999) Relationships among crustal structure, volcanism and strike-slip tectonics in the Lipari-Vulcano volcanic complex (Aeolian Islands, Southern Tyrrhenian Sea, Italy). *Phys. Earth Planet. Inter.* 116, 31-52.
- Westaway R. (1993) Quaternary uplift of southern Italy. *J. Geophys. Res.* 98, 21741-21772.
- White M.J. and McPhie J. (1997) A submarine welded ignimbrite - crystal-rich sandstone facies association in the Cambrian Tyndall Group, western Tasmania, Australia. *J. Volcanol. Geotherm. Res.* 76, 277-295.
- Yevsyukov Y.D. (1994) Morphology of Palinuro and Poseidon seamounts (Southeastern Tyrrhenian Sea). *Oceanology* 34, 415-420.

IFM-GEOMAR Reports

No.	Title
1	RV Sonne Fahrtbericht / Cruise Report SO 176 & 179 MERAMEX I & II (Merapi Amphibious Experiment) 18.05.-01.06.04 & 16.09.-07.10.04. Ed. by Heidrun Kopp & Ernst R. Flueh, 2004, 206 pp. In English
2	RV Sonne Fahrtbericht / Cruise Report SO 181 TIPTEQ (from The Incoming Plate to mega Thrust EarthQuakes) 06.12.2004.-26.02.2005. Ed. by Ernst R. Flueh & Ingo Grevemeyer, 2005, 533 pp. In English
3	RV Poseidon Fahrtbericht / Cruise Report POS 316 Carbonate Mounds and Aphotic Corals in the NE-Atlantic 03.08.-17.08.2004. Ed. by Olaf Pfannkuche & Christine Utecht, 2005, 64 pp. In English
4	RV Sonne Fahrtbericht / Cruise Report SO 177 - (Sino-German Cooperative Project, South China Sea: Distribution, Formation and Effect of Methane & Gas Hydrate on the Environment) 02.06.-20.07.2004. Ed. by Erwin Suess, Yongyang Huang, Nengyou Wu, Xiqu Han & Xin Su, 2005, 154 pp. In English and Chinese
5	RV Sonne Fahrtbericht / Cruise Report SO 186 – GITEWS (German Indonesian Tsunami Early Warning System 28.10.-13.1.2005 & 15.11.-28.11.2005 & 07.01.-20.01.2006. Ed. by Ernst R. Flueh, Tilo Schoene & Wilhelm Weinrebe, 2006, 169 pp. In English
6	RV Sonne Fahrtbericht / Cruise Report SO 186 -3 – SeaCause II, 26.02.-16.03.2006. Ed. by Heidrun Kopp & Ernst R. Flueh, 2006, 174 pp. In English
7	RV Meteor, Fahrtbericht / Cruise Report M67/1 CHILE-MARGIN-SURVEY 20.02.-13.03.2006. Ed. by Wilhelm Weinrebe und Silke Schenk, 2006, 112 pp. In English
8	RV Sonne Fahrtbericht / Cruise Report SO 190 - SINDBAD (Seismic and Geoacoustic Investigations Along The Sunda-Banda Arc Transition) 10.11.2006 - 24.12.2006. Ed. by Heidrun Kopp & Ernst R. Flueh, 2006, 193 pp. In English
9	RV Sonne Fahrtbericht / Cruise Report SO 191 - New Vents "Puaretanga Hou" 11.01. - 23.03.2007. Ed. by Jörg Bialas, Jens Greinert, Peter Linke, Olaf Pfannkuche, 2007, 190 pp. In English

- 10 FS ALKOR Fahrtbericht / Cruise Report AL 275 - Geobiological investigations and sampling of aphotic coral reef ecosystems in the NE-Skagerrak, 24.03. - 30.03.2006, Andres Rüggeberg & Armin Form, 39 pp.
In English
- 11 FS Sonne / Fahrtbericht / Cruise Report SO 192-1: MANGO: Marine Geoscientific Investigations on the Input and Output of the Kermadec Subduction Zone, 24.03. - 22.04.2007, Ernst Flüh & Heidrun Kopp, 127 pp.
In English
- 12 FS Maria S. Merian / Fahrtbericht / Cruise Report MSM 04-2: Seismic Wide-Angle Profiles, Fort-de-France – Fort-de-France, 03.01. - 19.01.2007, Ernst Flüh, 45 pp.
In English
- 13 FS Sonne / Fahrtbericht / Cruise Report SO 193: MANIHIKI Temporal, Spatial, and Tectonic Evolution of Oceanic Plateaus, Suva/Fiji – Apia/Samoa 19.05. - 30.06.2007, Reinhard Werner and Folkmar Hauff, 201 pp.
In English
- 14 FS Sonne / Fahrtbericht / Cruise Report SO195: TOTAL TONGA Thrust earthquake Asperity at Louisville Ridge, Suva/Fiji – Suva/Fiji 07.01. - 16.02.2008, Ingo Grevemeyer & Ernst R. Flüh, 106 pp.
In English
- 15 RV Poseidon Fahrtbericht / Cruise Report P362-2: West Nile Delta Mud Volcanoes, Piräus – Heraklion 09.02. - 25.02.2008, Thomas Feseker, 63 pp.
In English
- 16 RV Poseidon Fahrtbericht / Cruise Report P347: Mauritanian Upwelling and Mixing Process Study (MUMP), Las-Palmas - Las Palmas, 18.01. - 05.02.2007, Marcus Dengler et al., 34 pp.
In English
- 17 FS Maria S. Merian Fahrtbericht / Cruise Report MSM 04-1: Meridional Overturning Variability Experiment (MOVE 2006), Fort de France – Fort de France, 02.12. - 21.12.2006, Thomas J. Müller, 41 pp.
In English
- 18 FS Poseidon Fahrtbericht /Cruise Report P348: SOPRAN: Mauritanian Upwelling Study 2007, Las Palmas - Las Palmas, 08.02. - 26.02.2007, Hermann W. Bange, 42 pp.
In English
- 19 R/V L'ATALANTE Fahrtbericht / Cruise Report IFM-GEOMAR-4: Circulation and Oxygen Distribution in the Tropical Atlantic, Mindelo/Cape Verde - Mindelo/Cape Verde, 23.02. - 15. 03.2008, Peter Brandt, 65 pp.
In English
- 20 RRS JAMES COOK Fahrtbericht / Cruise Report JC23-A & B: CHILE-MARGIN-SURVEY, OFEG Barter Cruise with SFB 574, 03.03.-25.03. 2008 Valparaiso – Valparaiso, 26.03.-18.04.2008 Valparaiso - Valparaiso, Ernst Fluh & Jörg Bialas, 242 pp.
In English



IFM-GEOMAR

Leibniz-Institut für Meereswissenschaften
an der Universität Kiel

Das Leibniz-Institut für Meereswissenschaften
ist ein Institut der Wissenschaftsgemeinschaft
Gottfried Wilhelm Leibniz (WGL)

The Leibniz-Institute of Marine Sciences is a
member of the Leibniz Association
(Wissenschaftsgemeinschaft Gottfried
Wilhelm Leibniz).

Leibniz-Institut für Meereswissenschaften / Leibniz-Institute of Marine Sciences

IFM-GEOMAR
Dienstgebäude Westufer / West Shore Building
Düsternbrooker Weg 20
D-24105 Kiel
Germany

Leibniz-Institut für Meereswissenschaften / Leibniz-Institute of Marine Sciences

IFM-GEOMAR
Dienstgebäude Ostufer / East Shore Building
Wischhofstr. 1-3
D-24148 Kiel
Germany

Tel.: ++49 431 600-0
Fax: ++49 431 600-2805
www.ifm-geomar.de